**Sharif University of Technology**

**(Aerospace Engineering Department)**

**A Thesis Submitted in Partial Fulfillment of the Requirement for the M.Sc. Degree**

# Numerical Investigation of Vortex Shedding Control Behind a Cylinder with Swinging Thin Plates

**By:**
**Babak Bagherzadeh Chehreh**

**Supervisor:**
**Dr. Khodayar Javadi**

**Advisor:**
**Dr. Mohammad Taeibi Rahni**

January, 2016

**Abstract**

Von-Karman vortex shedding is a transient aerodynamic instability which occurs in laminar flows over a bluff body in a certain condition. When this phenomenon occurs, vortices take form on upper and lower parts of the bluff body and begin to shed into an oscillatory manner affecting a significant part of the flow domain.

This research focuses on Karman vortex shedding control by using two thin swinging splitter plates. Length ratio of plates to cylinder diameter is 1 p = 1) and plates are attached at +55 degrees (trigonometric angle). Plates are forced to oscillate at different ratios of natural vortex shedding frequencies (0.75, 1, 1.25, 1.5 and 2) for different amplitudes.

Simulations were conducted for Reynolds numbers 200, 250 and 300 by numerically solving Naiver-Stokes equations using finite Volume method.

Our results show that in certain configurations the oscillatory nature of side force (lift force) is completely suppressed. The effects of splitter plates oscillation on Drag force, flow behavior and vortex shedding frequency are also presented.

**Key Words**: *Aerodynamic instability, Pressure Field Fluctuation, Circular Cylinder, Splitter Plate, Strouhal Number*

# Contents

1.1. Overall definition of the research topic ..... 6
1.1.1. Strouhal number ..... 8
1.1.2. Flow control- vortex shedding control ..... 9
1.1.2.1. What is the flow control? ..... 9
1.2. Research motivation ..... 10
1.3. Research background ..... 10
1.4. Targets and innovation of the research ..... 13
1.5. Detailed project definition ..... 14
1.6. Summary and overview of the following seasons ..... 15
2.1. Fluid dynamic equations ..... 17
2.1.1. Conservation laws ..... 18
2.1.1.1. Mass continuity (mass conservation) ..... 18
2.1.1.2. Momentum conservation ..... 18
2.1.1.3. Energy conservation ..... 19
2.2. Simplification and correction of equations for the problem ..... 19
2.3. Boundary conditions ..... 20
3.1. Finite volume method ..... 22
3.2. Equations and settings ..... 22
3.2.1. Pressure-based solution ..... 22
3.2.1.1. Pressure-velocity coupling ..... 22
3.2.2. Time ..... 23
3.2.2.1. Time step ..... 23
3.2.3. Space discretization ..... 23
3.3. Grid ..... 23
3.3.1. Dynamic grid ..... 25
3.3.1.1. Smoothing ..... 25
3.3.1.2. Layering ..... 27
3.3.1.3. Remeshing ..... 27
3.4. Validation ..... 31
3.4.1. Comparison of solutions with analytical relations ..... 31
3.4.2. Comparison of results with available simulations ..... 32
3.4.3. Study the mesh independency ..... 33
3.4.4. Study the time step independency of solution ..... 39
4.1. Checking and determining the arrangement of wings around the cylinder ..... 42

4.1.1. Study the installation location of wings.....43
4.1.2. Studying the installation angle of wings .....47
4.2. Studying the effect of swinging of wings on the flow .....51
4.2.1. Effect of oscillations of the wings on the drag force .....52
4.2.2. Properties of lift force and oscillations result from oscillation of wings.....62
4.2.3. Qualitative Properties of the flow and shape of vortices.....70
4.2.3.1. Classifying the flow behavior using the dimensionless numbers .....86

# Chapter 1

# Introduction

Vortex dominated flow always has attracted the attention of researchers and engineers which work on the concepts and phenomena of the fluid flow. These types of the flow include complicated wakes which can be two- or three-dimensional. Unstable vortex wakes occur when a fluid flows over a non-streamlined structure and/or in a simpler term over a bluff body. These unstable wakes induce fluctuations created by vortices which can cause the serious and scientific challenges arise in different engineering fields. The severe induced vortices can cause very considerable structural damages. Generally, the problems related to the fluctuations created by vortices are observed in the designation of towers, buildings, oil platforms, offshore structures, bridges, pipe lines, heat exchangers and so on. Any non-streamlined geometry is considered as a bluff body, if the pressure drag dominance over the viscous drag. The well-known examples for a bluff body include circular cylinder, sphere, square and rectangle. Even an airfoil, which is a streamlined geometry, considered as a bluff body at high attack angles. The aim of the present thesis is to investigate the behavior of the separated vortices over a 2D circular cylinder. Despite of having simple geometry, circular cylinder enables the study of all vortex shedding phenomena, therefore it is a popular and widely used geometry. in this thesis, the study will be done over this geometry.

## 1.1. Overall definition of the research topic

Most of the previous researches done on the bluff bodies, investigated the flow passing over a 2D circular cylinder ([1]-[15]). As it was mentioned by Roshko [11], the circular cylinder is the fundamental of the bluff body concept. The reason behind the popularity of this geometry is its simple geometry and its practical applications in engineering and constructions such as sea pipelines, bridge legs, docks and so on. In experimental studies, it is simpler to use circular pipes and bars with circular cross-section which are easily available. However, it should be noted that the flow passing over a circular cylinder can be very complicated and its solution can be very useful for obtaining an overall understanding about flow passing over a bluff body in different conditions. The history of the researches done in the field of flow passing a circular cylinder can be tracked back until the period of French scientist and mathematician Jean le Rond d'Alembert and his famous paradox. He was surprised by the results obtained from his calculations on the potential flow passing over the circular cylinder. Because the drag force he obtained was zero which was in paradox with the result of his physical experiment and observation of the resistance force in opposite direction of cylinder's movement in the fluid. The problem was the lack of viscosity in his calculations. With the help of the studies done after his experiment, which most of them were experimental tests, effective steps have been taken for understanding the concept and the role of viscosity in producing the drag force caused by flow passing over bluff bodies. Since the real fluid is viscos, therefore creates a resistance against the shear stress when a geometry moves respect to the fluid. The behavior of the vortex wakes depends on the balance between inertia and the viscos forces, and as a result, the flow regimes are categorized using dimensionless Reynolds number:

$$Re = \frac{\rho U x}{\mu} \tag{1.1}$$

where ρ, U, x and μ are density of fluid, velocity of the free stream, the characteristic length and dynamic viscosity, respectively. It should be noted that, diameter of the 2D cylinder is

considered as its characteristic and the Reynolds number for a 2D cylinder is corrected as follows:

$$Re = \frac{\rho U D}{\mu} \tag{1.2}$$

When the Reynolds number approaching zero, the flow can be considered as artificial because this creates a flow pattern which is ideally symmetric respect to the centerline of the bluff body and the upstream streamlines (respect to the centerline) are completely same as the downstream streamlines. In fact, flow of a high-viscosity fluid and/or flow passing very small geometries where in $Re \ll 1$ have the symmetric patterns. These types flow called creeping flow or Stokes in which the inertia force of the fluid is neglected. Laminar flow occurs in very low Reynolds numbers where the order of fluid's viscous forces is much larger than that of the inertia forces. Stagnation pressure which occurs at the attack edge of the geometry is enough to direct the fluid flow around the geometry. By increasing the Reynolds number, the boundary layer's thickness increases and the effect of the inertia force become more pronounced to the extent that the stagnation pressure of the attack edge will not be enough for rotating the flow around the geometry to the scape edge. Eventually, this process continues to the extent that the flow separated from the surface of the structure and the separation phenomenon occurs. Instability properties of the flow changes in a wide range of the Reynolds number. This interval can range from the coherent, repeating and rotating vortices called the Von-Karman vortex street which occurs in Reynolds number lower than 100, to a very irregular and random regime of the turbulent eddies which occurs in very high Reynolds number (about several millions). Roshko found that for a circular cylinder, the creation of the vortices to some extent depends on the base pressure coefficient ($C_{pb}$) which calculates at the trigonometric angle of 180-degree respect to the attack angle. He used this result to classified the vortex shedding regimes ([11] and [13]):

1. $Re<49$: Steady flow regime
2. $49 \leq Re<180$: laminar vortex shedding regime
3. $180<Re<260$: transient regime of the 3D wakes
4. $260<Re<10^3$: increase in disorder in the 3D small structures
5. $10^3<Re<10^5$: shear layer transient regime
6. $10^5<Re<4\times10^5$: asymmetric reattachment regime (critical transition regime)
7. $4\times10^5<Re<8\times10^5$: symmetric reattachment regime (supercritical transition regime)
8. $Re>8\times10^5$: boundary layer transient regime (post-critical regime)

Despite of researches done on the flow passing over circular cylinder, several experimental and numerical studies have been done on the flows passing over bluff rectangular and square geometries ([16]-[26]). The interest on studying the rectangular geometries rooted in designation of buildings and vehicles. For example, many of buildings such as skyscrapers are constructed with rectangular cross-section, and for this reason they are exposed against the vortex induction oscillations created by the wind blow. A big vehicle such as truck and/or trailer can simply be considered as a rectangular geometry. Such studies can be very effective for designing a vehicle to reduce the drag and as a result to reduce the fuel consumption. Another example of flow passing over a rectangular and/or square geometry, is the moving arm of in the hard disc drive (HDD).

### 1.1.1. Strouhal number

While the unstable vortices and their inductive oscillations topic is very wide, in this thesis the attention is focused on the laminar flow regime where the Von-Karman vortices occur. In this regime, the flow behavior as a result of the instabilities is complicated. After more than a century since Strouhal, a Czech scientist, for the first encountered this phenomenon, in 1887, there are also several unknowns to this day. Strouhal studied the rapture of telegraph wire occurs by this phenomenon and derived his famous formula for describing the frequency of this phenomenon. Generally, the value of the non-dimensionless Strouhal number describes the oscillation mechanism of this phenomenon. Strouhal number defined as follows:

$$Sr = \frac{fL}{V} \tag{1.3}$$

where denotes the vortices separation frequency from the surface, L is the characteristic length and V is the velocity of fluid flow. For example, for a circular cylinder, the characteristic length is equal to diameter of cylinder and the relation (4-1) is corrected as follow,

$$Sr = \frac{fD}{V} \tag{1.4}$$

where D is diameter of the cylinder.

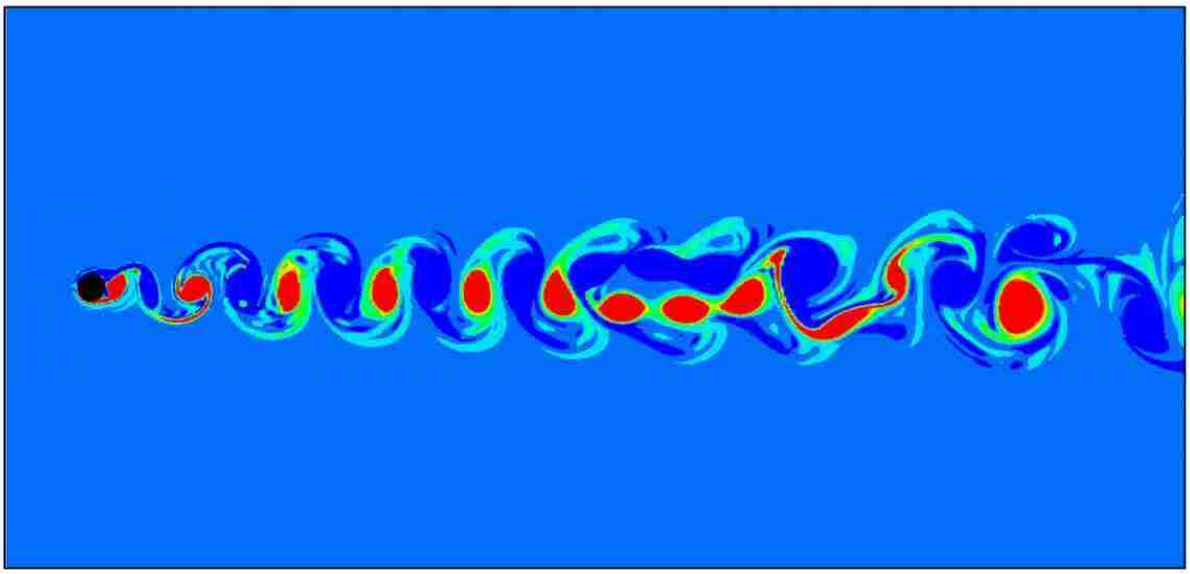

**Fig. (1-1).** Von-Karman vortices separated from the surface of a 2D cylinder in a numerical simulation.

Figs. (1-1) and (1-2) show the flow rotation plots in a numerical simulation of the separated Karman vortices from the surface of the 2D cylinder and the Karman vortices created in the atmosphere of the earth, respectively.

In the next years, Theodore Von-Karman, an American-Polish aerospace engineer and mathematician studied this phenomenon in more details and was able to detect this phenomenon. After his service this phenomenon was named in his honor

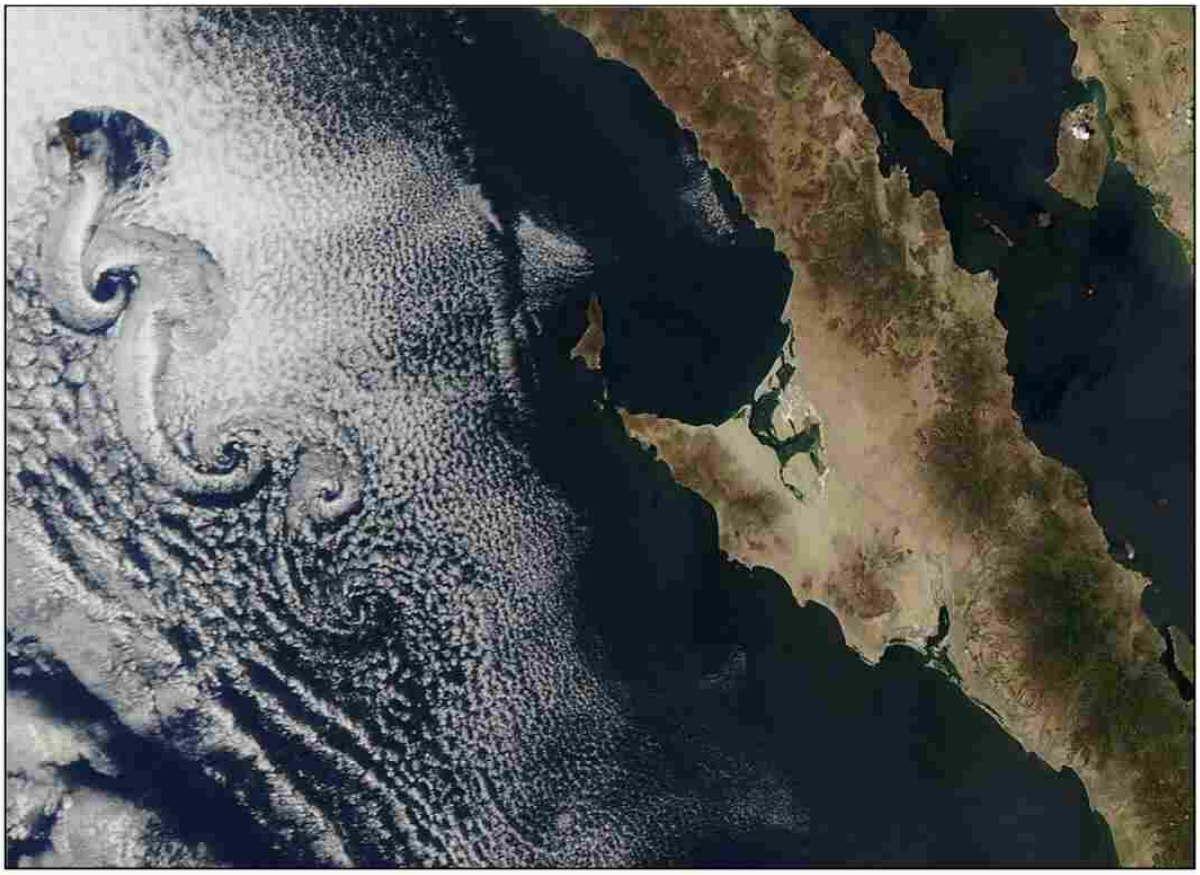

**Fig. (2-1):** Created Von-Karman vortices in the atmosphere of the earth.

### 1.1.2. Flow control- vortex shedding control

With an overview on the researches done on the vortex shedding, it can be found that one of the most important targets of the researches has been controlling the vortex shedding; because, as it was mentioned earlier, controlling the vortex shedding has several designation and engineering advantages.

#### 1.1.2.1. What is the flow control?

Flow control is one of the main branches of fluid dynamic which is growing rapidly. Flow control means creating a small change in the configuration of the problem. This results in very useful advantages in the engineering application include drag reduction, lift increase, increasing the mixing quality or reducing the noise. This change can be created using active or passive devices. The active devices include turbulators or stable surface roughness elements that do not need energy consumption for their operation. The active control needs actuators which can moves time dependently and needs energy for moving. The examples of such devices include plasma actuators and valves. The actuation command can be predefined (open-loop control) and/or can be depend on the sensors which check the flow parameters (close-loop control).

In this thesis, the numerical method and solution of Navier-Stokes equations were used. A code was developed using Matlab software and The Gambit software and the commercial Ansys Fluent software were used to generate the mesh and solving the problem for validation, respectively. As mentioned earlier, in the present study the laminar flow regime is investigated. Therefore, given that the range of Reynolds number is from 200 to 300, the diameter of cylinder was selected to be 1. The velocity of free stream (m/s) is calculate using Eq. (1-2):

$$Re = \frac{\rho U D}{\mu} \Rightarrow U = \frac{Re\mu}{\rho D} \Rightarrow 0.292 < U < 0.438$$

To define the boundary conditions, the Velocity Inlet was used as inlet and for the remaining boundaries the Pressure Outlet condition was used.

The final target is to install two solid swinging planes on the cylinder and investigate the effect of interaction between vorticity produced by them and the separated vortices from the surface of the cylinder.

## 1.2. Research motivation

During the time, study and research on the Von-Karman vortices phenomena is composed of three main sections. In the initial steps, the aim of the researches was to find a way to prevent the destructive effect of this phenomena on the structures. Then, the researches focused on inventing control methods, either active or inactive, to control the vortex shedding. But, in recent years, the attention was focused on recognizing the physic of the flow. Because of presence of the instabilities, the behavior of flow in this type regime is complicated and after about a century since the Strouhal observed this phenomenon, there still very unknowns about this phenomenon. for example, in some researches the effect of different parameters of the separator planes have been investigated, but their mutual effect on each other is still open for discussion. Using the ideas such as energy harvesting from the blood flow for cardiovascular patients need the full understanding about this phenomenon. At a time in which the energy crisis has engulfed the whole world, the importance of optimizing the systems and finding ways to harvest the reversible energy is obvious, even if its effect is initially very small. Therefore, targeting the further understanding the physics and behavior of the fluid flow in this regime seems to be helpful, because given its applicable designs (which of course still are at the conceptual stage), further understanding and finding more optimal control methods can lead to greater dominance over the physic of the flow.

## 1.3. Research background

As mentioned earlier, Strouhal for the first time, in 1887, found this phenomenon by observing the rapture of telegraph wire, and in the following years after that, Von-Karman was succeeded to detect this phenomenon by studying this phenomenon more accurately.

For many years, this phenomenon has been at the center of scientists' attention. Different topics such as the ability to control the periodic forces applied on the objects as a result of this phenomenon have been among the most important topics. Another interesting topic for scientists has been understanding the fluid-solid interaction phenomenon, which Von-Karman vortices is the most important topic among them. In the field of fluid-solid interaction, the

attention has been focused on investigating how to control this phenomenon by applying the periodic changes on the solid surface as well as how the resonance phenomena occur. Interaction of the Von-Karman vortices with the acoustic waves is also a new topic which recently gained a specific attention.

To date, many methods, either active or inactive, have been studied and used to control the vortices shedding around a bluff body, where their aim has been reducing the drag and lift forces and/or regulating the aerodynamic vortices created behind these objects, especially Von-Karman vortices.

One example of the works done on studying and proposing the active control method for controlling the vortex is the work done by Gillies [27] in 1998. By pointing out that the stability of vortices is due to the fluid flow and also the peripheral fluctuations only play a role in creating instabilities, he investigated an active control method using one to several sensors. An example which he presented in his work about instability persistence due to flow was the Von-Karman vortices created behind a cylinder which occur for a Reynolds more than the critical Reynolds. By saying that controlling the vortex shedding need stabilizing most of the intrinsically unstable modes, he succeeds to control a simplified model of the vortex behind a cylinder with a control method using several sensors in Reynolds number more than the Reynolds number that a single-sensor system had not responded to.

In 1999, Gattulli and Ghanem [28] investigated and simulated the mutual effects of fluid vortices and inductive vibrations to structures using Morison's equation and proposed an active control method for controlling the created vortices. They investigated the oscillatory behavior of induction vortices and invented an active control method by targeting the flow inductive forces exerted on the structures and marine industries such as oil platforms and transfer pipelines and even lateral elements such as holding cables and by proposing a design which has the ability to bear the oscillations caused by these oscillatory instabilities. They described the fluid-solid interaction using Morison's equation and continued their work by embedding a tuned mass damper on the structure and by using an adaptive and active control method. Their works have two positive outcomes: first, they successfully control the vortex shedding and reduce the oscillatory induction force; second, they were succeeded in estimating the hydrodynamic coefficient and verification and calibrating the Morison's equation for modeling the induction forces of the flow.

In 2002, Homescu et al. [29] controlled the Von-Karman vortices behind a rotating cylinder. Their main target was controlling the Karman vortex shedding behind the rotating cylinder by controlling the rotational speed of the cylinder. They found a relation between regularization coefficient and Reynolds number in the range 60 to 140, using an empirical logarithmic relation. Based on their results, they found the optimal rotational speed of the cylinder for Reynolds number between 60 to 1000. By these researches, they significantly reduced the amplitude of the vortex-induce swinging drag force using the optimal rotational speed.

In 2005, Akilli et al. [30], have tried to control the behavior of fluid flow around the cylinder vertically located in the shallow water using a separator plane. In this research, the length of the separator plane was considered constant and equal to the diameter of the cylinder, but its location at the downstream was considered as a variable. Also, the width of the plane was another parameter investigated in this research. For this purpose, three planes with different width were used, so that for three planes, three ratios of the plane's width to cylinder's diameter

(T/D) were measured 0.016, 0.04 and 0.08, respectively. Another parameter investigated in this experiment was the cylinder-plane gap. The variation of this parameter was applied so that a 1000mm interval was traversed in each stage by 1.25mm steps. In their experiment, they used particle image velocimetry (PIV) method to detect the flow and to obtain the speed vector field. The obtained results showed that in the ratio T/D between 0 to 1.75, using the separator plane for controlling (in this case stopping) the Von-Karman vortex shedding was very effective. Among the numerical studies done in this field, the work of Turki [31] in 2008 can be mentioned. It is worth noting that he used the square geometry instead of a circular cylinder. He also used a separator plane at downstream and behind the geometry, but the difference was that he fixed the separator plane. Therefore, his control method is an inactive method. He selected the range 110 to 200 for Reynolds number and the blockage ratio of $\beta = h/H = 1.4$ to perform the numerical simulation. The governing equation were solved using the finite element method (FEM) and on a staggered grid. He investigated the plane's length and its effect on the Strouhal number and drag force, but his main achievement in this research was obtaining a linear relation between the critical length od the plane and the Reynolds number. he observed that if the length of separator plane calculated by this relation, the vortex shedding is completely stopped.

Sudhakar and Vengadesan [32], In 2012, have addressed a numerical study on this phenomenon. In their work, they investigated the flow behavior behind a 2D circular cylinder where a periodic separator plane was installed behind it and at the downstream of the flow. The moving plane hinged the cylinder from the junction and has forced vibrating. The Reynolds number of the flow was selected 100. It is worth noting that the main characteristic of this work is the complicated interference and behavior between vortices separated from the moving plane and the cylinder, therefore to prevent the undesirable complicated, most of the equations were solved in the Cartesian coordination. They observed that given the amplitude and frequency of the vibration of the separator plane three kinds of the vortex system can be seen: normal separation, chain of vortices, and vortices which are separated from the separator plane. They found that if the plane vibrates, the reverse relation between the vortex formation length and Strouhal number is not applicable anymore.

In 2013, Hu Ye and Wang [33], carried out an experimental study on the effect of installing a flexible plane at the end of vibrating cylinder on the vortex generation using the PIV method. These two scientists investigated the effect of separator plane length parameter on the flow behavior and how the vortices created. In the previous studies, the length of separator plane was considered as an effective parameter on the flow behavior. Therefore, since they used a flexible plane and the length parameter was their main target, their obtained results provided a great help in completing the aerodynamic science in the field of laminar flow instabilities. As expected, they observed that the more the plane's length become flexible, their deformation will be larger. They found a relation between the power of the rotational vortices and the escape edge velocity of the separator plane in order to study the effect of flexible plane's length on the creation and developing pattern of the vortices. Also, by changing the flexibility of the plane, they measured the power of the created vortices and investigated their creation pattern.

An experimental study on the separator planes done by Kunze and Brucker [34] in 2012 is another experimental research. They investigated the flow behavior and the motion of hairy flaps installed behind the cylinder. It is worth nothing that the Reynolds number was in the range 5,000 to 31,000 which represents a turbulent flow regime. Dynamic of the fluid flow and

the motions of flaps was recorded, observed and analyzed using the PIV method. They observed that the existence of flaps completely changes the nature of vortex formation, means that unlike the flap-free case where the vortices are formed in a zigzag shape (such as Von-Karman vortices), they formed in a line along the cylinder axis, which causes a reduction in force vibration resulted from the severe variations of the pressure field. They also investigated the relation between Reynolds and Strouhal number in different flaps states and published their results.

Igbalajobi et al. [35], in 2013, repeated the experiment of separator planes behind the cylinder. The main difference was that the length of cylinder was not considered infinite and indeed unlike the previous experiments wherein the cylinder's length was considered equal to the width of test section of wind tunnel so that the its 3D effects can be neglected, they selected different aspect ratios for cylinder to investigate this parameter. The Reynolds number was set to74,000 and the plane's length was changes respect to the cylinder's diameter in 7 steps. They observed that by taking in to account the 3D effect in this phenomenon, the reduction in drag forces which was quite evident in 2D case, in 3D case it almost does not exist. They observed a considerable reduction in drag force only for a cylinder with aspect ratio 9 and the ratio of plane's length to cylinder's diameter (L/D) equal to 1 to 3. In other cases, the value of drag force was almost remained unchanged. For preventing the vortex shedding for the cylinder, their results showed that there is not an important difference between the2D case (long infinite cylinder) and 3D case; in other word, for a cylinder with any aspect ratio, the length of plane can be selected so that the formation and shedding of vortices prevented. For example, for a cylinder with aspect ratio 9, if the length selected so that $L/D \geq 9$, the formation and shedding of vortices is prevented which is exactly equal to a 2D case or an infinite cylinder.

Qiu et al. [36], in 2014, by referring that several researches and experiments have been done so far to reduce the drag and to eliminate the force vibrations around a cylinder due to the periodic instabilities using the separator planes, they performed an experimental test in large size wind tunnel and investigated the effect of installing separator plane at upstream of the flow in front of the cylinder. Installing two separator planes, one behind and the other one in front of the plane, and also a half-cylinder that is cut longitudinally in the middle were the other cases they experimentally tested. They found that the separator plane installed at upstream is able to bring the flow to critical state in low Reynolds number. Their results validated the length of separator plane needed to overcome the vortex generation obtained from the previous researches. The innovation of their work was investigating the width and behavior of boundary layer as well as finding their relation with Reynolds number.

## 1.4. Targets and innovation of the research

As mentioned earlier, the control method proposed and used till now can be divided in to two categories: active and inactive. In active method, the flow behavior is controlled by consuming and injecting the energy to the flow. For example, an active control system can act on the Von-Karman vortices so that the velocity of flow measured by a sensor installed at the upstream, therefore the Reynolds number of flow is calculated respect to the cylinder's diameter and fluid specifications. The result of this calculation is sent as a signal to a stimulator (for example a separator plane) which is installed at downstream of the flow and the based on this signal the swinging motion speed of the plane is set to prevent the vortices generation. In an inactive method, the flow behavior controlled by changing the geometry or using the porous or smart

(in novel applications) surfaces without consuming energy. An important example of this method is long chimneys which the Karman vortices' effect is neutralized by embedding a spiral band around it.

Therefore, given the importance of more understanding of the kind of instabilities and the flow behavior, continuing the work of researchers seems reasonable. Using the separator planes for controlling the behavior of vortices is a method which still has many unknown parameters.

Controlling Von-Karman vortex shedding using a separator plane, either actively (along with energy consumption and forced motion of plane) or inactively (using a fixed plane behind the cylinder), have been works wherein the good results obtained; but as mentioned earlier, more understanding the behavior of this phenomenon is among the main targets of this project. For this purpose, two separator planes were installed behind the cylinder and were forced to oscillate which in turn is a novel work. Installing two planes brings the geometry shape close to a geometry coincides on the streamline and the obtained results can be used as a guidance to investigate the airfoil in laminar flow and in the presence of instabilities of Von-Karman vortices. On the one hand, because the problem gets more complicated, the number of effective parameters on the flow behavior increases and therefore, investigating their effect provides more understanding about physic and behavior of the flow. on the other hand, since two separator planes will be used, their locations on the cylinder and the rotational speed are the other important parameters which will be investigated in this research. Of course, it should be pay attention that this problem is inherently complicated so increasing the number of the variables is out of the scope of a MSc's thesis; therefore, it is necessary that the number of parameters under study remains limited.

## 1.5. Detailed project definition

In this section, the detailed project definition will be addressed and the physics and the conditions of the problem under study are defined in details. Also, the initial conditions, properties of fluid and the type of boundary conditions will be described.

In the present study, the fluid-solid interaction caused by two solid movable planes installed on a circular cylinder in a laminar flow in 2 dimensional is simulated. The aim of study is to investigate the effect of these arrangement on the behavior of the Von-Karman vortices. Three Reynolds numbers 200, 250 and 300 were selected to study the effect of this dimensionless parameter on the responses. The diameter of cylinder 1cm selected and the fluid is air and the condition considered as standard. Therefore, the flow velocity for three Reynolds numbers in terms of cylinder's diameter are calculated using Eq. (1-2):

$D = 1\ cm = 0.01m$

$\mu = 1.7894 \times 10^{-5}\ kg/m - s$

$\rho = 1.225\ kg/m^3$

$$Re = \frac{\rho U D}{\mu}$$

- $Re = 200 = \frac{(1/225 \times U \times 0\backslash 01)}{1/7894 \times 10^{-5}} \Rightarrow U = 0.292\ m/s$
- $Re = 250 = \frac{(1/225 \times U \times 0\backslash 01)}{1/7894 \times 10^{-5}} \Rightarrow U = 0.365\ m/s$
- $Re = 300 = \frac{(1/225 \times U \times 0\backslash 01)}{1/7894 \times 10^{-5}} \Rightarrow U = 0.438\ m/s$

The velocity used as inlet boundary. The upper and lower boundaries are satisfied with the pressure condition and the gauge pressure is used for the outlet boundary.

Same as the previous researches, the length of planes was selected equal to cylinder diameters (i.e. 1cm). Therefore, the ratio of plane's length to cylinder's diameter L/D=1 was used.

The solution will be unsteady and the time step of the solution will be discussed in the next chapter. Because of motion of the planes in the field, the dynamic mesh method is used. The equations of the flow are elliptical, the solution is pressure-based and the SIMPLE method is used to discretize the equations. The equations of momentum and pressure are of second order.

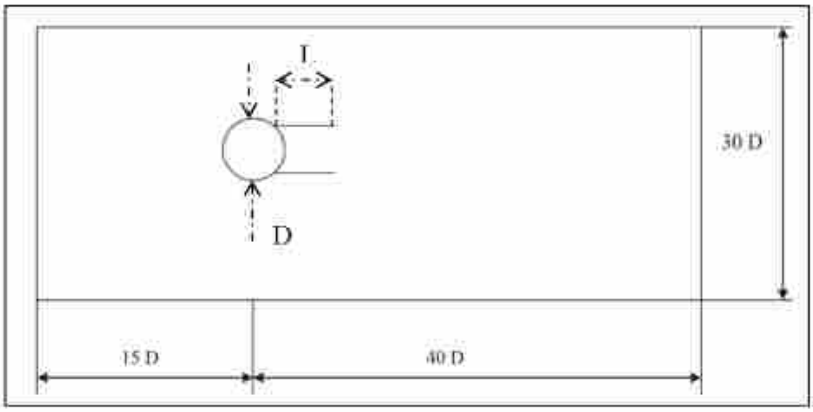


**Fig. (1.3):** Physics of the problem and the calculation domain.

## 1.6. Summary and overview of the following seasons

Understanding and controlling the unsteady vortices on the bluff bodies have been long time the topic of the researches. After over a half century since this phenomenon has been discovered, there are also unknowns and challenges remained in several design and engineering problems. The complexity of the physic and the behavior of the fluid flow in the event of these instabilities is a motivation for the further investigations. By advancement in technology and empowering computers and also progress in the field of computational fluid dynamic, numerical simulation is used with high reliability, speed and accuracy.

In chapter 2, the governing equations of the problem are investigated. Then, in chapter 3, the numerical method and validation of the solution are studied. Chapter 4 presented the results and finally the summary and conclusions are reported in chapter 5.

# Chapter 2

# Governing equations and boundary conditions

In this chapter, the governing equations and boundary conditions will be defined. In physic science, the fluid dynamic is branch of fluid mechanic which describes the fluid flow. In other word, it is a inherit science of fluids (liquids and gases) in motion. Fluid dynamic itself has several subcategories such as aerodynamic (the science of studying motion of air and other gases) and hydrodynamic (the science of studying the motion of liquid fluids). Fluid dynamic has wide applications such as calculating the forces and momentums applied on the aircrafts, calculating the oil mass transfer rate inside the pipes, predicting the weather condition and the behavior of the nebula between the interstellar. Even some of the concepts of this science can be used in traffic engineering, where in this field the traffic is assumed as the continues fluid flow.

Fluid dynamic presents a systematic structure which is the foundation of the scientific applications mentioned earlier and is resulted from the empirical and semi-empirical rules obtained by measuring the behavior of the fluid. The response of a fluid dynamic problem is the calculation of different properties of the fluid such as flow, pressure, density and temperature as the functions of time and space [37].

## 2.1. Fluid dynamic equations

Principles and the main basis of the fluid dynamic are conservation laws, or more exactly the conservation of mass, conservation of linear momentum (or the second newton's law) and the conservation of energy (or the first law od thermodynamic). In fluid dynamic these rules are defined by Reynolds transport theorem.

Despite of the laws mentioned, the continuum assumption governed the fluids. Fluids are composed of molecules which collide with each other or the other objects. However, based on the mentioned assumption, fluid considered continuum rather discrete. Therefore, properties such as density, pressure, temperature and flow velocity are attributed to the infinitesimal points and assume that the properties of change from one point to another continuously. Therefore, the fact that fluid is composed of the discrete molecules is ignored [38].

For fluids which are dense enough so that they assumed as continuum, do not have ionic properties and their flow velocity is lower than the speed of light, the momentum equations for the Newtonian fluids are the Navier-Stokes equations. These equations are a set of nonlinear differential equations that describe the fluid flow wherein the stress is linearly depends on the pressure and velocity gradients. These equations, in their non-simplified form, have not general closed-form solution, therefore to solve these equations the numerical dynamic fluid is used. These equations can be simplified in different ways which all make the equations to be solved more easily. In special problems of fluid dynamic, the exact solution can be obtained by proper simplification.

It should be noted that in addition to the equations of mass conservation, momentum and energy, one thermodynamic equation of state is needed to express the pressure as a function of the other thermodynamic variables so that the problem completely defined. The perfect gas equation of state is an example:

$$p = \frac{\rho R_u T}{M} \tag{2.1}$$

Where p, ρ, Ru, M and T are pressure, fluid density, gas universal constant, molar mass and temperature, respectively.

### 2.1.1. Conservation laws

Three conservation laws are used for solving fluid dynamic problems and can be written in both integral and differential forms. The mathematical formulation of the laws is derived using the control volume concept. Control volume is a definite hypothetical volume in space where the fluid can enter in and exit out. The integral form of the conservation, mass variation, momentum and/or energy laws can be assumed inside a control volume. In differential form of the conservation laws, the Stokes theorem is used. The result is some forms of this rules which attributed to the infinitesimal points inside the control volume where the set of these points, is the same integral form of the equations.

#### 2.1.1.1. Mass continuity (mass conservation)

Based on this law, the rate of change of fluid mass inside the control volume should be equal to the net mass flux of the fluid flow entering the control volume. The physical concept of this balance is that the mass inside the control volume neither destroyed nor created. The integral form of this law is as follows:

$$\frac{\partial}{\partial t}\iiint_V \rho dV = -\oiint_S \rho u.dS \qquad (2.2)$$

where ρ is the flow density, u is the flow velocity and t is time. The left-hand side of the equation include a triple integral on the control volume and the left-hand side is a surface integral on the surface of the control volume. The differential form of the mass conservation equation is obtained from divergence theorem as follows:

$$\frac{\partial \rho}{\partial t} + \nabla.(\rho u) = 0 \qquad (2.3)$$

#### 2.1.1.2. Momentum conservation

The equation of momentum conservation, applies the second Newton's equation on the control volume. Based on this equation, the change in the momentum of fluid inside the control volume is due to the net rate of fluid flow enters the control volume and the effect of the forces outside the control volume on the fluid inside the control volume. In the integral form of this equation, Eq. (2.4), $f_{body}$ denotes the volume force applied on the control volume per mass unit. The surface forces such as viscous forces are also denote by $F_{surf}$.

$$\frac{\partial}{\partial t}\iiint_V \rho u dV = -\oiint_S (\rho u.dS)u - \oiint_S p dS + \iiint_V \rho f_{body} dV + F_{surf} \qquad (2.4)$$

Deferential form of equation of momentum conservation is shown in Eq. (2.5). in this equation the body forces and surface forces are both denotes by F parameter. For example, F can be converted to two expressions of friction (surface) force and gravitational (body) force inside a tube.

$$\frac{Du}{Dt} = F - \frac{\nabla p}{\rho} \tag{2.5}$$

In aerodynamic, air is assumed as a Newtonian fluid in which the relation between shear stress (results from the frictional forces within the fluid) and the stain rate of the fluid elements is linear. Eq. (2.5) is a vector equation and in a 3D flow it can be expressed as 3 scalar equations. The equation of momentum conservation for an incompressible and viscos fluid called Navier-Stokes equations.

#### 2.1.1.3. Energy conservation

Although the energy can convert from one form to another one, but the net energy value within a closed system remains constant. The Eq. (2.6) is the mathematical expression of this concept:

$$\rho \frac{Dh}{Dt} = \frac{Dp}{Dt} + \nabla.(k\nabla T) + \Phi \tag{2.6}$$

where h, k, T and ϕ denote the enthalpy, thermal conductivity of fluid, temperature and viscous dissipation function, respectively. Viscous dissipation function defined the rate of conversion of mechanical energy of flow to heat. Based on the second law of thermodynamic, the sign of viscous dissipation function is always positive, which means that the viscosity cannot be produced inside the control volume.

## 2.2. Simplification and correction of equations for the problem

In the following problem, because of the low Reynolds number and as a result the negligible temperature variation and the lack of heat transfer, solving the energy equation was ignored. Therefore, the equation of momentum conservation should be corrected for an unsteady, incompressible and laminar flow. Since flow is unsteady, the expressions having derivation in terms of time remain and since the flow is 2D, the expressions in z-direction are eliminated. By assuming the constant density (incompressibility condition), the equation of momentum conservation simplified as follows:

$$\frac{\partial u}{\partial t} + (u.\nabla)u - \nu\nabla^2 u = -\nabla w + g \tag{2.7}$$

Where w is the specific thermodynamic work.

The tensor form of Eq. (2.7) is shown in Eq. (2.8).

$$\left(\frac{\partial}{\partial t} + u_j \frac{\partial}{\partial x_j} - \nu \frac{\partial^2}{\partial x_j \partial x_j}\right) u_i = -\frac{\partial w}{\partial x_i} + g_i \tag{2.8}$$

Where $\nu = \mu/\rho_0$ is kinematic viscosity.

## 2.3. Boundary conditions

As mentioned earlier, Velocity inlet is set as the inlet boundary. In this type of boundary condition, for a 2D flow the magnitude and vector direction of velocity are defined. In the present problem, in all arrangement cases the attack angle set to 0 and velocity defined in x direction. The outlet boundary and upper and lower boundaries of the domain are set by outlet Pressure condition in which the gauge pressure was set to zero so that introduce the free stream conditions. Also, the cylinder and wings were defined by Wall condition (no-slip boundary condition). Wings are exposed under a simple harmonic function defined in Eq. (2.9) and were oscillated in the form of a code and using user defined function (UDF) option in Fluent software.

$$y = A\,Sin(\omega t) \tag{2.9}$$

By differentiating the Eq. (2.9) respect to time, the Eq. (2.10) is obtained which indicates a linear speed of the wings.

$$y' = A\omega Cos(\omega t) \tag{2.10}$$

where A is the oscillation amplitude of the wings' tip in terms of radian and ω is the angular speed of wings in terms of radian per second and its relation with frequency (as a basis for the oscillation speed of the wings) defined as follows:

$$\omega = 2\pi f \tag{2.11}$$

The range of planes' motion is defined so that in a point having the maximum acceleration or a point having zero velocity (the upper bound for top plane and the lower bound for bottom plane) be the planes which are horizontal and parallel to the flow. Fig. (2.1) shows the boundary conditions on the solution domain.

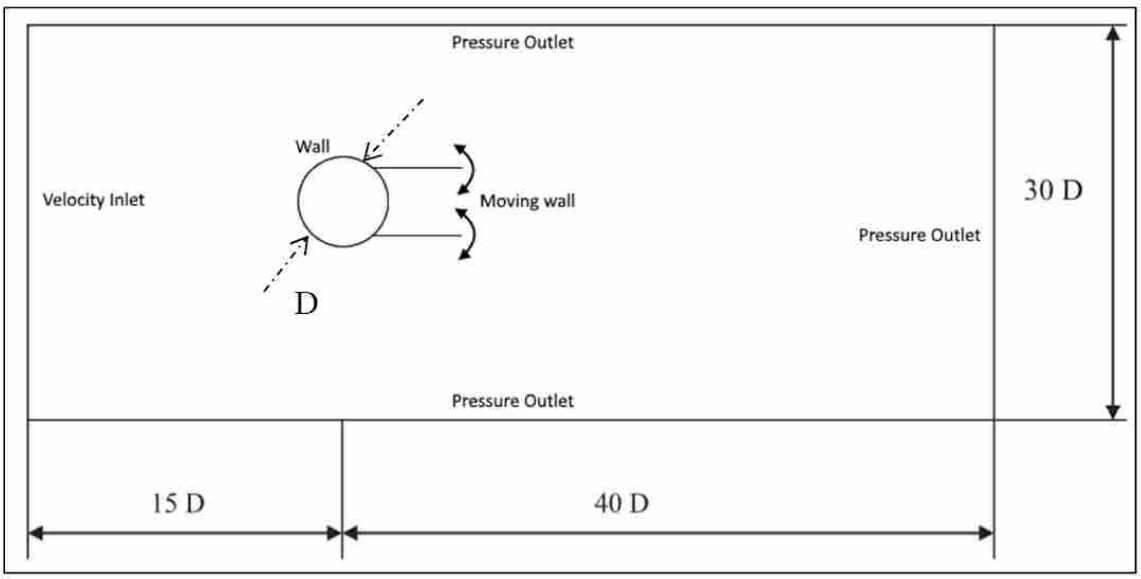


**Fig. (2.1):** Boundary conditions of the problem.

# Chapter 3

# Numerical method and validation

Computation fluid dynamic which generally called CFD is a branch of fluid dynamic which uses the numerical algorithms and analysis to solve and study the problem involving the fluid flow. In this method, the possibility of solving these equations numerically provided by converting the governing partial differential equations to algebraic equations. By dividing the solution domain to smaller elements and applying boundary conditions for boundary nodes and using some approximations a linear equation system obtains, that the temperature, pressure and velocity fields in desired area obtain by solving this algebraic equations' system. By using the results obtained from the solution of these equations, the resultant forces applied on the surfaces, both lift and drag coefficients and the other parameters can be calculated. The AnsysFluent commercial software was used to validate the problem, this software uses the finite volume method (FVM).

## 3.1. Finite volume method

FVM is a method which is used generally in CFD codes. The advantages of this method include the solution speed and lower RAM consumption. In FVM, the governing partial differential equations (Navier-Stokes, mass conservation and energy conservation equations) rewritten to a conservative form and then are discretized in the control volume. This discretization ensures the conservation of flux passing through control volume. Based on the finite volume equations, the governing equations are as follows

$$\frac{\partial}{\partial t}\iiint Q dV + \iint F dA = 0 \tag{3.1}$$

where Q is the vector of conserved variables, F is the vector of fluxes passing through an element of the control volume, V is the volume of the control volume element and A is the surface area of the control volume element.

## 3.2. Equations and settings

In this section, the solution method, order of equations, coupling method of equations and the other setting are described.

### 3.2.1. Pressure-based solution

Using a pressure-based solution is suitable for solving problems with low Ma number wherein the variations of density is negligible against the pressure changes.

Pressure-based solver used an algorithm belongs to a general class of the solution methods called projection method. In the projection method, the mass conservation of velocity field obtains by solving one pressure (or pressure correction) equation. This pressure equation obtained from the continuity and momentum equations so that the velocity field which corrected by pressure satisfies the continuity equation. Since the governing equations are nonlinear and are coupled, the solving process requires an iterative process; the governing equations are solved iteratively so that converged to the solution.

#### 3.2.1.1. Pressure-velocity coupling

As mentioned earlier, the pressure and velocity equations are solved separately. For solving the problems with laminar and incompressible regime, usually two SIMPLE and SIMPLEC coupling methods are used. for problems which are not relatively complicated (laminar flow

regime without presence of another model) and the convergence is only limited to the pressure velocity coupling method, selecting SIMPLEC method causes an increase in convergence rate and as a result reduces the solution time. But, given the variable nature of dynamic mesh due to the motion of wings, in this problem the SIMPLE method has been selected because increases the stability of solution compare with the SIMPLEC method.

### 3.2.2. Time

Due to the unsteady nature of the problem, the solution is done as time-dependent so that the vortex shedding solved and recorded step-by-step.

#### 3.2.2.1. Time step

The size of time step should be smaller than the smallest time scale of the problems so that all phenomenon exists in the problem recorded. The base for selecting time step, is set to correct record of frequency of vortex shedding and the force coefficients. By calculating the time scale of vortex shedding and the oscillation motion of the wings as the time criterions of the problem, the initial time step is defined.

By considering the vortex shedding as the criterion, and knowing the frequency of shedding (From previous works), time scale calculated as follows:

$$f \approx 7 \Rightarrow \tau_1 = \frac{1}{f} = \frac{1}{7} = 0.14\ s$$

Another important phenomenon in the problem is the oscillation of the wings. By calculating the speed of the wigs' tip using Eq. (2.10) at maximum frequency and knowing the oscillation altitude, the second time scale is also determined:

$$y' = A\omega Cos(\omega t) \Rightarrow V_{Max} = A\omega \approx (0.157 \times 0.01) \times 100 = 0.157\, m/s$$

$$\tau_2 = \frac{A}{V} = \frac{1.57 \times 10^{-3}}{0.157} = 1 \times 10^{-2}\ s$$

Given that $\tau_1$ is smaller than $\tau_2$, therefore $1\times10^{-2}$ is the maximum time step. The selection of final size of the time step will be described in the time resolution study section.

### 3.2.3. Space discretization

In the section of space discretization settings, the pressure and momentum equations will be of second order. The reason behind this selection, is the higher precision of the solution that the first order equations as well as the higher solution rate than the higher order equation along with preserving the phenomena of the problem.

## 3.3. Grid

Grid generation was done using Gambit software. Given that the dynamic mesh was used to solve the problem of wings' motion, the domain is divided in to two parts so that the remeshing calculations only performed in the dynamic part of the domain and the computational cost reduced as much as possible. In Fig. (3.1), the boundary of the desired area has been shown in red.

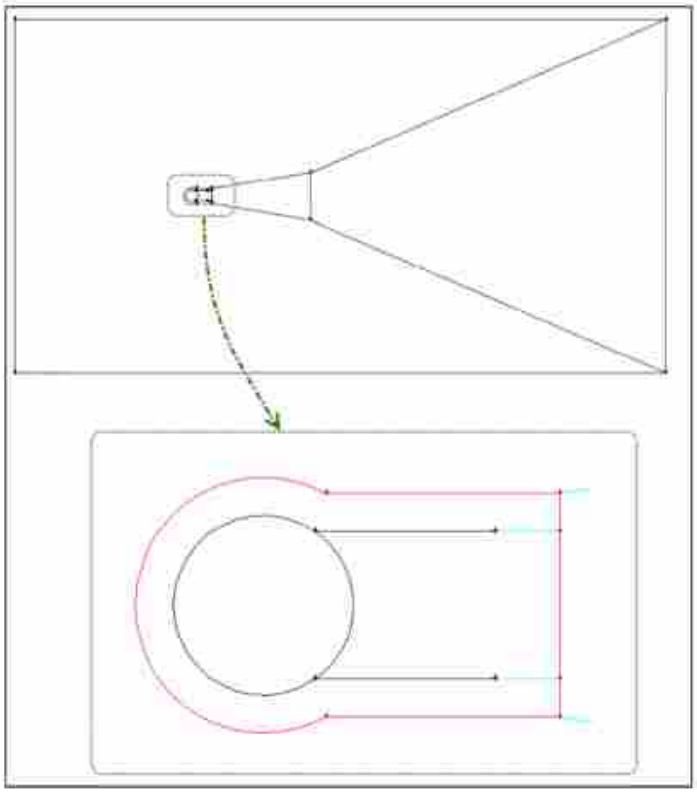

**Fig. (3.1).** Segmentation of the area of solution domain.

The application of dynamic mesh is only possible using the unstructured triangle grid. Since the boundary layer and the vorticity created within it are the most parts of the phenomenon of forming and shedding vortices and modeled using unstructured grid, the grids in areas around the problem geometry is also generated using the unstructured triangle grid. Fig. (3.2) shows the generated grid and the grid's information are provided in Table (3.1).

**Table (3.1).** Information of the generated grid.

| | |
|---|---|
| The number of grid cells within the dynamic domain | 20,956 |
| The number of grid cells outside the dynamic domain | 5,210 |
| Total number of grid cells | 26,166 |
| Maximum angular tilting of the cell | 0.78 |
| Percentages of total number of cells having angular tilting more than 75% | 0.13% (35 of 26,166) |
| Maximum size change | 7 |
| Percentages of the total number of cell with size change more than 3 | 0.18% (48 of 26,166) |

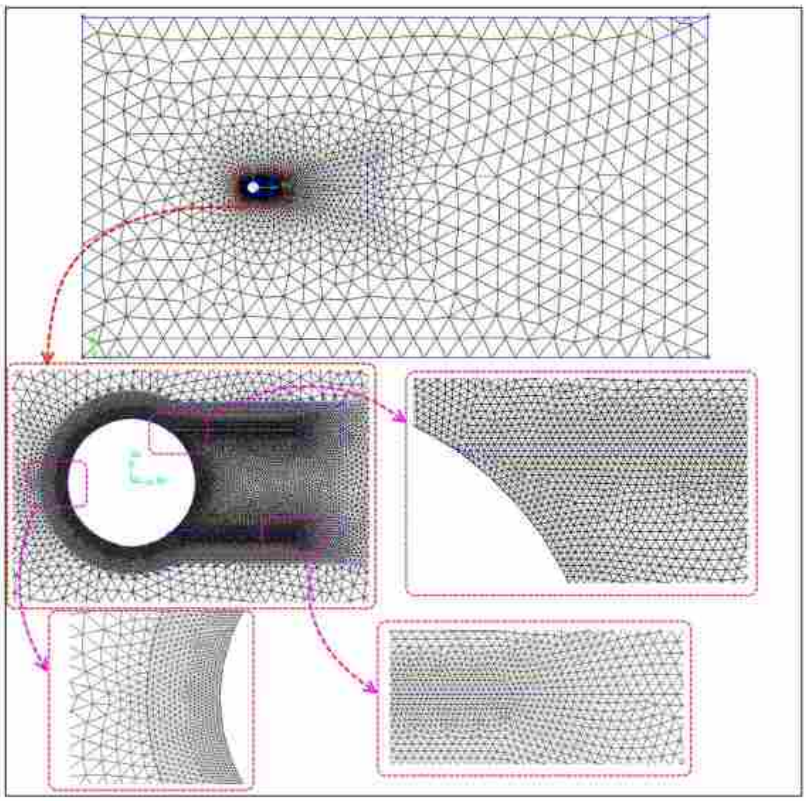

**Fig. (3.2):** Generated grid.

The number of grid points on the walls was selected so that their distance from each other obtained equal to $1.25\times10^{-4}$ which is a good number for recording and solving the boundary layer.

### 3.3.1. Dynamic grid

In the dynamic grid, with the change in the location of the solid boundaries in each time step, the grid around it is modified. In fact, with time step advancement, despite of the calculation of the flow equations, a calculation is also performed to modify the grid. One of the limitations of the size of time step is related to the method used in dynamic mesh; because as the size of the time step becomes larger than the limit, the equation of grid modification diverged and eventually cells with negative volume will appeared. There are three options in the dynamic mesh section which can be used alone or simultaneously. In following, these methods are described.

#### 3.3.1.1. Smoothing

In smoothing method, to modify the grids around the dynamic boundary and/or a deformable boundary, the nodes within the grid move but the number of nodes and their connections (cells' wall) do not change. In fact, it can be said that the interior nodes attract the motion of the boundary. Three subcategories of this method change the variations of the equations. These three subcategories are:

- Spring-based
- Diffusion
- Linearly elastic solid

#### 3.3.1.1.1. Spring-based method

In the first smoothing method (spring-based), the connecting lines of the grid nodes are considered as a grid of springs. The initial distance between the nodes before every movement of solid boundary considered as the balance state of the spring. Therefore, by movement of solid boundary, a virtual force is distributed in this hypothetical grid which lead to movement and length change in these lines. The forces applied on these grid's nodes obtained using the Hooke's law as follows:

$$\vec{F_i} = \sum_{j}^{n_i} k_{ij} \left( \Delta\vec{x_j} - \Delta\vec{x_i} \right) \tag{3.2}$$

where $\Delta\vec{x_i}$ and $\Delta\vec{x_j}$ are displacements of node i and its neighbor j, $n_i$ is the number of neighbor nodes connected to node I and $k_{ij}$ is the spring constant (or the spring stiffness coefficient) between nodes I and j. The spring constant is calculated by Eq. (3.3):

$$k_{ij} = \frac{k_{fac}}{\sqrt{\left|\vec{x_i} - \vec{x_j}\right|}} \tag{3.3}$$

where, $k_{fac}$ is the dimensionless spring constant which is defined for the code. In the balance state, the net force applied on a single node from all nodes connected to it must be equal to zero. This condition results in an iterative equation which is as follows:

$$\Delta\vec{x_i}^{m+1} = \frac{\sum_j^{n_i} k_{ij} \Delta\vec{x_j}^{m}}{\sum_j^{n_i} k_{ij}} \tag{3.4}$$

where m is the number of the iteration. After every time step, by updating the location of the nodes on the solid boundary, the mentioned equation solved iteratively so that the balance of the forces satisfied. The result is a updated grid based on the variations of the boundary.

However, since in this method the number of points and their connections do not changed, this method is not lonely responsible for movement of the solid boundary with high amplitude and is appropriate only for small variations (such as surface vibration).

#### 3.3.1.1.2. Diffusion method

In the diffusion-based smoothing method, the diffusion equation (5.3) governs the grid motion:

$$\nabla.(\gamma\nabla\vec{u}) = 0 \tag{3.5}$$

where, $\vec{u}$ is the displacement speed of the grid. The boundary conditions of the above equation calculate by the motion of the solid boundary. The above-mentioned Laplacian equation defines that how the motion of the solid boundary diffused in to internal space of the grid. The diffusion coefficient $\gamma$ shows how it control the effect of boundary motion on the internal space of the grid. For example, a constant diffusion coefficient means that the motion of solid boundary has been diffused normally within the grid.

#### 3.3.1.1.3. Linearly elastic solid method

In linearly elastic solid-based smoothing method, the connecting lines between the grid nodes are considered as solid structures and their deformations calculate based on the EQs. (3.6) - (3.8).

$$\nabla.\sigma(\vec{y}) = 0 \tag{3.6}$$

$$\sigma(\vec{y}) = \lambda\left(tr\varepsilon(\vec{y})\right)I + 2\mu\varepsilon(\vec{y}) \tag{3.7}$$

$$\varepsilon(\vec{y}) = \frac{1}{2}\left(\nabla\vec{y} + (\nabla\vec{y})^T\right) \tag{3.8}$$

where, σ is the stress tensor, ε is strain tensor and $\vec{y}$ is the displacement vector of the grid. To solve the above-mentioned equations the relation between shear module μ and parameter λ is needed. This relation is defined by user and by using the Poison ratio. Eq. (9.3) shows the relation equation between these two parameters.

$$v = \frac{1}{2\left(1 + \mu/\lambda\right)} \tag{3.9}$$

### 3.3.1.2. Layering

In layering method, which is suitable for prismatic 3D grids, the layers of the cell are defined in the vicinity of the moving boundary. The height of these layers is proportional to the first layer stick to the solid boundary. In this method, there is a possibility that an ideal height defined for each layer. By movement of the boundary, the height of the adjacent cells to the wall can increases based on the following condition:

$$h_{min} > (1 + a_s)h_{ideal} \tag{3.10}$$

where, $h_{min}$ is the minimum layer height, $h_{ideal}$ is the defined ideal height and as is the layer cutting factor. By exceeding the defined limit, the layer cuts in to two layers using the cutting factor.

### 3.3.1.3. Remeshing

As mentioned earlier, in areas with triangular or pyramidal (3D) grid, the spring-based smoothing method is used to modify the grid; but, when the displacement of the solid boundary is large compare with the size of the adjacent cells, the quality of the cells decreased dramatically to the extent in which there is a possibility that the cell destroyed. Eventually, this trend caused the grid be useless (for example due to creation of cells with negative volume) and the solution diverged.

In the local remeshing method, the software identified the cells which get out of the defined size and angular tilting limit and modifies the grid connections by changing the location of the nodes. If the new cells satisfy the tilting condition, the grid is updated locally (the responses of the flow solution of the cells in the previous time step transferred to the new cells).

In this method, the software checks the cells inside the defined area and signed the cells which have one or more of following conditions:

- The angular tilting of the cell is more than the defined limit.
- The cell is smaller than the minimum defined characteristic length.
- The cell is larger than the maximum defined characteristic length.
- The cell height is out of the defined characteristic length limit.

If the local remeshing method is not able to sufficiently reduce the maximum angular tilting of the desired cells, then the cell zone remeshing is used. in this method, all the cells in the dynamic area are checked and if necessary, they modified to ensure the quality of the cells in the whole area.

Three parameters, angular tilting, minimum and maximum characteristic length of dynamic grid have the most important effect on the grid quality and are defined by users.

Given the high motion range of the wings than the adjacent cells, in the present problem the spring-based smoothing method and zone and local remeshing methods are used to ensure a good quality for recording boundary layer and vorticity created on the solid surface.

In the following figures, it has been tried to show the effect of the changing and modifying the grid caused by the top wing. Time step was set to $1\times10^{-3}$sec, the maximum cell tilting set to 0.4 and the minimum and maximum characteristic length were set to $5\times10^{-5}$ and $1\times10^{-4}$m, respectively.

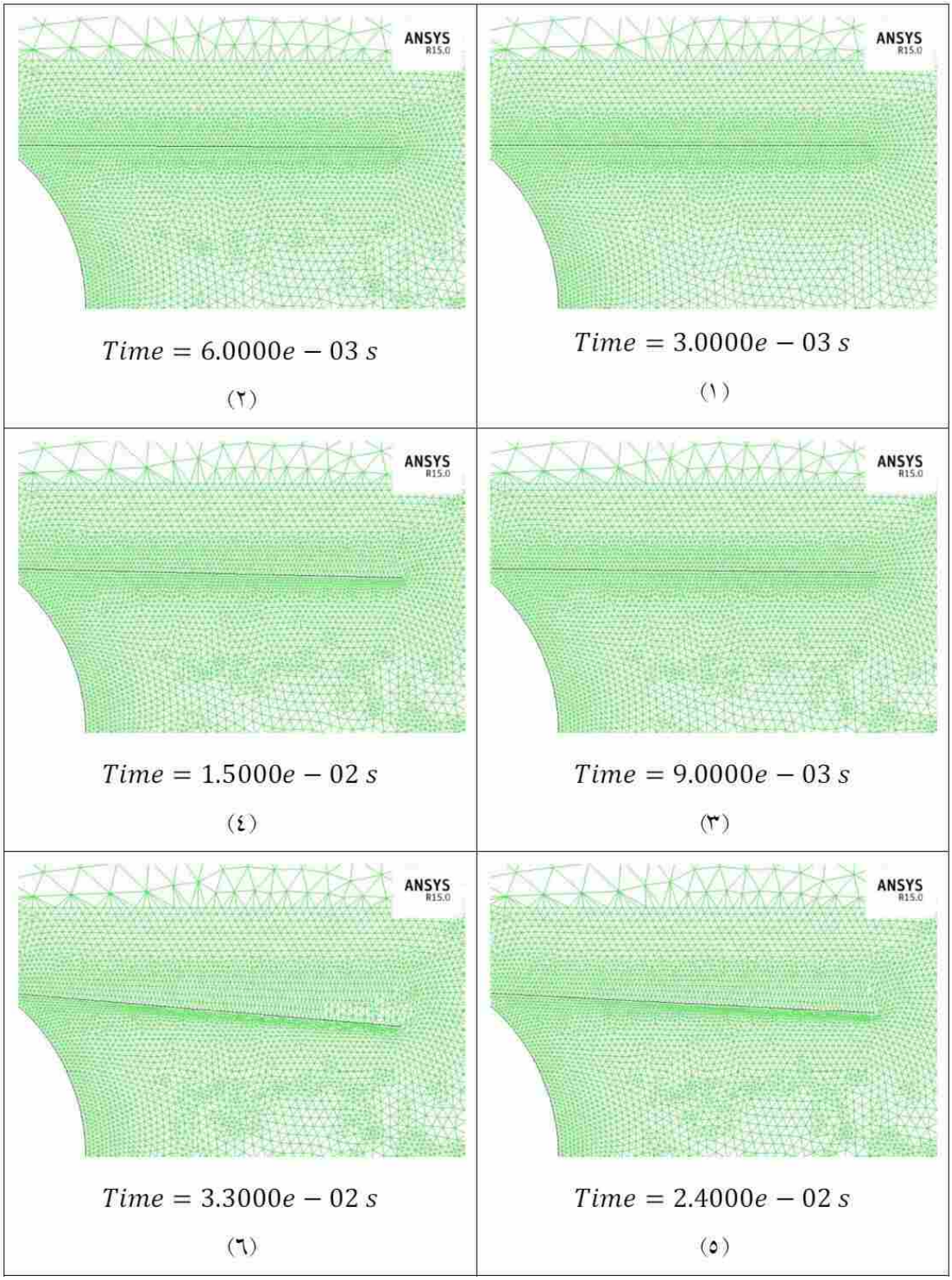


**Fig. (3.3):** Modifying the dynamic grid.

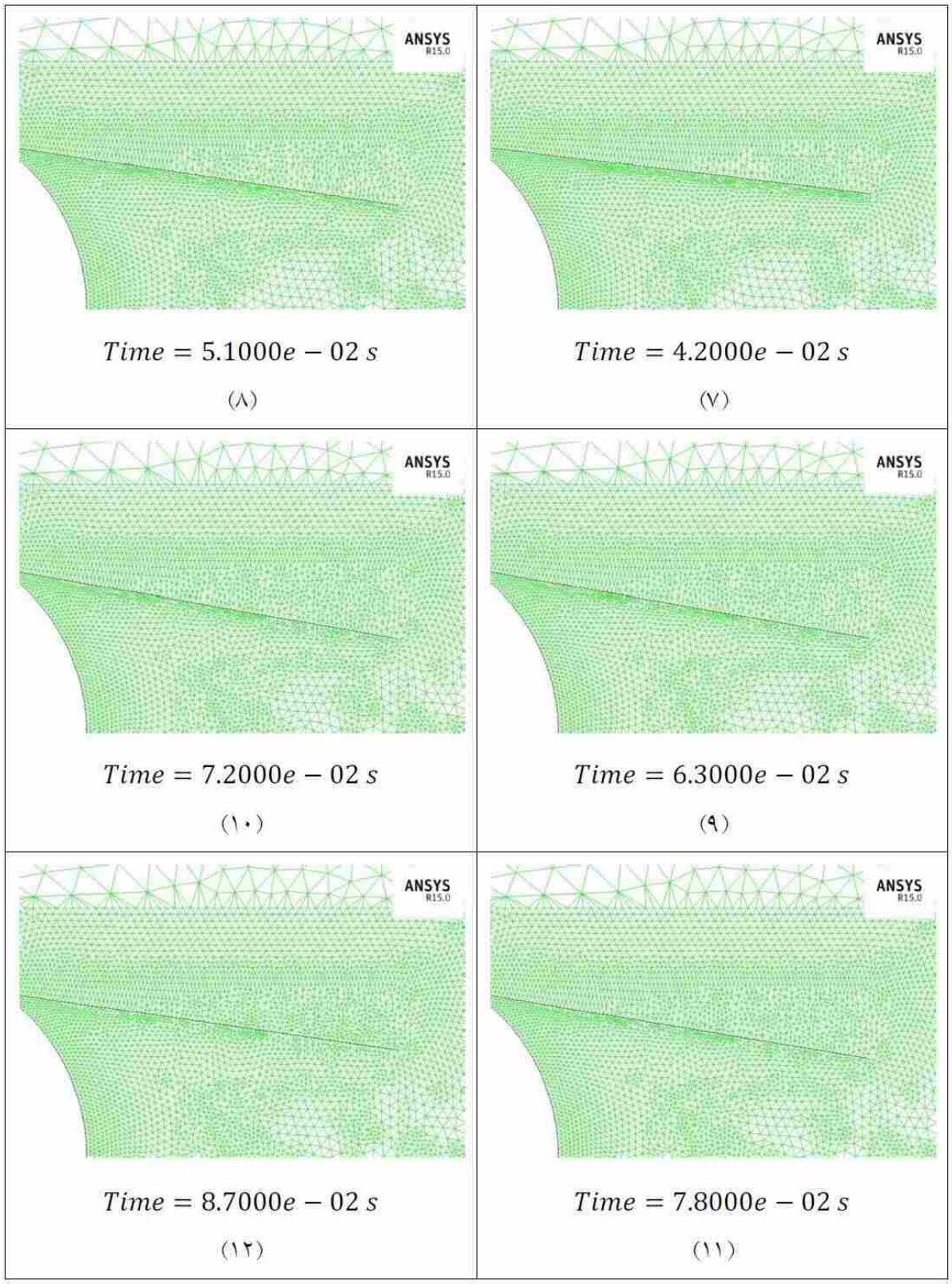


**Fig. (3.4):** Modifying the dynamic grid.

## 3.4. Validation

In this section, the experimental and numerical results of the papers are used for validation.

### 3.4.1. Comparison of solutions with analytical relations

During the last half-century, many efforts have been made with the aim of defining the coefficients of the relations between Reynolds and Strouhal numbers for vortex shedding in the laminar flow regime which have led to extracting different coefficients. These researches were mainly followed the work on Roshko [39]. He plotted the $(fD^2/\nu)$ against the Reynolds number and by linear estimation of data using mean square method found the A and B coefficients of the Eq. (3.11).

$$S_r = A + \frac{B}{Re} \tag{3.11}$$

Since then, the parameter $Ro = (fD^2/\nu) = S_r Re$ known as the dimensionless Roshko number.

Also, following the Triton [40] and Berger [41], a trinomial approximation has been used. The Eq. (3.12) shows this relation.

$$S_r = ARe + B + \frac{C}{Re} \tag{3.12}$$

Williamson and Brown [42] by proposing the Eq. (3.13) based on the square of the Reynolds number minimized the error. The precision of their relation even with two first sentence is more the previous relations.

$$S_r = \left( A + \frac{B}{\sqrt{Re}} + \frac{C}{Re} + \ldots \right) \tag{3.13}$$

They used the information of 2D numerical solution provided by Henderson (1997), determined the Eq. (3.11) and Eq. (3.13).

$$S_r = 0.2175 - \frac{5.106}{Re}$$

$$S_r = 0.2731 - \frac{1.1129}{\sqrt{Re}} + \frac{0.4821}{Re}$$

The defined relation is valid for Reynolds number between 50 to 1000. In following, the Strouhal number for vortex shedding on the 2D cylinder without wings for Reynolds number 200, 250 and 300 will be compared with the result obtained from the first binomial relation and the trinomial relation Williamson and Brown. For this purpose, the lift coefficient ($C_t$) is recorded for every time step. Then, the oscillation frequency of lift coefficient graph (which is the same frequency of vortex shedding) is extracted using the fast Fourier transform (FFT) command in MATLAB software. Then, the Strouhal number is calculated using the obtained frequency:

- $Re = 200\,, f = 5.694 \Rightarrow S_r = \frac{fD}{v} = \frac{5.694\times0.01}{0.292} = 0.195$
- $Re = 250\,, f = 7.409 \Rightarrow S_r = \frac{fD}{v} = \frac{7.264\times0.01}{0.365} = 0.203$
- $Re = 300\,, f = 9.102 \Rightarrow S_r = \frac{fD}{v} = \frac{9.102\times0.01}{0.438} = 0.208$

The comparison of the results obtained from Eqs. (3.11) and (3.13) are shown in Table (3.2).

| Percentages of difference with trinomial relation | Williamson trinomial relation | Percentages of difference with binomial relation | Roshko binomial relation | The obtained value | Reynolds number |
|---|---|---|---|---|---|
| 0.93 | 0.1968 | 1.554 | 0.1919 | 0.195 | 200 |
| 0.81 | 0.2046 | 2.918 | 0.197 | 0.203 | 250 |
| 1.18 | 0.2104 | 3.615 | 0.2005 | 0.208 | 300 |

According to Table (3.2), the percentages of calculation error comparing with the Williamson trinomial relation is about 1% which is an acceptable value.

### 3.4.2. Comparison of results with available simulations

In this section, some of the results of Sudhakar and Vengadesan [6] were simulated since in this paper the arrangement is close to the arrangement of the present study and the results are used for validating the numerical method. As mentioned in chapters 1 in the research background section, Sudhakar and Vengadesan [6] installed a wing on the trailing edge of the 2D cylinder with different frequencies and amplitudes, investigated their effect on the frequency of the vortex shedding (Strouhal number), drag force and formation and shedding pattern of the vortices (by investigating the vorticity field). According to the Fig. (3.5), three highlighted values are selected and simulated.

**Table 2**
Strouhal number for different amplitude and oscillation frequencies.

| $f_s$ | A | | | | |
|---|---|---|---|---|---|
| | 0.1 | 0.2 | 0.3 | 0.4 | 0.5 |
| 0.0825 | 0.14 (0.0825) | 0.0825 | 0.0825 | 0.0825 | 0.0825 |
| 0.1 | 0.1 | 0.1 | 0.1 | 0.1 | 0.1 |
| 0.165 | 0.165 | 0.165 | 0.165 | 0.165 | 0.165 |
| 0.2 | 0.133 (0.2) | 0.2 (0.128) | 0.2 | 0.2 | 0.2 |
| 0.3 | 0.14 | 0.14 | 0.3 (0.126) | 0.3 | 0.3 |
| 0.33 | 0.138 | 0.138 | 0.33 (0.138) | 0.33 | 0.33 |
| 0.4 | 0.138 | 0.138 | 0.148 (0.4) | 0.4 (0.148) | 0.4 (0.138) |
| 0.5 | 0.135 | 0.135 | 0.148 (0.5) | 0.247 (0.5) | 0.5 (0.125) |

**Fig. (3.5):** Selected arrangement from the reference paper for simulation and validation of the solving method.

It should be noted that the swinging of flat solid wing is under the simple harmonic function and the swinging amplitude considered as coefficients of diameter of cylinder and the swinging frequency was considered as dimensionless and defined as follows:

where, $f_s$ is the dimensionless frequency and $f$ is the wing's frequency. The comparison of the Strouhal number obtained with the results of the reference paper is shown in Table (3.3).

**Table (3.3).** Comparison of Strouhal number obtained in this paper with the numerical result of reference paper.

| | Obtained result | Reference result | Difference (%) |
|---|---|---|---|
| $f_s$=0.3, A=0.2 | Sr=0.14 | Sr=0.14 | 0 |
| $f_s$=0.4, A=0.3 | Sr=0. 4 | Sr=0.3988 | 0.3 |
| $f_s$=0.5, A=0.1 | Sr=0.135 | Sr=0.135 | 0 |

Of course, it should be noted that the error percentage is not absolutely zero. But, given the number of decimal places in the Strouhal number reported in the reference paper, the obtained results are rounded up so that the number of decimal places be equal to that of the reference paper. Therefore, there is rounding error in the results.

Also, the drag coefficient calculated by the presented drag force in the paper was compared. It should be noted that the drag force was oscillating and its average value is calculated in a range where the flow is semi-steady. Table (3.4) shows the values of the drag coefficient.

**Table (3.4).** Comparison of the drag coefficient value obtained in this paper with the numerical result of reference paper.

| | Obtained result | Reference result | Difference (%) |
|---|---|---|---|
| $f_s$=0.3, A=0.2 | $C_d$=1.1 | $C_d$ =1.153 | 4.6 |
| $f_s$=0.4, A=0.3 | $C_d$ =1.054 | $C_d$ =1.0944 | 3.7 |
| $f_s$=0.5, A=0.1 | $C_d$ =1.12 | $C_d$ =1.151 | 2.6 |

According to the results obtained and their comparison with reference paper (Tables (3.3) and (3.4)), the difference percentage of results is in an acceptable range.

### 3.4.3. Study the mesh independency

In order to study the independency of results to mesh, two kinds of grids are investigated. The first grid is especially fine at the downstream of the geometry and the location of vortex shedding (Vortex Street). Fig. (3.6) shows this grid. Second grid is coarser than the grid used in this project. This grid is shown in Fig. (3.7). Data related to these grids are shown in Table (3.5).

**Table (3.5).** Data related to the grids used to study the mesh independency.

| | Total number of cells | Number of cells in the dynamic region | Number of the cells outside of the dynamic region |
|---|---|---|---|
| Main grid | 26,166 | 20,956 | 5,210 |
| Fine grid | 87,640 | 45,631 | 42,009 |
| Coarse grid | 9,184 | 6,740 | 2,444 |

In following, the results obtained from these two grids used in this project and finally some images of these grids are presented. The Reynolds number in all scenarios is 250, the oscillation amplitude of the planes is 10 degree and the angular speed of the moving wings is

44.25rad/sec[1]. The comparison of the value of shedding frequency in the main, fine and coarse grids is compared with each other in Table (3.6).

**Table (3.6).** Comparison of vortex shedding frequency in different arrangements and different grids.

| | Shedding frequency in no-wings scenario | Shedding frequency in scenario with fixed wings | Shedding frequency in scenario with moving wings |
|---|---|---|---|
| Main grid | 7.264 | 7.187 | 7.924 |
| Fine grid | 7.268 | 7.237 | 7.005 |
| Coarse grid | 7.081 | 7.026 | 6.612 |

Given that the results of the fine, coarse and main grids are close enough, therefore in order to reduce the computational costs the grid with 26,166 cells is selected as the main grid and the solution is independent of the grid.

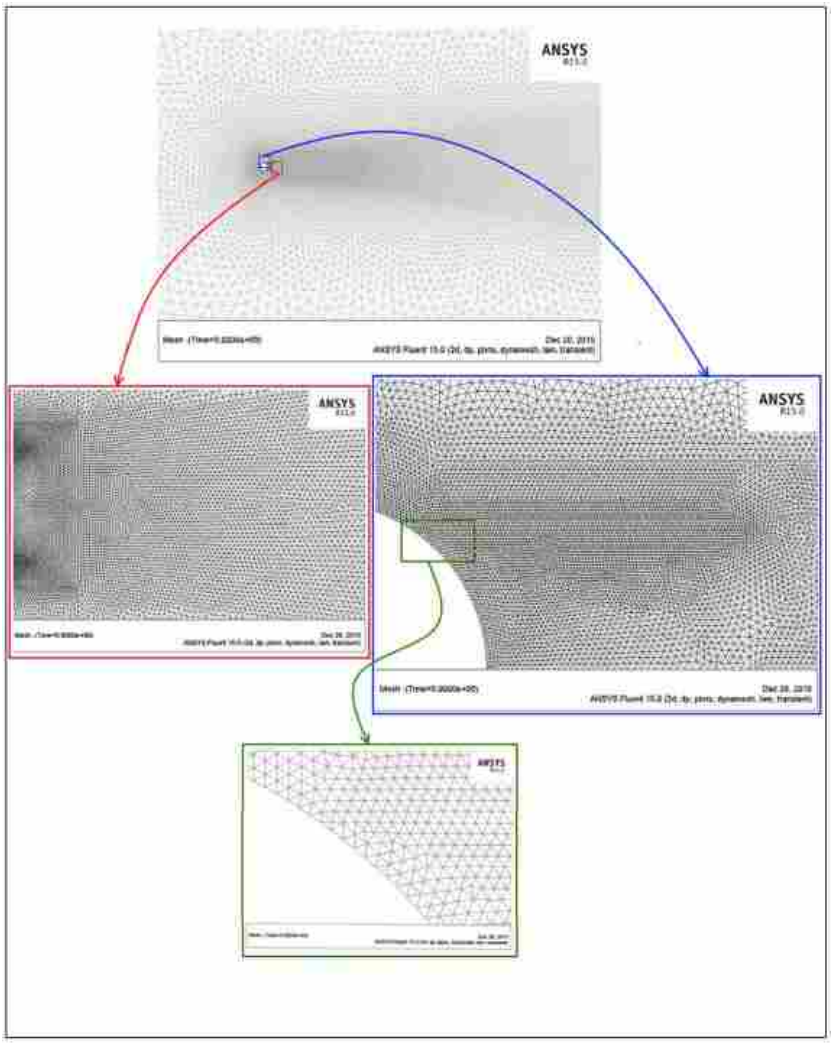


**Fig. (3.6):** the fine grid used to study the mesh independency.

[1] It will be proved that this value of natural shedding frequency in a case with wings obtained as a constant value.

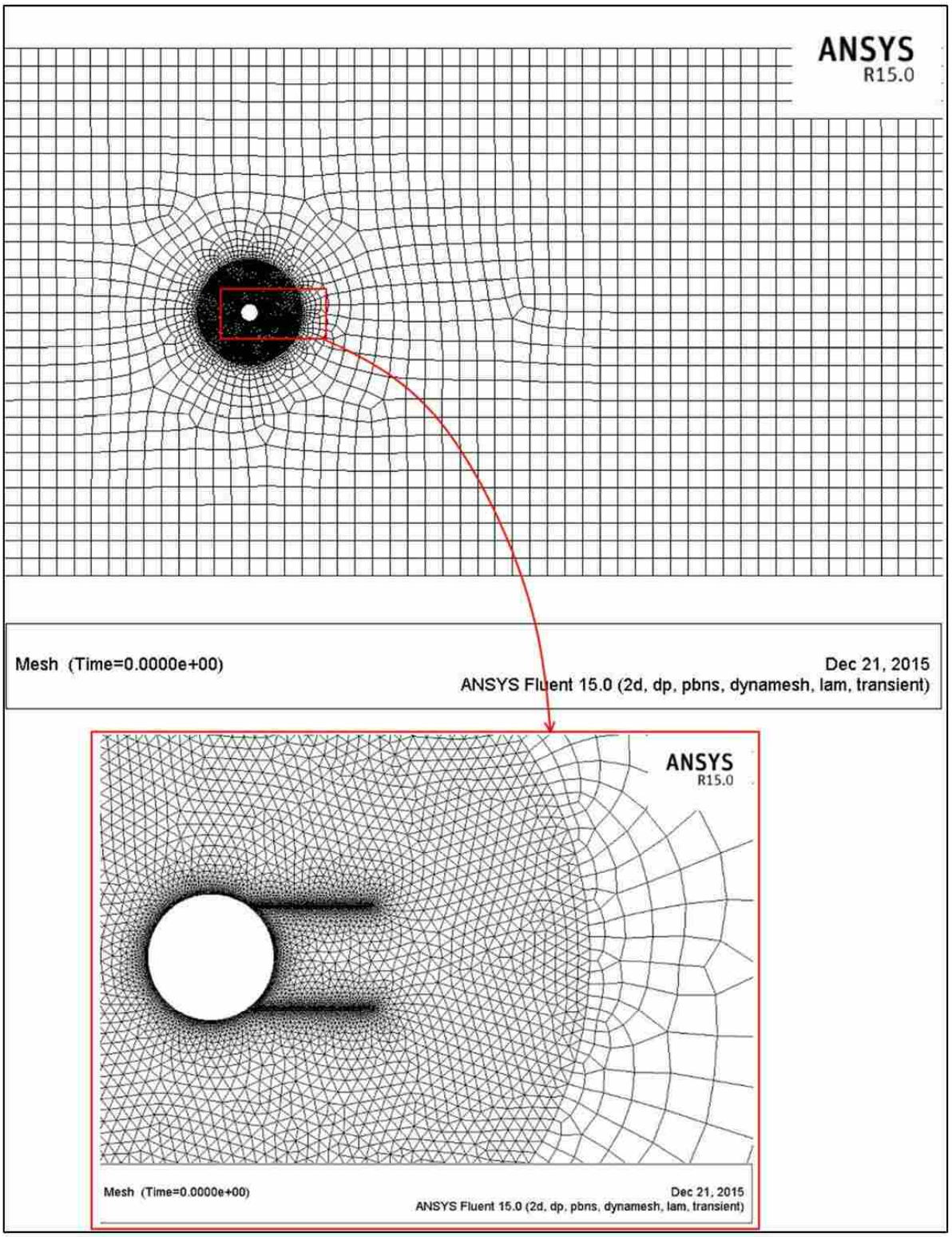


**Fig. (3.7):** The coarse grid used to study the mesh independency.

Given that the lift and drag coefficient are of integral value kind, they can not alone ensure the full similarity between the flow solved in different grids. In numerical solutions, in order to ensure the similarity between the solved flow in different grids and demonstrating the mesh independency, the comparison of local variables is used. for example, the pressure coefficient distribution on the body surface and/or the shape of the velocity vectors distribution can be used.

In the present study, in addition to investigate the dynamic behavior of lift coefficient and comparison of vortex shedding frequency, the comparison of the velocity vectors distribution shape in different locations is used. for this purpose, at a same time, the shape and the size of the velocity vectors in same locations are compared.

The locations used to investigate the velocity vector distribution is defined as follows. It should be noted that the length of all three lines is equal to the cylinder radius and their directions pass the center of cylinder. Also, these three lines are considered at angles 125, 90 and 50 degree, respectively.

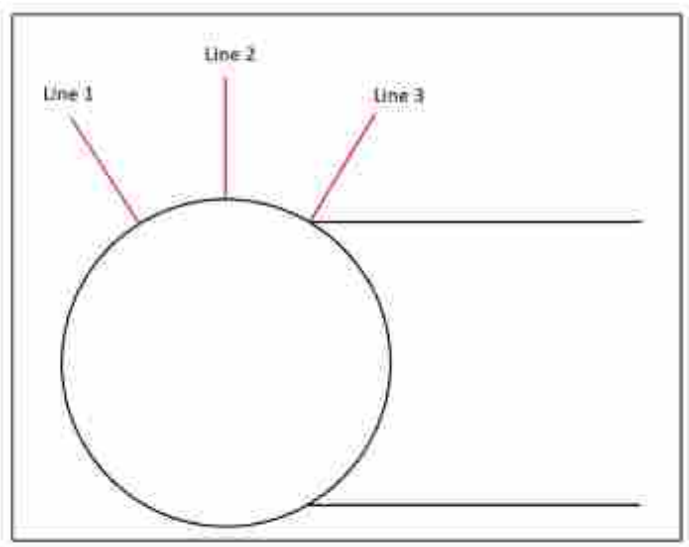


**Fig. (3.8):** Defining the location of measuring the velocity vector profile.

In order to present the overall view of the velocity vectors profile, the velocity vectors are shown on the pre-defined lines at time 8.64sec. This figure is related to the main grid.

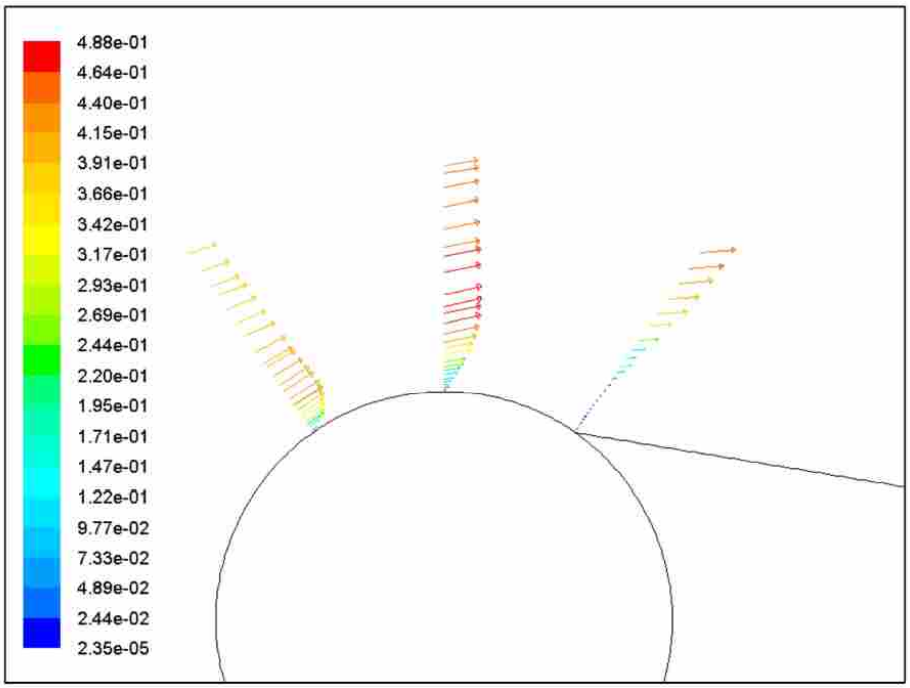


**Fig. (3.9):** Overall view of velocity vector distribution on the pre-defined reference lines.

To more detailed comparison, the values of the velocity vectors in different grids on the pre-defined reference lines against the vertical distance from the cylinder surface are shown in the following figure at time 8.46sec. Due to the great agreement between these plots, it can be concluded that the mesh independency and appropriateness of the grid are great to be used in the following calculations.

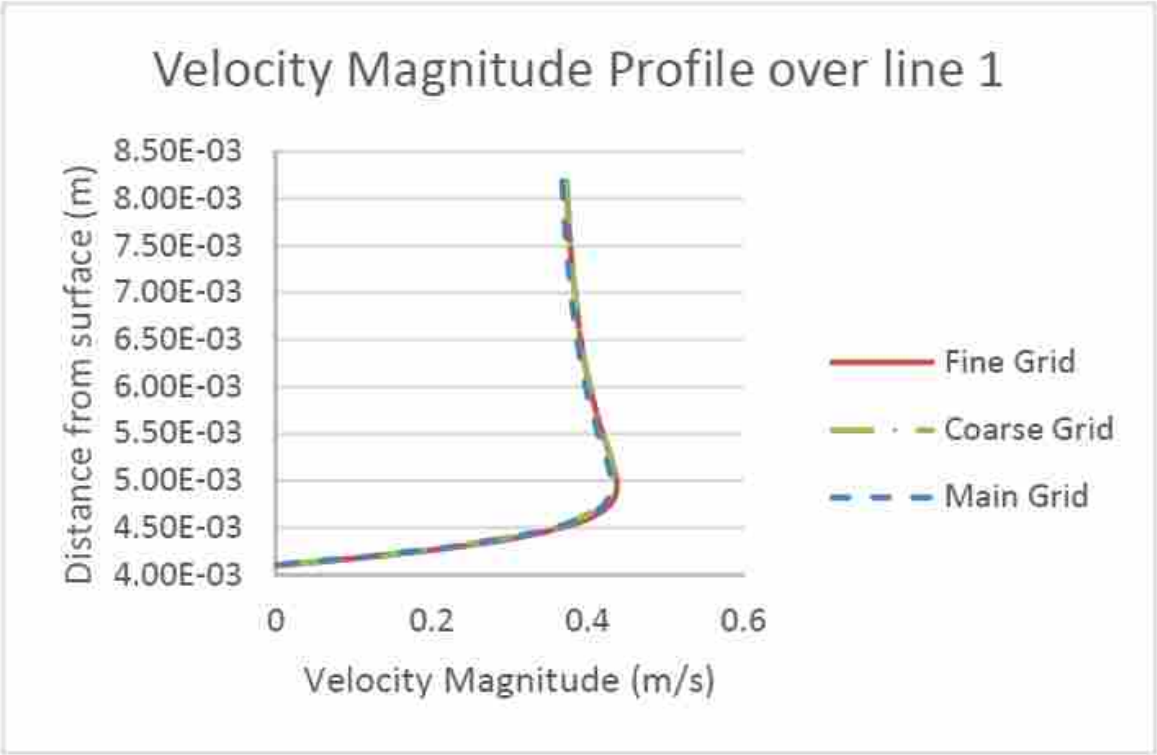


**Fig. (3.10):** Velocity size distribution on the first reference line.

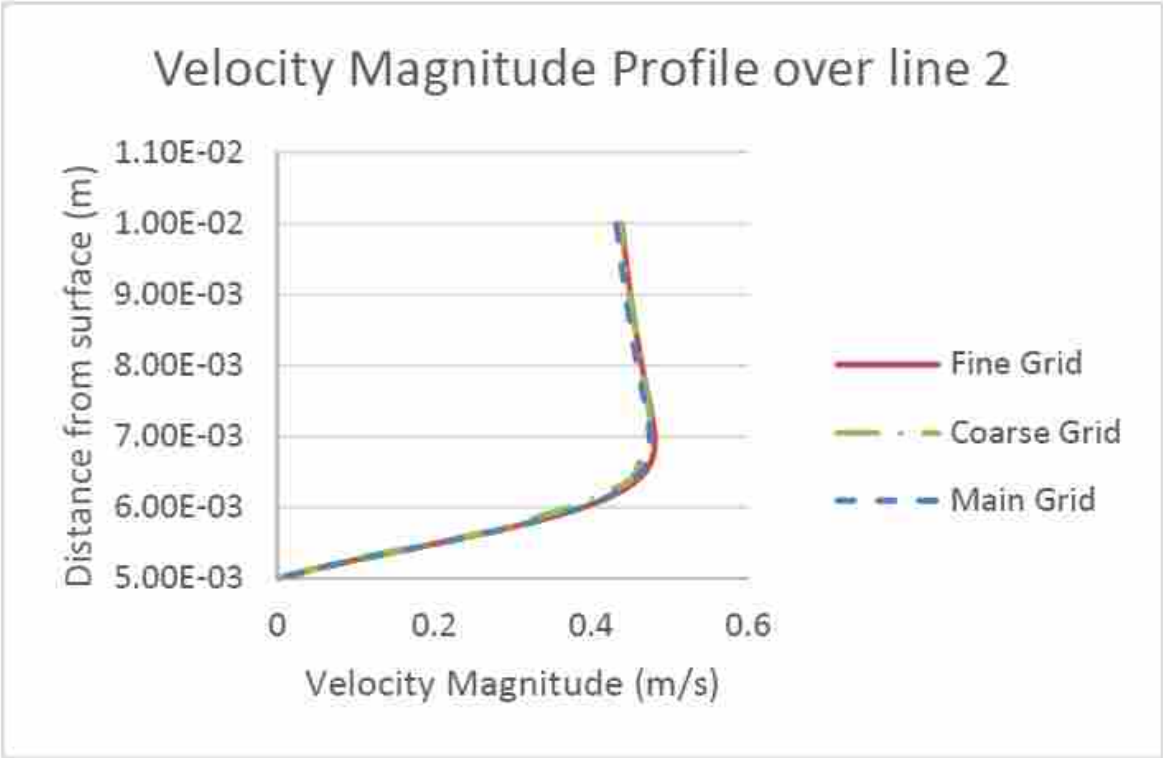


**Fig. (3.11):** Velocity size distribution on the second reference line.

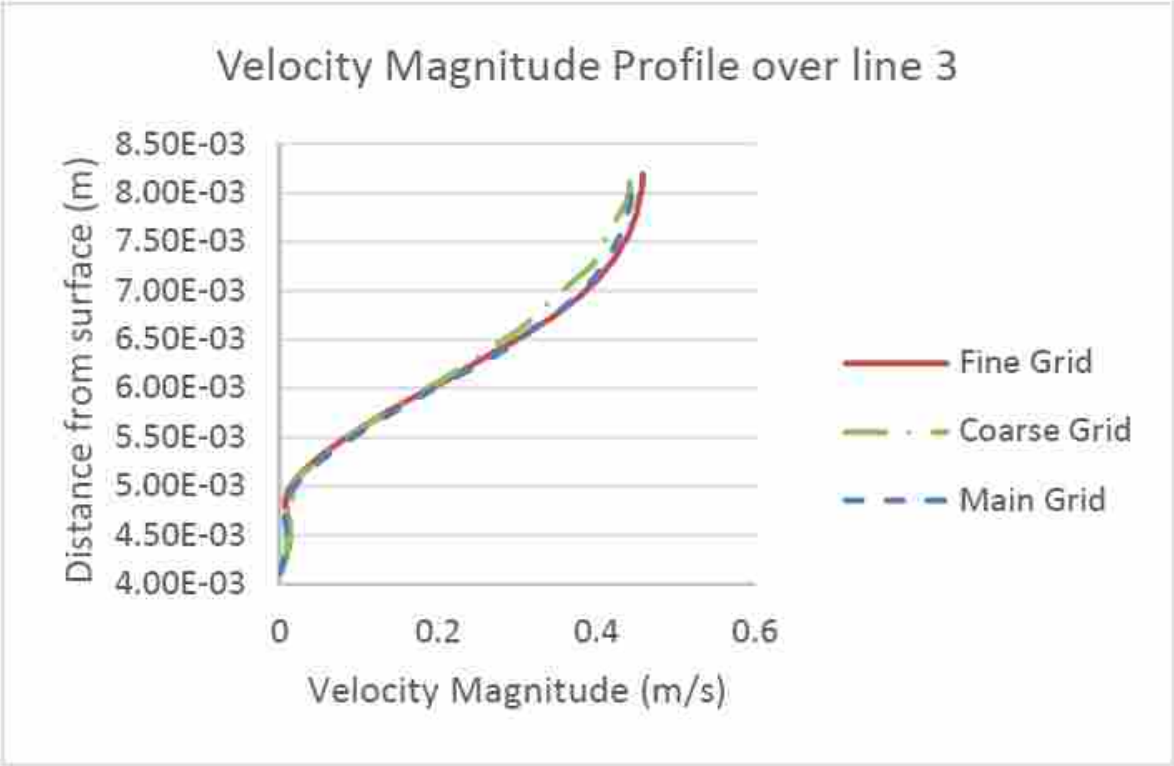


**Fig. (3.12):** Velocity size distribution on the third reference line.

### 3.4.4. Study the time step independency of solution

For more detailed recording of phenomena available in this research, the time step has been calculated an order smaller than the physical value of phenomena and assumed to be$1\times10^{-3}$ sec. In the validation section it was observed that the solution results were in good agreement with the results of the reference papers and the previous researches at this time step. It should be noted that this value ensures the quality of modifying the dynamic grid.

In order to study the time step independency of solution, in addition to selected time step, the solution is also done for the time step $1\times10^{-5}$ sec. Then, by investigating the drag force coefficient it was found that the fast Fourier transform obtained from this coefficient was same for both time steps and the extracted frequency was nearly same in both simulations with a small difference. Therefore, given that the solution with lower time step is more time consuming, and also given the acceptable equality of frequency of drag force coefficient in both cases, time step $1\times10^{-3}$ sec was selected as the base. Figs. (3.8) and (3.9) show the fast Fourier transform results obtained from the drag coefficient with time steps $1\times10^{-5}$ sec and $1\times10^{-3}$ sec, respectively. The Reynolds number is 250, angular speed of wings is 44.5 rad/sec (frequency ratio 1) and frequency amplitude is 10 degree.

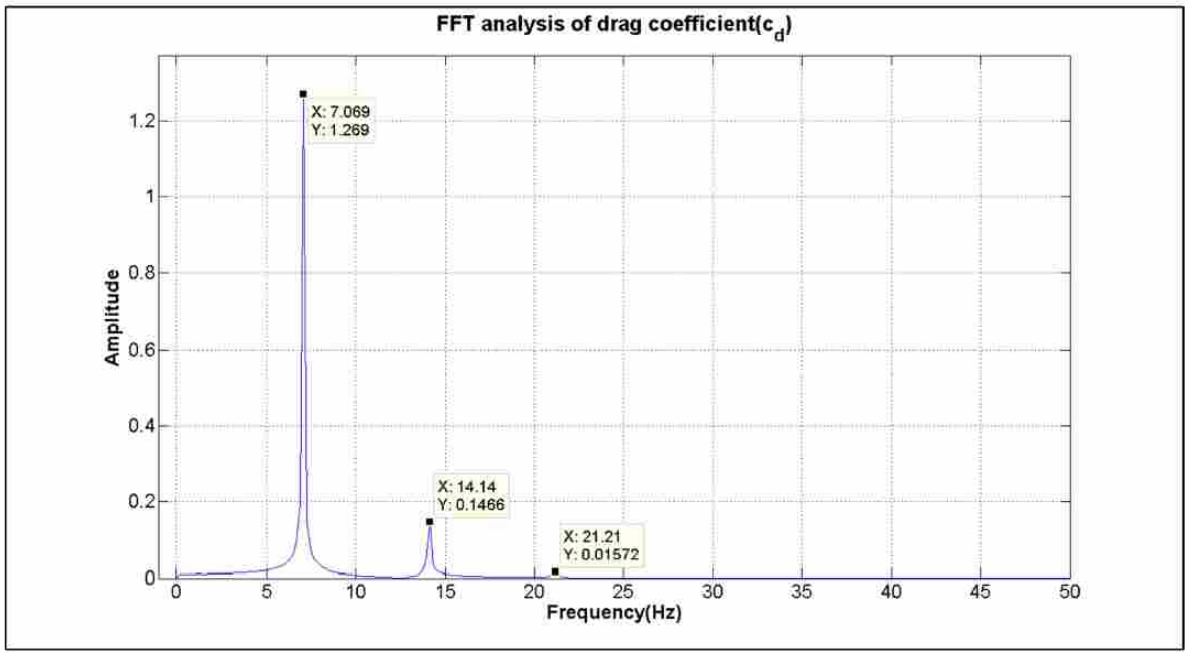


**Fig. (3.13):** The results of fast Fourier transform of drag coefficient with time step $1\times10^{-5}$ sec.

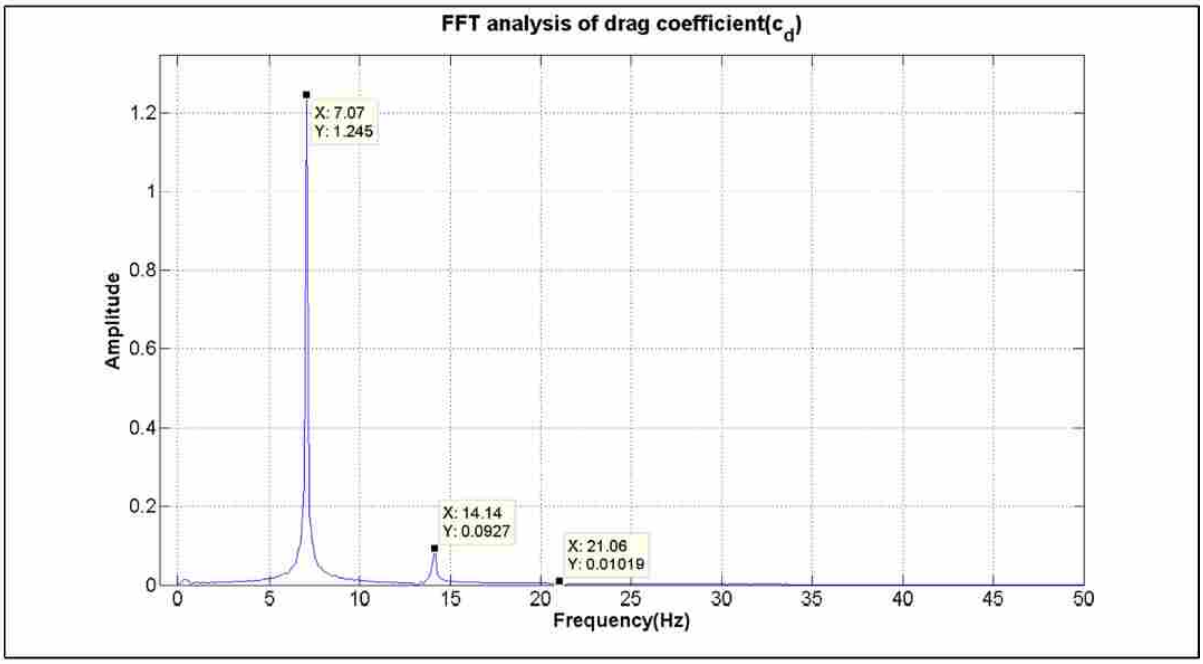


**Fig. (3.14):** The results of fast Fourier transform of drag coefficient with time step $1\times10^{-3}$ sec.

The difference percentage of the drag coefficient frequency is:

$$Difference\ percentage: \left|\frac{7.069-7.07}{7.069}\right| \times 100 = 0.01\%$$

In the results of the fast Fourier transform presented, the waves with frequencies 2, 2, 4 and … equal to the frequency of the dominant wave were observed which their amplitude decrease logarithmically. It seems that these waves are not physical waves and resulted from the reflection of the pressure reflective boundary condition.

# Chapter 4

# Results

The results obtained are presented in this chapter. By solving the flow in a scenario with fixed wings in three Reynolds numbers 200, 250 and 300, three frequencies of vortex shedding are extracted. This frequency assumed as the natural shedding frequency and the criterion of the frequency changes, assumed to be swinging of wings. Then, the problem has been solved in different coefficients of natural frequency and at different swinging amplitudes of the wings. Then, the coefficients of drag and lift forces as well as the frequencies available in these coefficients are obtained using fast Fourier transform. Table (4.1) provides the information of different arrangements of the problems.

**Table (4.1):** Presentation of different arrangement of the problem.

| Frequency ratio<br><br>Frequency amplitude (degree) | Reynolds number | | |
|---|---|---|---|
| | 200 | 250 | 300 |
| 0.75 | | | |
| 10 | ✓ | ✓ | ✓ |
| 14 | ✓ | ✓ | ✓ |
| 16 | ✓ | ✓ | ✓ |
| 18 | ✓ | ✓ | ✓ |
| 1 | | | |
| 10 | ✓ | ✓ | ✓ |
| 14 | ✓ | ✓ | ✓ |
| 16 | ✓ | ✓ | ✓ |
| 18 | ✓ | ✓ | ✓ |
| 1.25 | | | |
| 10 | ✓ | ✓ | ✓ |
| 14 | ✓ | ✓ | ✓ |
| 16 | ✓ | ✓ | ✓ |
| 18 | ✓ | ✓ | ✓ |
| 1.5 | | | |
| 10 | ✓ | ✓ | ✓ |
| 14 | ✓ | ✓ | ✓ |
| 16 | ✓ | ✓ | ✓ |
| 18 | ✓ | ✓ | ✓ |
| 2 | | | |
| 10 | ✓ | ✓ | ✓ |
| 14 | ✓ | ✓ | ✓ |
| 16 | ✓ | ✓ | ✓ |
| 18 | ✓ | ✓ | ✓ |

## 4.1. Checking and determining the arrangement of wings around the cylinder

Studying the flow behavior and the forces exerted on the cylinder equipped with swinging wings is based on the arrangement of wings on the cylinder. In this study, the ration of wings' length to cylinder's diameter is a predefined value. However, the location and angle of wings installed on the cylinder should be studied. To prevent the extreme complexity, the arrangement has been determined based on the forced at fixed geometry. In the following section, the determining strategy of these variables and the related plots are presented.

### 4.1.1. Study the installation location of wings

The installation location of the wings is the first arrangement variable which is investigated in this research. To determine the installation location, the smallest variation amplitude of the drag forces is of concern.

**Problem definition**

Wings assumed to be fixed and parallel to the flow. Studying the installation location of the wings has been done at angles ±50, ±55, ±60, ±67.5, ±70, and ±80 degree. The amplitude of oscillation of drag and lift forces has been derived based on the fast Fourier transform and then an arrangement with minimum oscillations has been selected. It is worth noting that all simulations have been perform for Reynolds 250 and time step 0.001. According to the defined domain, the Velocity inlet is set for inlet boundary, and the Pressure outlet is set for top, bottom and behind boundaries.

**Results and determination of installation location**

In following, the results related to the coefficients of drag and lift forces are presented for simulation the flow around the cylinder equipped with two fixed wings.

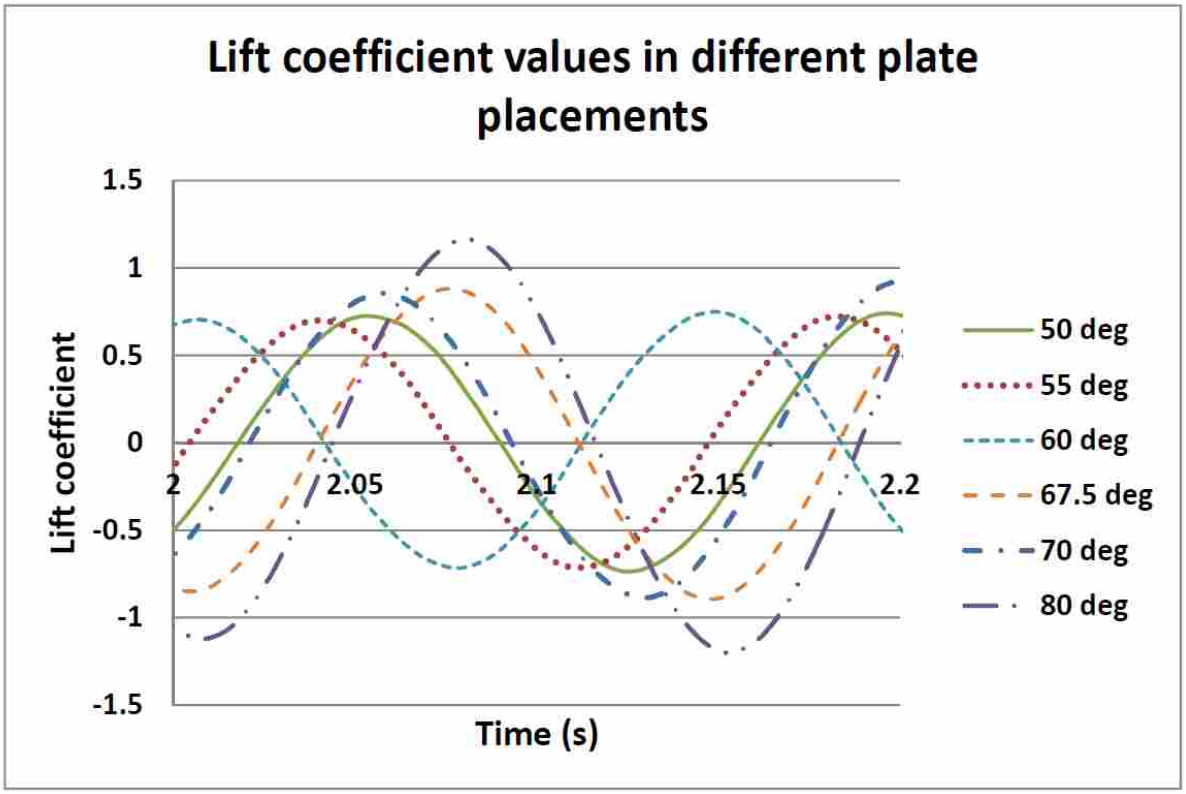


**Fig. (4.1):** Comparison of oscillation amplitude of the lift force at the installation location of different wings.

As can be seen in Fig. (41), all graphs show a sinusoidal function around the zero value. In other word, the maximum value of the graph is equal to the oscillation amplitude of the lift

coefficient with high precision. Given that the minimum value occurs in oscillation amplitudes of the lift coefficient for 55-degree changes in installation location, therefore the most possible choice for installation location is the angle 55-degree. More detailed decision making on this can be obtained by investigating the fast Fourier transform graphs for every oscillation shown in Figs. (4.2) to (4.7).

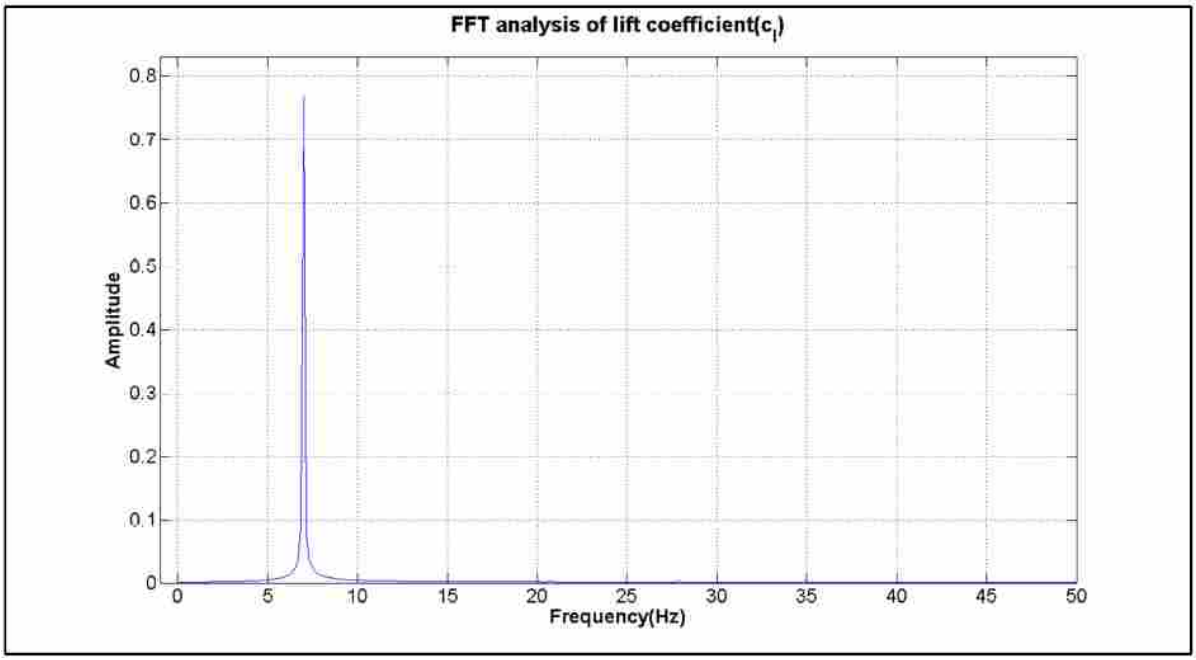


**Fig. (4.2):** Fast Fourier graph of coefficient of lift force for installation location arrangement at 50 degree.

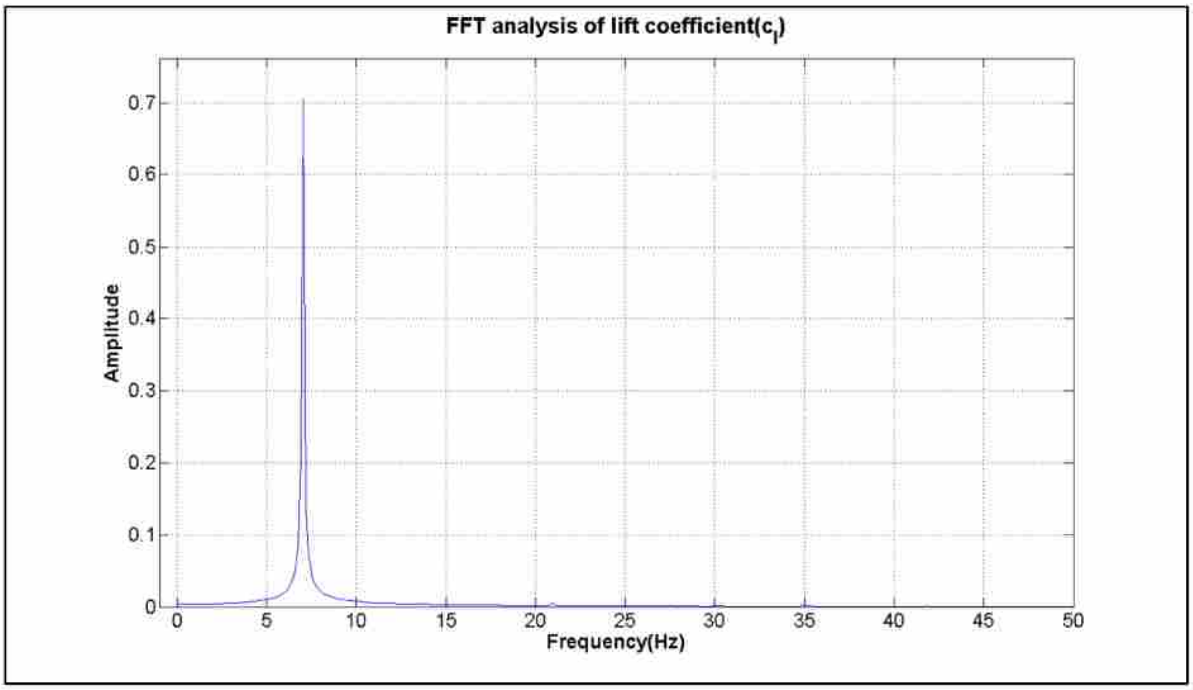

**Fig. (4.3):** Fast Fourier graph of coefficient of lift force for installation location arrangement at 55 degree.

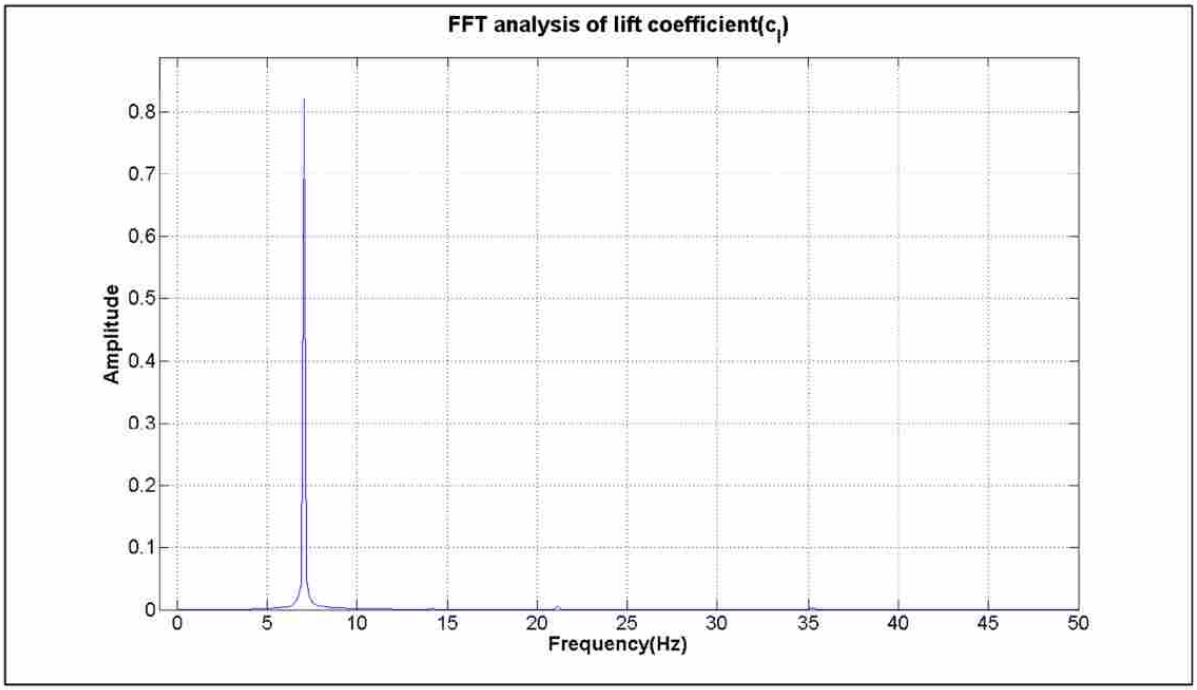


**Fig. (4.4):** Fast Fourier graph of coefficient of lift force for installation location arrangement at 60 degree.

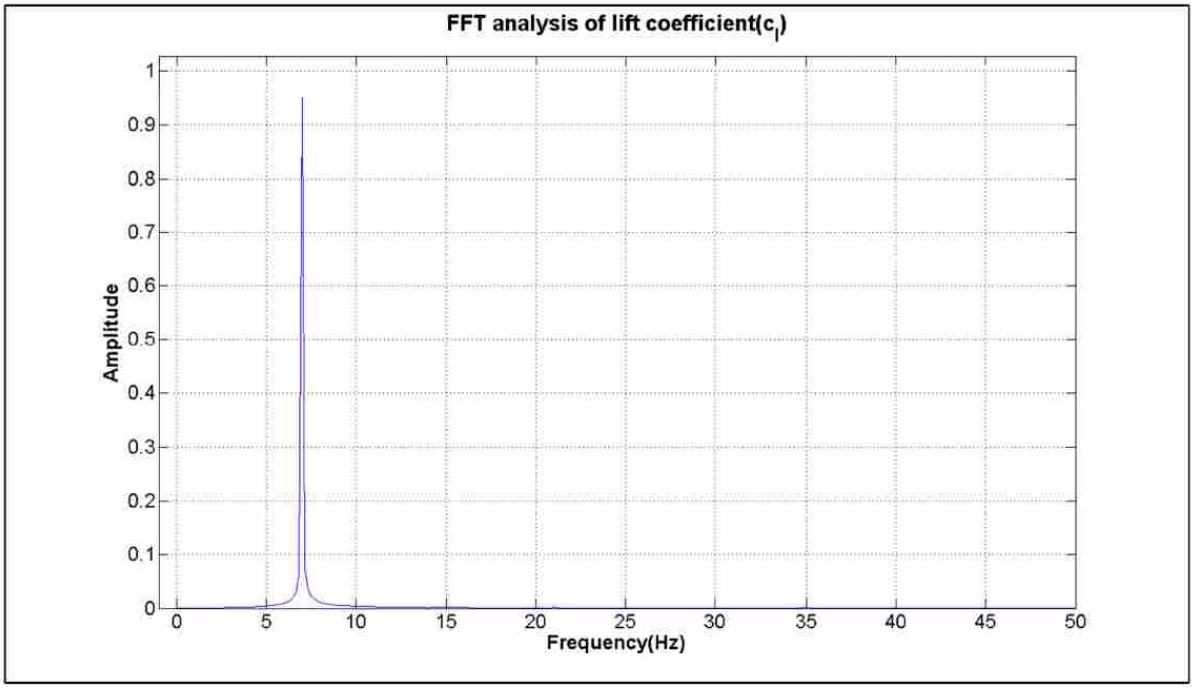


**Fig. (4.5):** Fast Fourier graph of coefficient of lift force for installation location arrangement at 60 degree.

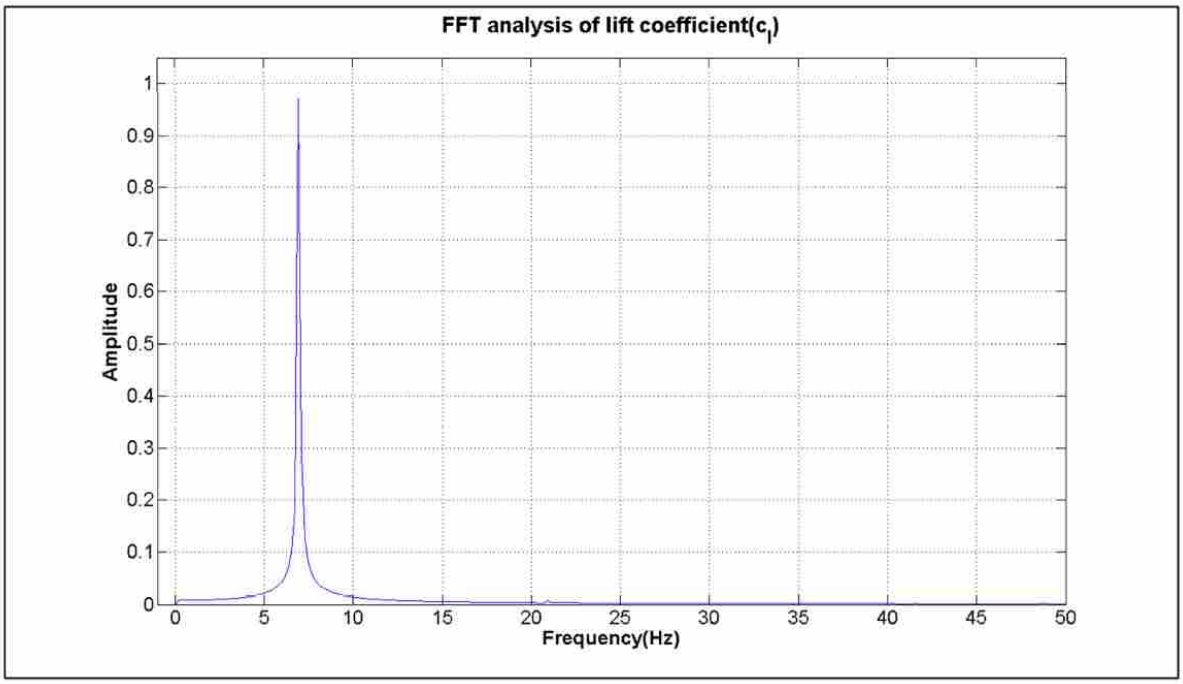


**Fig. (4.6):** Fast Fourier graph of coefficient of lift force for installation location arrangement at 70 degree.

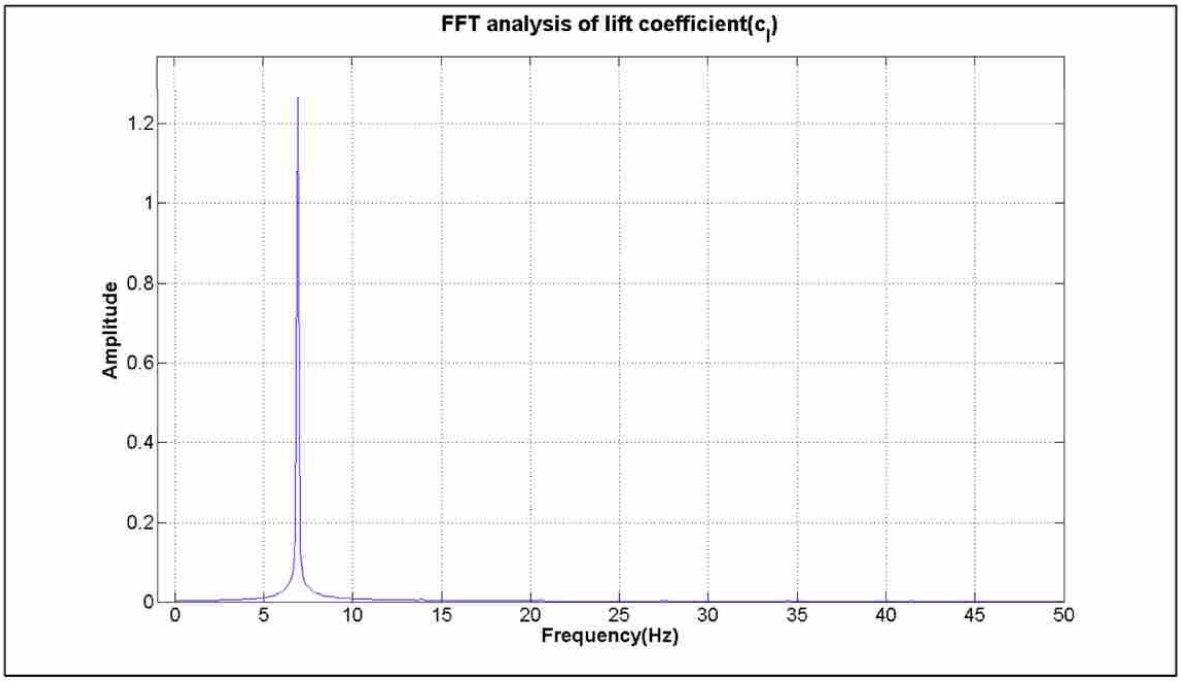


**Fig. (4.7):** Fast Fourier graph of coefficient of lift force for installation location arrangement at 80 degree.

Given the graphs shown in Figs. (4.2) to (4.7), it can be seen that all graphs have one pick. Therefore, with very good precision it can be claim that the behavior of the lift coefficients is completely sinusoidal. The value of the amplitudes of the sinuses is equal to the value of each pick and the frequency of the sinusoidal function is equal to the location of the pick in the graphs. Therefore, in order to find an appropriate option for installation location of the wings, a case is desired in which its fast Fourier transform graph has the minimum value on the vertical axis.

**Table. (4.2):** Oscillation amplitude of the lift force coefficient in different installation location of wings results from fast Fourier transform.

| Installation location (degree) | Oscillation amplitude of lift coefficient |
|---|---|
| 50 | 0.7729 |
| 55 | 0.5106 |
| 60 | 0.8103 |
| 67.5 | 0.915 |
| 70 | 0.9712 |
| 80 | 1.266 |

In Table (4.2), the values of the oscillation amplitude of the lift coefficient per the variations of the installation location are presented. In this table, it can clearly observe that the minimum oscillation amplitude occurs ate installation location of 55 degree. Therefore, this option selects as the installation location.

### 4.1.2. Studying the installation angle of wings

Another variable which defines the arrangement of the wings is the installation angle of wings. The installation angle is indeed an angle in which the wings have that maximum distance from each other. This angle defines as the angle between direction of wings' location in its maximum case with the flow direction. In this section, the effect of this angle is investigated and the appropriate angle is determined.

**Problem definition**

According to the results of the previous section, wings are installed on the cylinder at the angles $\pm$ 55-degree respect to the center of the cylinder. Also, same as before, to prevent the excessive complexity, wings are assumed fixed. The strategy for selecting the proper option, a case is selected in which the minimum oscillation of forces occurred. The values of the forces are defined using the fast Fourier transform at every time step. All simulations have been performed with Reynolds number 250 and time step 0.001. According to the defined domain, the Velocity inlet is set for inlet boundary, and the Pressure outlet is set for top, bottom and behind boundaries.

**Results and determining the installation angle**

In this section, the results related to coefficients of drag and lift forces are provided for simulation of flow around the cylinder equipped with two fixed wings.

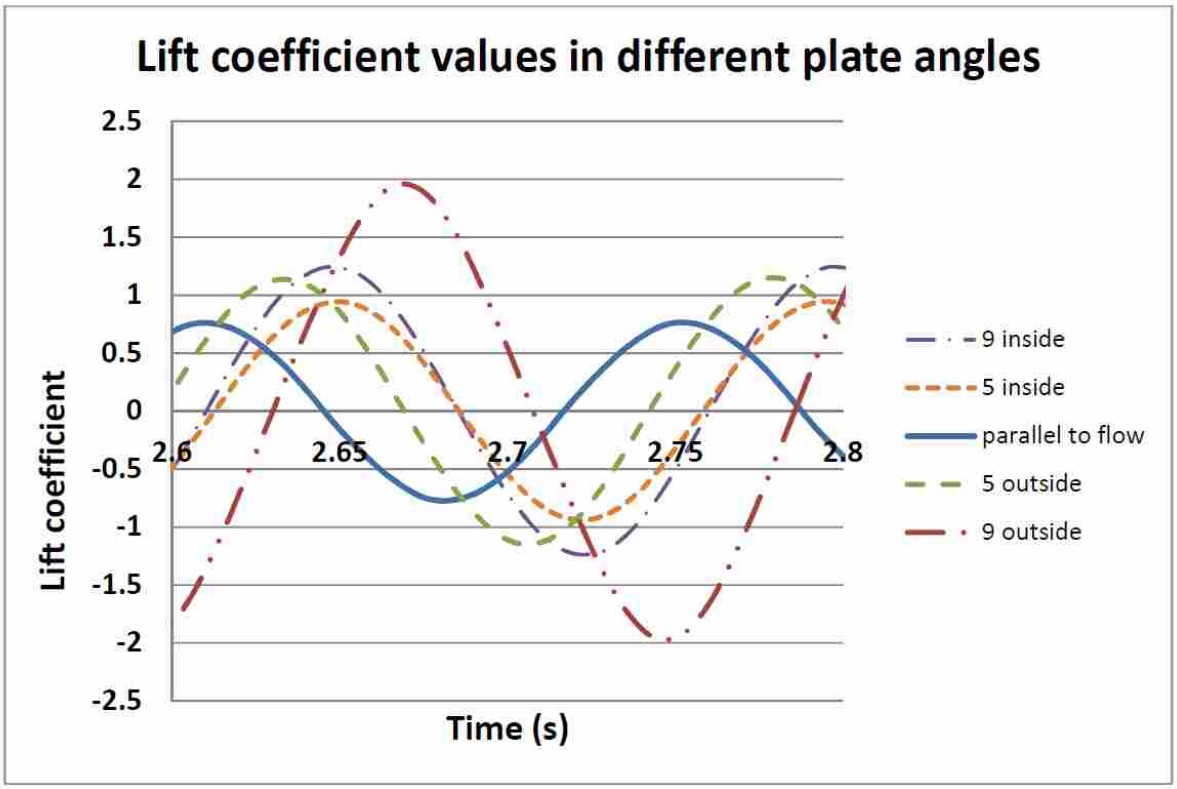


**Fig. (4.8):** Comparison of oscillation amplitude of lift force at different installation angles of wings.

Same as before, the appropriate installation angle can be determined by investigating the graph showing variations of oscillation amplitude of the lift coefficient for different installation angle. According to Fig. (4.8) wherein all oscillations are sinusoidal and occur around the zero value; it can claim that the minimum value of oscillation amplitude occurs at zero installation angle. In other word, in a case where the planes are installed parallel to the flow, the minimum oscillation value of lift coefficient occurred. It should be noted that, in a case where the distance of free end of the planes is shorter than their distance at the cylinder junction called the inside planes. In this case, the installation angle of the planes is negative. To perform more detailed investigation, the information related to lift coefficient are exposed under the fast Fourier transform. The results of this transform are presented in the following figures.

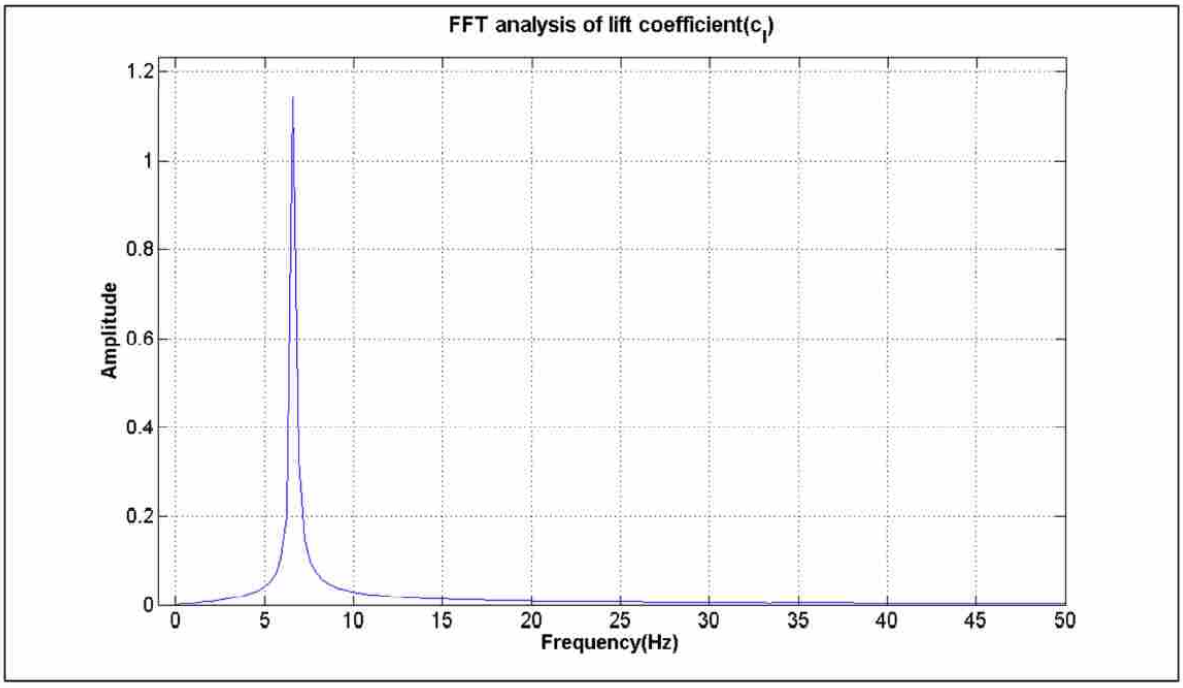


**Fig. (4.9):** The fast Fourier transform plot of lift force coefficient for an arrangement at installation angle at -9 degree.

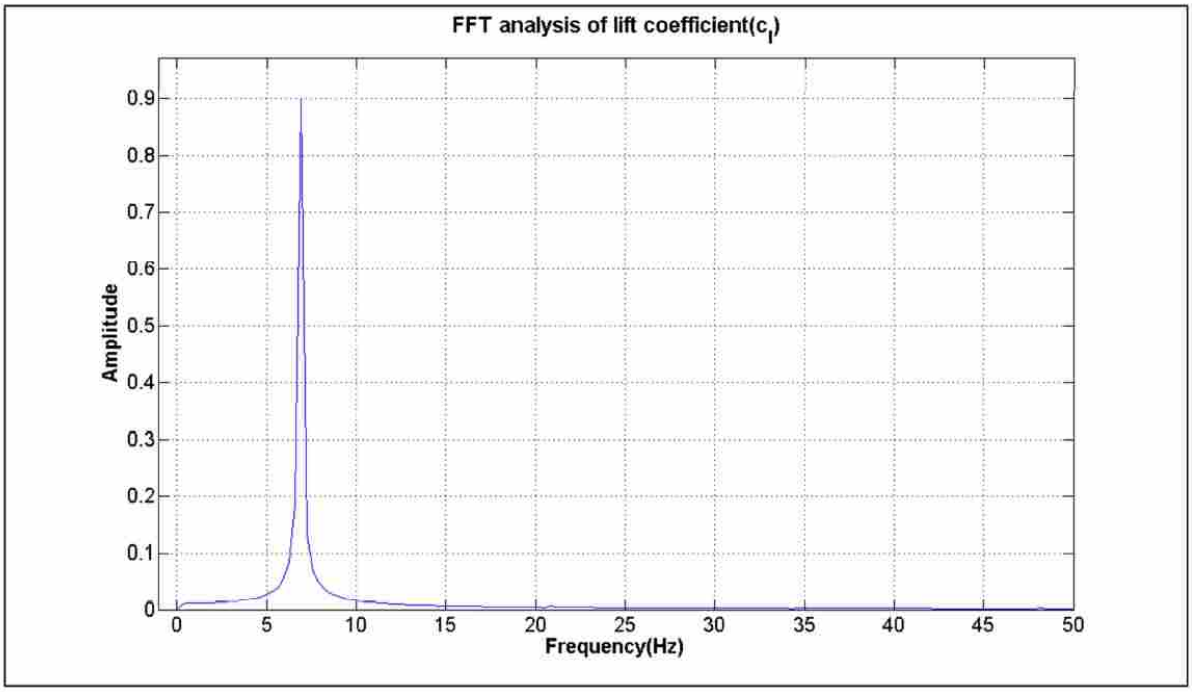


**Fig. (4.10):** The fast Fourier transform plot of lift force coefficient for an arrangement at installation angle at -5 degree.

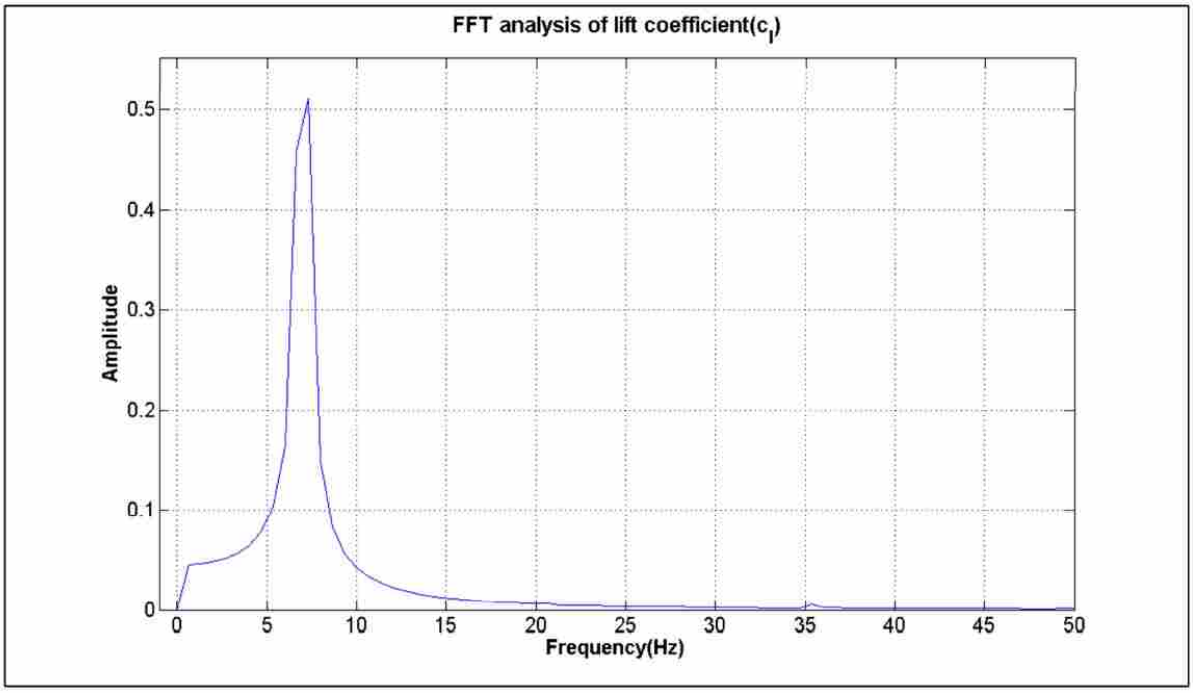


**Fig. (4.11):** The fast Fourier transform plot of lift force coefficient for an arrangement at installation angle at 0 degree.

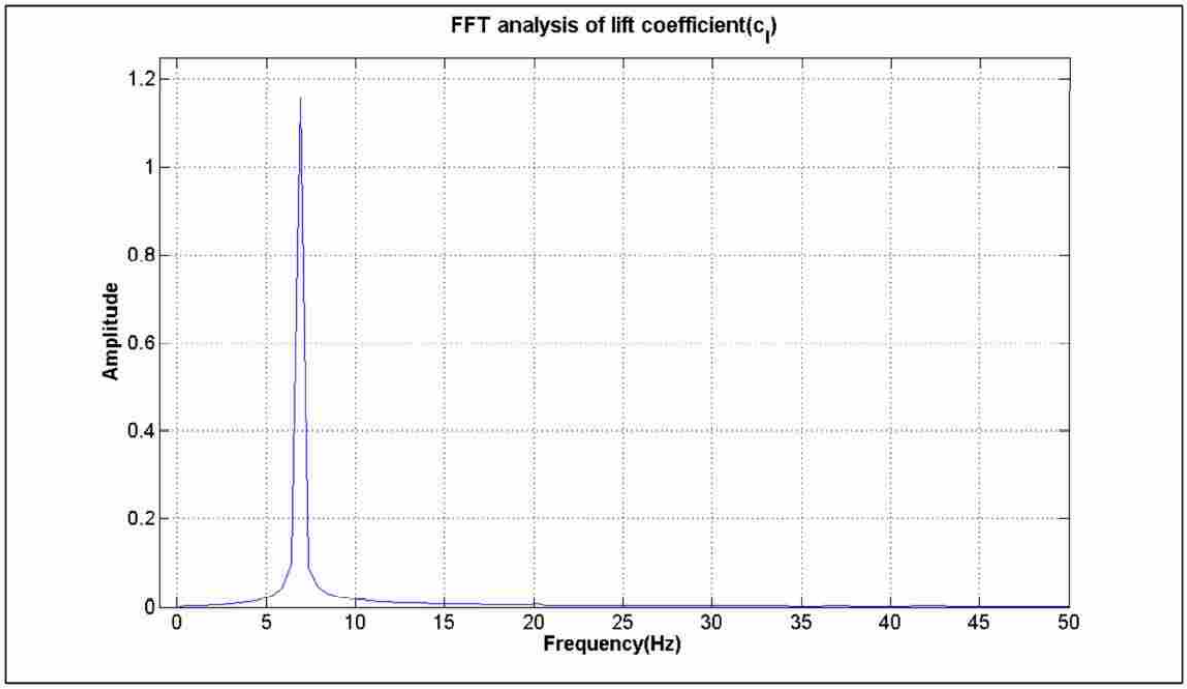


**Fig. (4.12):** The fast Fourier transform plot of lift force coefficient for an arrangement at installation angle at +5 degree.

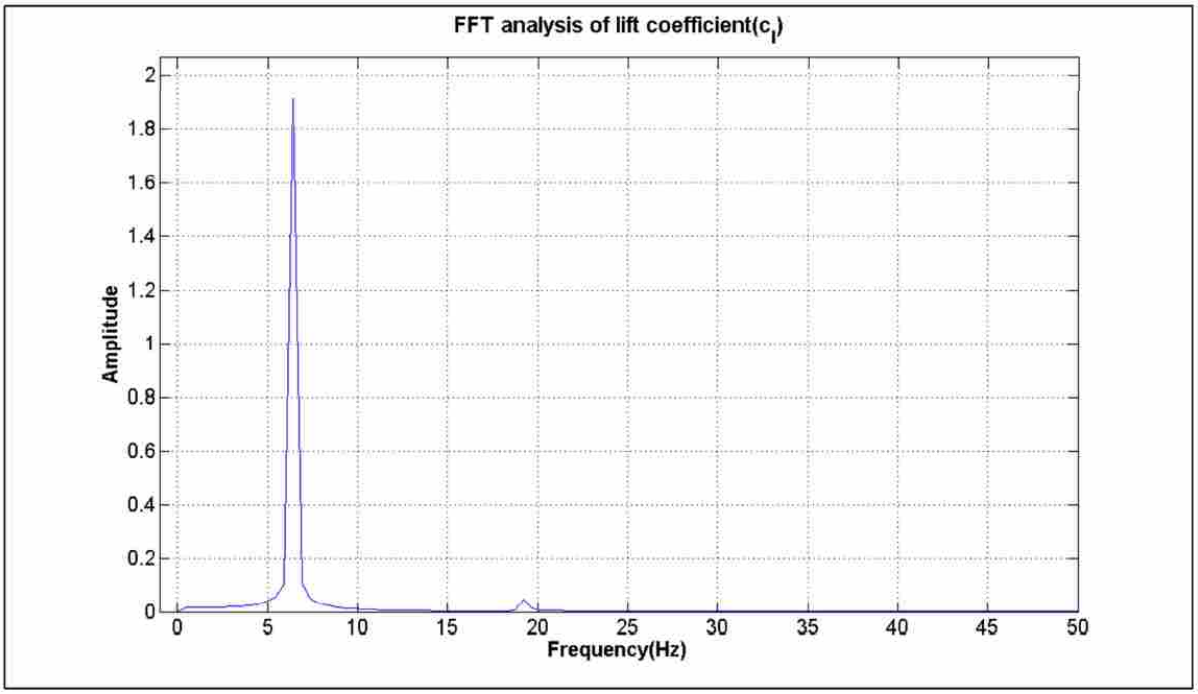


**Fig. (4.13):** The fast Fourier transform plot of lift force coefficient for an arrangement at installation angle at +9 degree.

Given the graphs shown in Figs. (4.9) to (4.13), it can be seen that all graphs have one pick. Therefore, with very good precision it can be claim that the behavior of the lift coefficients is completely sinusoidal. The value of the amplitudes of the sinuses is equal to the value of each pick and the frequency of the sinusoidal function is equal to the location of the pick in the graphs. Therefore, in order to find an appropriate option for installation location of the wings, a case is desired in which its fast Fourier transform graph has the minimum value on the vertical axis.

**Table. (4.3):** Oscillation amplitude of the lift force coefficient in different installation angle of wings results from fast Fourier transform.

| Installation angle (degree) | Oscillation amplitude of lift coefficient |
|---|---|
| -9 | 1.114 |
| -5 | 0.853 |
| 0 | 0.5106 |
| +5 | 1.157 |
| +9 | 1.911 |

According to Table (4.3) it can be found that the minimum oscillation amplitude is related to a case wherein they are parallel to the flow. Therefore, this option is selected as the final shape of the arrangement of surfaces around the cylinder.

## 4.2. Studying the effect of swinging of wings on the flow

Generally, the aim of studies done on the effect of the geometrical factors on the flow around the cylinder is the investigation the effect of results of geometry variations on the qualitative behavior of flow and the changes in forces exerted on the cylinder. In this section, the result of the present study is presented in three stages. In the first stage, the effect of different variables

on the lift force and oscillatory behavior of this force due to the applied variations is investigated. Then, according to lift force, observations and the related analysis are presented. Finally, the shape of the vortices is shown and the behavior of vortices are described. As mentioned earlier, in every oscillation, the wings reached the installation angle at their highest mode. This oscillation is under the simple harmonic function. In this research, the amplitude of the sinusoidal function of angle between the wing and flow and also their frequency are two variables of the flow.

### 4.2.1. Effect of oscillations of the wings on the drag force

In aerodynamic phenomena which has the oscillating nature, the force coefficient reflects this oscillation. The drag force coefficient also shows this oscillation perfectly. Fig. (4.14) shows the oscillation of this coefficient which resulted from the simulation done at Reynolds number 200 with fixed wings which are installed parallel to the flow at angle $\pm$ 55 on the cylinder.

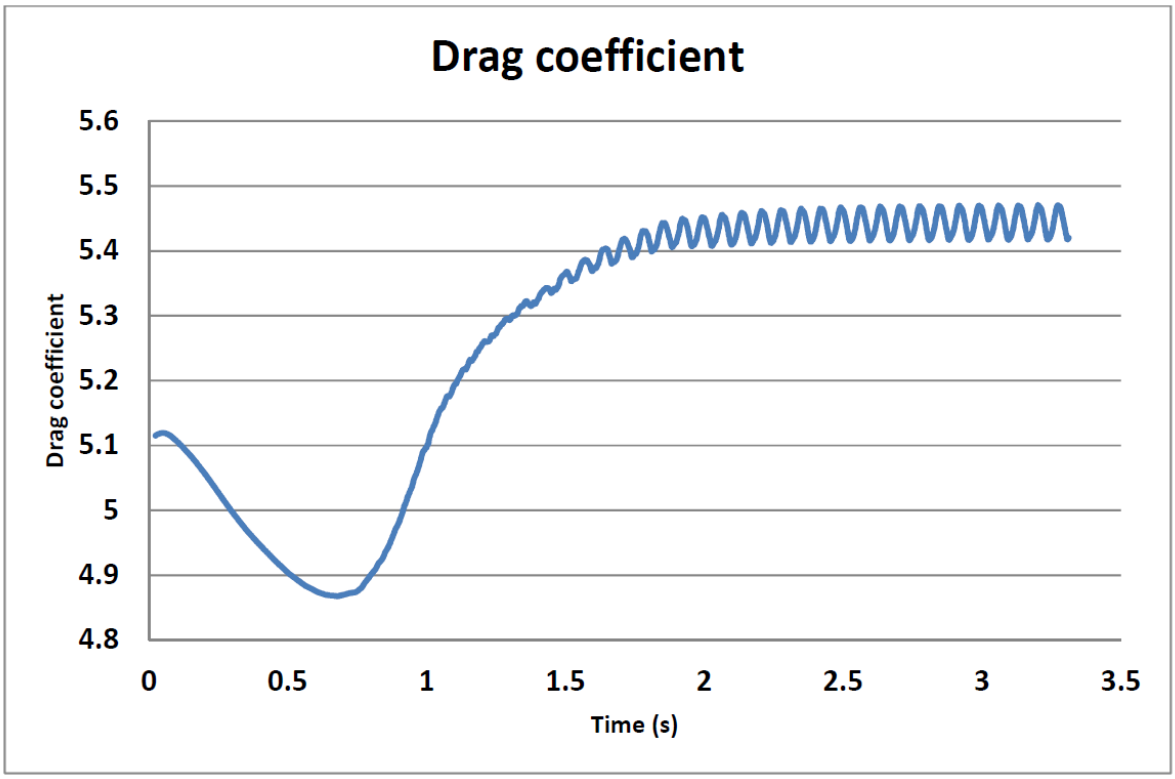


**Fig. (4.14):** The drag coefficient graph for fixed wings arrangement installed at angle zero at trigonometric degree $\pm$ 55.

According to Fig. (4.14), formation of flow continues until 2.5sec. From this time on, the oscillating the drag coefficient around a non-zero value (nearly 5.45) is quite evident. Then the flow reached its semi-steady mode.

The simulations performed based on the Table. (4.1) at different Reynolds, maximum deviation angle of the wings respect to the installation angle as well as the frequency ratio. The results obtained from these simulations are extracted and analyzed after applying the fast Fourier transform on the drag forces. In each scenario, the fast Fourier transform graphs can provide the information related to the amplitude of the drag force oscillations. Also, the oscillation frequency of this force is also extracted from these graphs. Comparison of these values by changing the different variables include Reynolds number, amplitude and frequency of wings'

oscillation can provide important information about the effect of these parameters on the behavior of the drag force.

**Results**

In this section, the results related to drag force coefficients in different simulations as well as the fast Fourier transform of these data are presented. Given that different simulations there is a difference in the amplitude, superposition of graphs is not allowed and given the multitude of graphs, only a part of graphs are shown as examples. Investigating the frequencies and amplitudes of the picks exist in the graphs of the force coefficient fast Fourier transform show that drag force is only a function of motion of the wings.

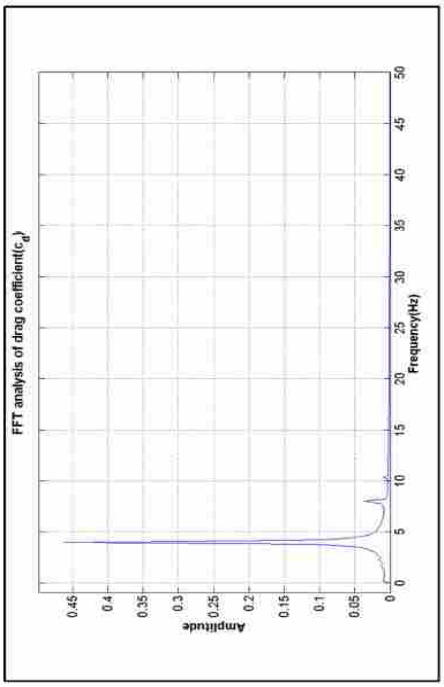


**Fig. (4.15):** Fast Fourier transform diagram of drag force coefficient at Reynolds number 200, frequency ratio 0.75 and oscillation amplitude 10 degree.

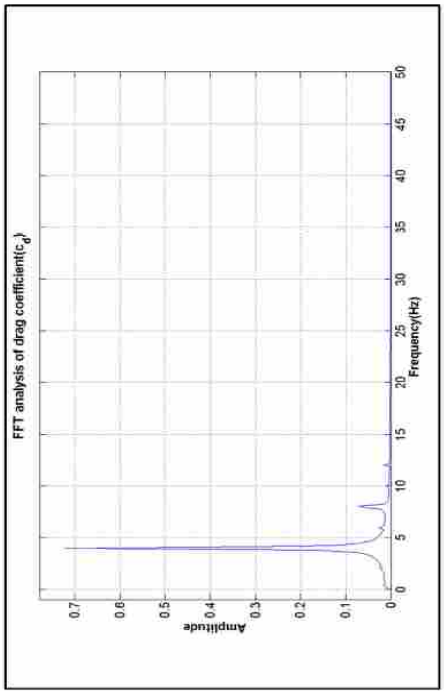


**Fig. (4.16):** Fast Fourier transform diagram of drag force coefficient at Reynolds number 200, frequency ratio 0.75 and oscillation amplitude 16 degree.

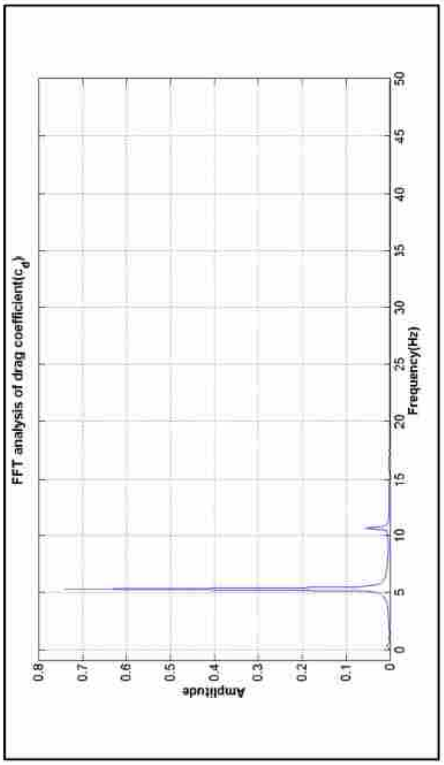


**Fig. (4.17):** Fast Fourier transform diagram of drag force coefficient at Reynolds number 200, frequency ratio 1 and oscillation amplitude 10 degree.

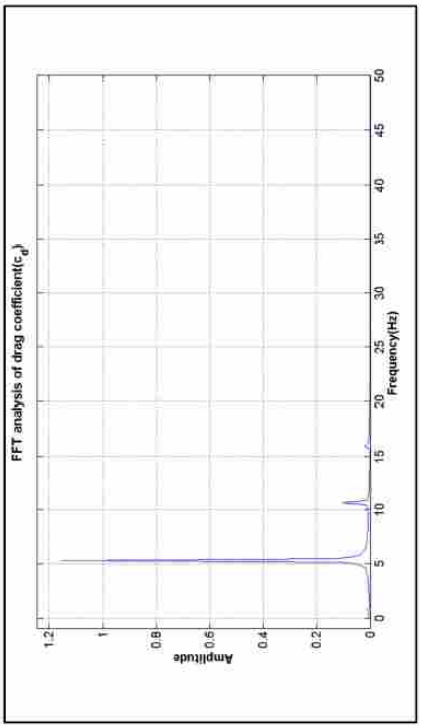


**Fig. (4.18):** Fast Fourier transform diagram of drag force coefficient at Reynolds number 200, frequency ratio 1 and oscillation amplitude 16 degree.

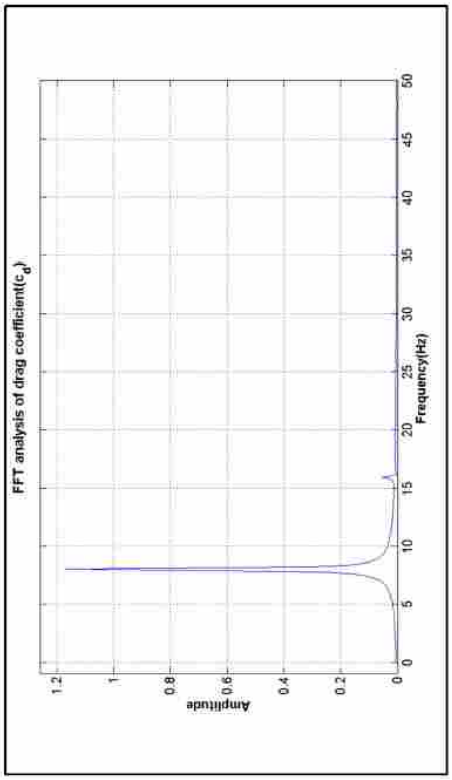


**Fig. (4.19):** Fast Fourier transform diagram of drag force coefficient at Reynolds number 200, frequency ratio 1.5 and oscillation amplitude 10 degree.

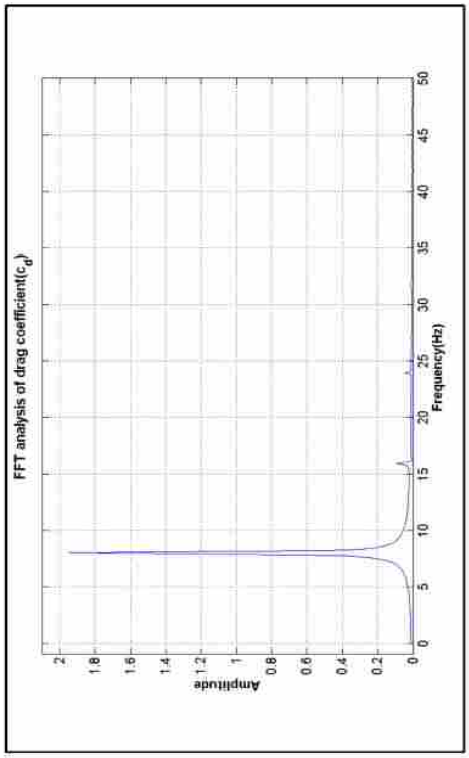


**Fig. (4.20):** Fast Fourier transform diagram of drag force coefficient at Reynolds number 200, frequency ratio 1.5 and oscillation amplitude 16 degree.

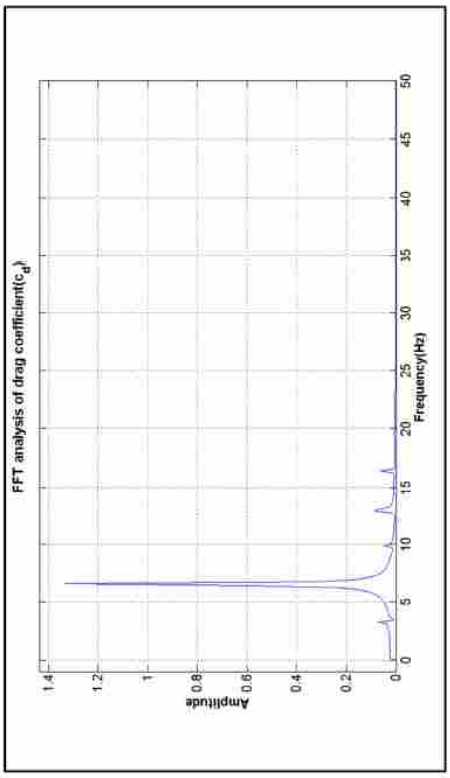


**Fig. (4.21):** Fast Fourier transform diagram of drag force coefficient at Reynolds number 300, frequency ratio 0.75 and oscillation amplitude 10 degree.

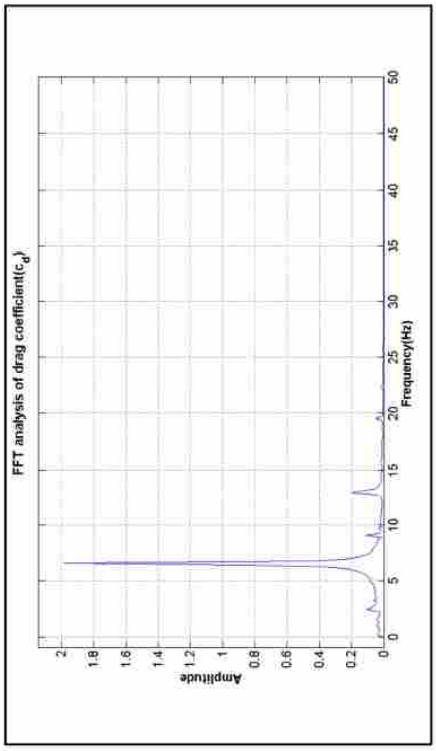


**Fig. (4.22):** Fast Fourier transform diagram of drag force coefficient at Reynolds number 300, frequency ratio 0.75 and oscillation amplitude 16 degree.

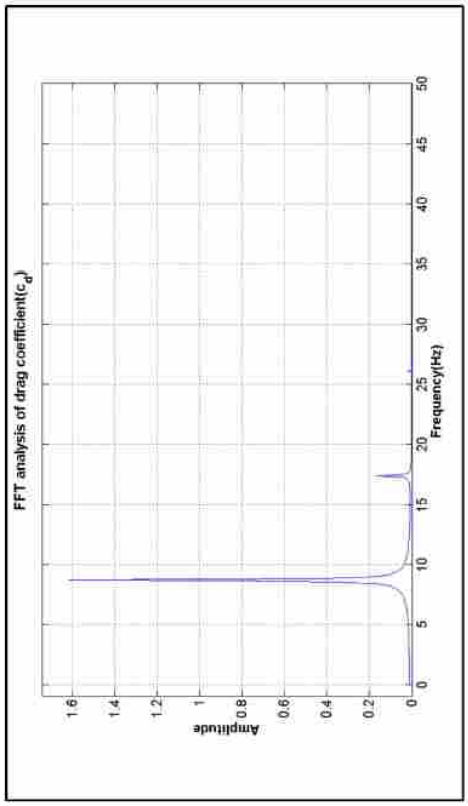


**Fig. (4.23):** Fast Fourier transform diagram of drag force coefficient at Reynolds number 300, frequency ratio 1 and oscillation amplitude 10 degree.

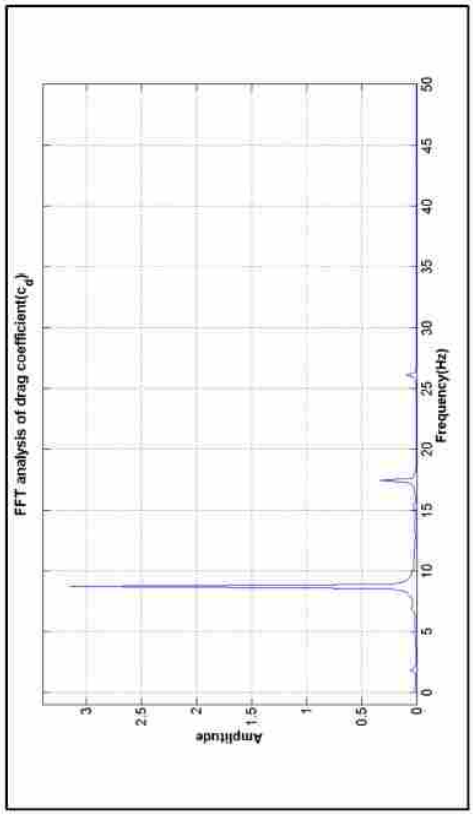


**Fig. (4.24):** Fast Fourier transform diagram of drag force coefficient at Reynolds number 300, frequency ratio 1 and oscillation amplitude 16 degree.

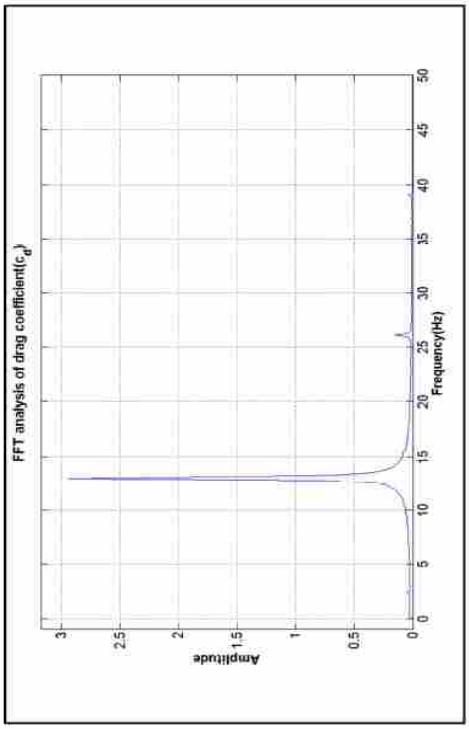


**Fig. (4.25):** Fast Fourier transform diagram of drag force coefficient at Reynolds number 300, frequency ratio 1.5 and oscillation amplitude 10 degree.

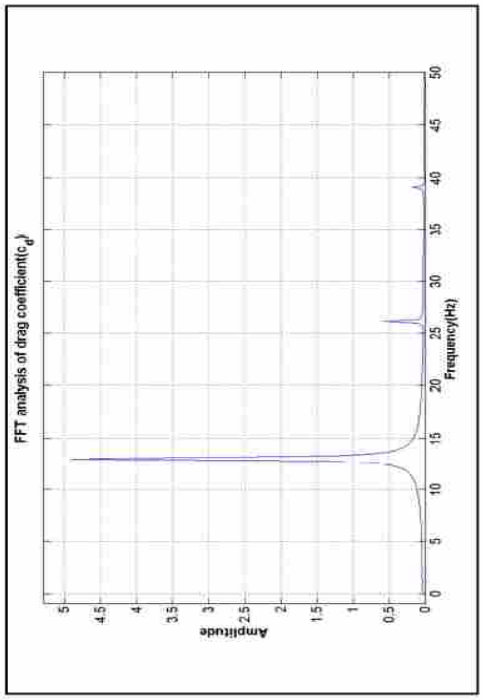


**Fig. (4.26):** Fast Fourier transform diagram of drag force coefficient at Reynolds number 300, frequency ratio 1.5 and oscillation amplitude 16 degree.

Generally, in all graphs of Figs. (4.15) to (4.26) only one pick is observed. In other word, only one oscillating phenomenon dominates on the behavior of the drag force. It can be seen that by increasing the Reynolds number, the oscillation amplitude of wings and their oscillation frequency, the oscillation amplitude of the drag force increases.

Table (4.4) shows the variations of the drag coefficient frequency in different simulations. The three columns on the left-hand side are separated by Reynolds number. the dray-colored rows repeated in this Tables separated the different simulations in terms the ratio of oscillation frequency of planes to the natural frequency. The frequency written in these rows show the frequency of the planes.

As can be seen from this table, all frequencies presented are equal to the oscillation frequency of planes with good accuracy. It was mentioned earlier that the oscillations of the drag coefficient are only a function of oscillatory phenomenon. according to this table, it can claim that the oscillations of drag force are only a function of oscillations of the planes.

**Table (4.4):** The values of frequency of drag force coefficient in simulations.

| **Frequency ratio**<br><br>Frequency amplitude (degree) | **Reynolds number** | | |
|---|---|---|---|
| | **200** | **250** | **300** |
| **0.75** | **3.992** | **5.282** | **6.552** |
| 10 | 3.994 | 5.333 | 6.572 |
| 14 | 3.944 | 5.28 | 6.57 |
| 16 | 3.947 | 5.26 | 6.572 |
| 18 | 3.945 | 5.255 | 6.57 |
| **1** | **5.323** | **7.043** | **8.696** |
| 10 | 5.309 | 7.07 | 8.727 |
| 14 | 5.309 | 7 | 8.7.3 |
| 16 | 5.308 | 7.059 | 8.711 |
| 18 | 5.306 | 7.033 | 8.703 |
| **1.25** | **6.663** | **8.804** | **10.87** |
| 10 | 6.675 | 8.859 | 10.84 |
| 14 | 6.675 | 8.815 | 10.9 |
| 16 | 6.673 | 8.87 | 10.84 |
| 18 | 6.671 | 8.818 | 10.84 |
| **1.5** | **7.985** | **10.564** | **13.023** |
| 10 | 8.04 | 10.51 | 12.98 |
| 14 | 8.04 | 10.58 | 13.01 |
| 16 | 8.038 | 10.54 | 12.98 |
| 18 | 8.042 | 10.64 | 13.03 |
| **2** | **10.666** | **14.085** | **17.391** |
| 10 | 10.67 | 14.07 | 17.41 |
| 14 | 10.67 | 14.12 | 17.37 |
| 16 | 10.67 | 14.13 | 17.38 |
| 18 | 10.67 | 14.13 | 17.4 |

Extracting the fast Fourier transform of drag coefficient is different from the lift force; because the drag force has an average value and its oscillations occur around this value. In order for similarity and increasing the accuracy of calculations of fast Fourier transform, first, the average value of data is subtracted from them and then the fast Fourier transform applied on the data. Generally, this causes that the oscillations occurred around the zero value. This leads

to an increase in accuracy of fast Fourier transform and reduces the final noises. Also, the initial frequency which is a constant value in values' function, is eliminated from the picks of the fast Fourier transform's graph.

After investigating the frequency of oscillations, the values of oscillation amplitude of drag coefficient per the variations of different studied variables are presented in the following graphs with aim of study the behavior of oscillation amplitude of drag coefficient.

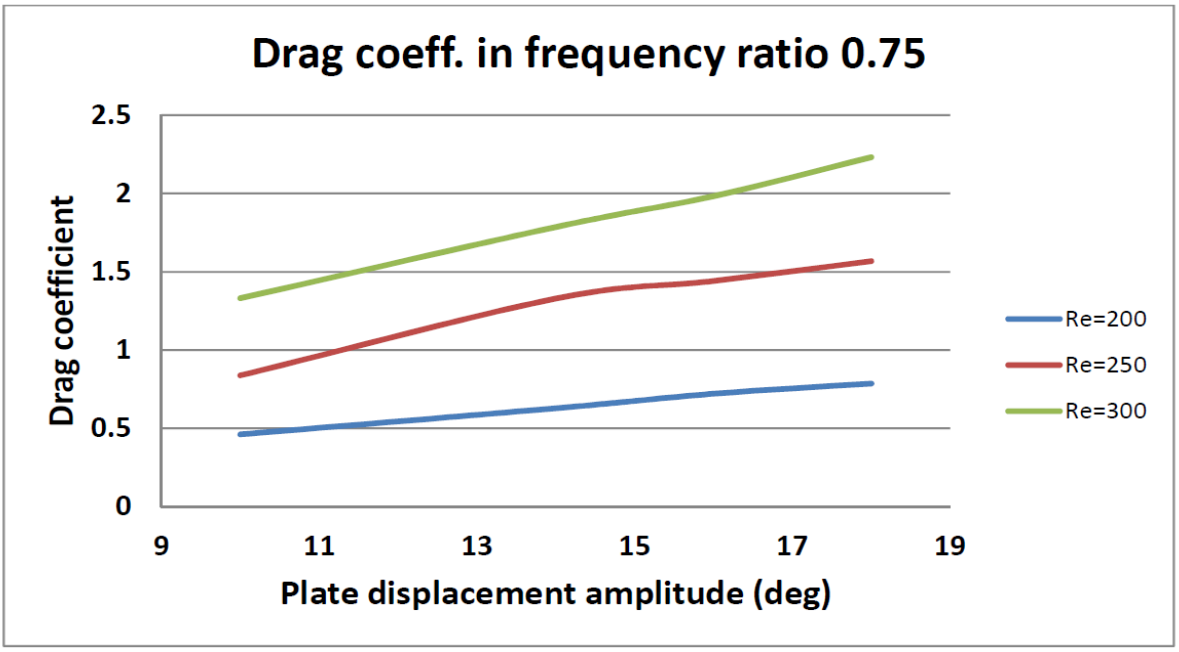


**Fig. (4.27):** Variations of drag force coefficient value at oscillations with frequency ratio 0.75, at Reynolds numbers 200, 250 and 300 and in different oscillation amplitudes.

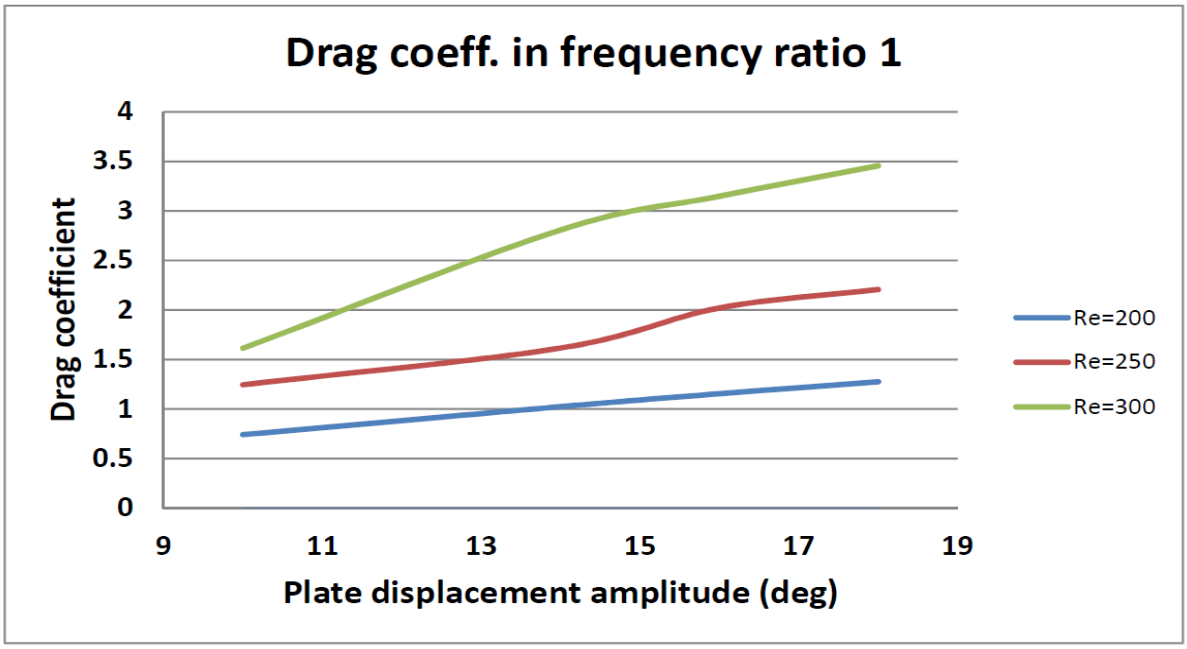


**Fig. (4.28):** Variations of drag force coefficient value at oscillations with frequency ratio 1, at Reynolds numbers 200, 250 and 300 and in different oscillation amplitudes.

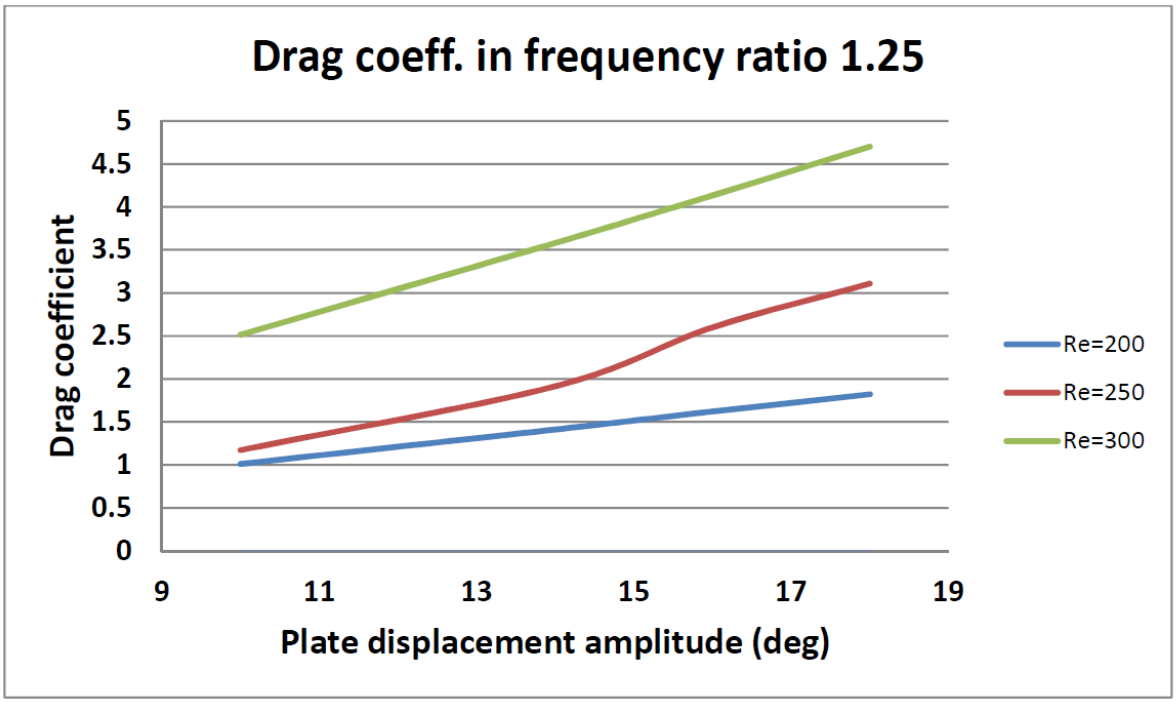


**Fig. (4.29):** Variations of drag force coefficient value at oscillations with frequency ratio 1.25, at Reynolds numbers 200, 250 and 300 and in different oscillation amplitudes.

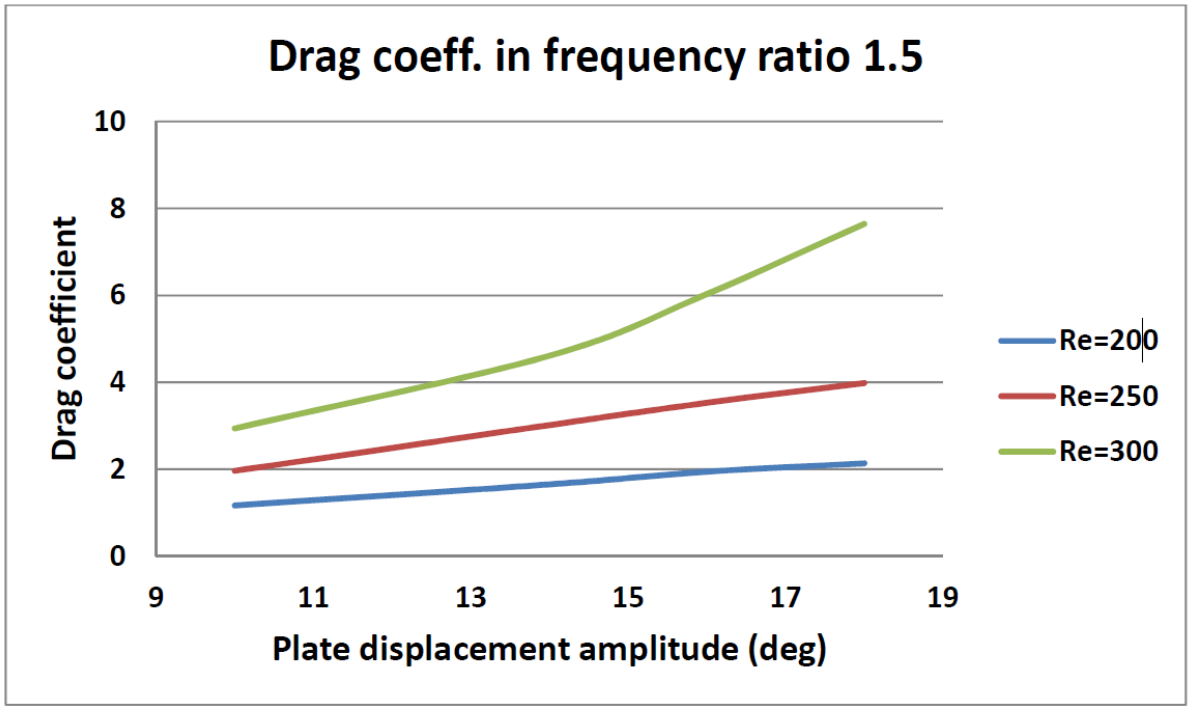


**Fig. (4.30):** Variations of drag force coefficient value at oscillations with frequency ratio 1.5, at Reynolds numbers 200, 250 and 300 and in different oscillation amplitudes.

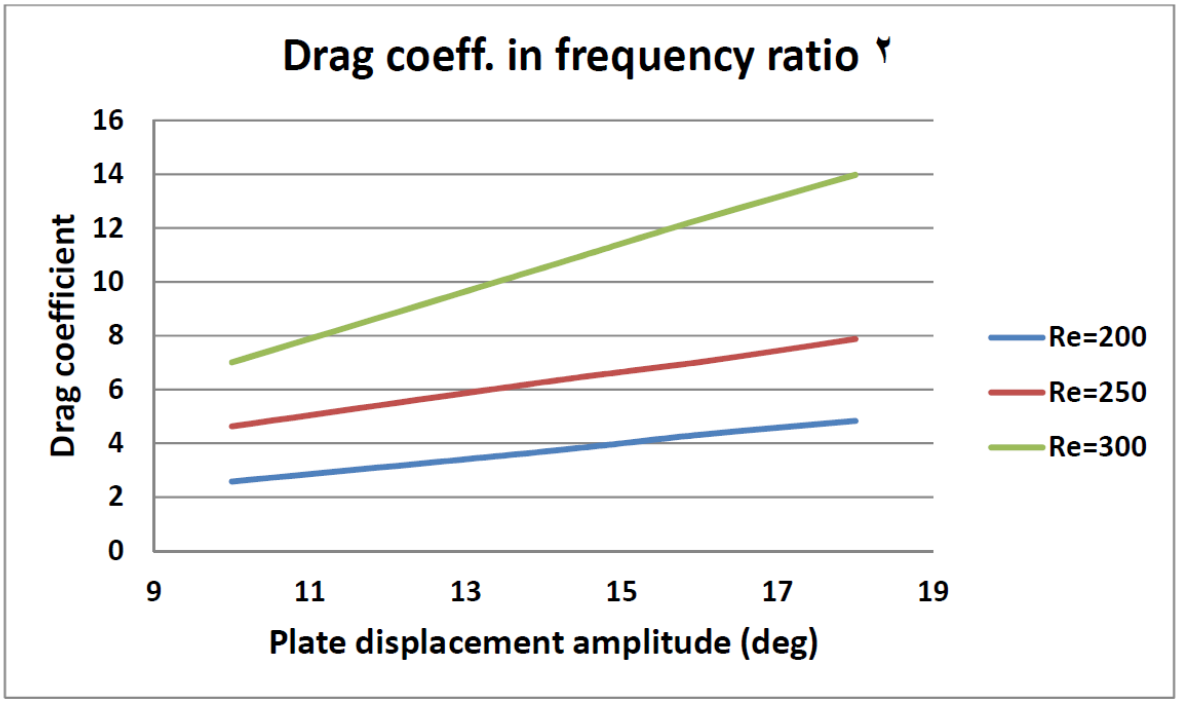


**Fig. (4.31):** Variations of drag force coefficient value at oscillations with frequency ratio 2, at Reynolds numbers 200, 250 and 300 and in different oscillation amplitudes.

Figs. (4.27) to (4.31) show that the by an increase in the Reynolds number as well as an increase in the amplitudes of wings' oscillations, the amplitudes of drag force oscillations increases. Also, it can be seen that all graphs have nearly follow the same linear trend. The lines resulted from linear fitting do not follow a clear trend and only show an increasing trend. In addition to comparison of the graphs of one plot, a comparison between the graphs of different figures is also interesting. By investigating the equivalent graphs in different figures, it can claim that by increasing the frequency ratio, the amplitude of the drag force oscillations increases.

The increasing trend of the amplitude of the drag force oscillations per an increase in the frequency oscillation of wings is shown in Figs (4.32) to (4.34).

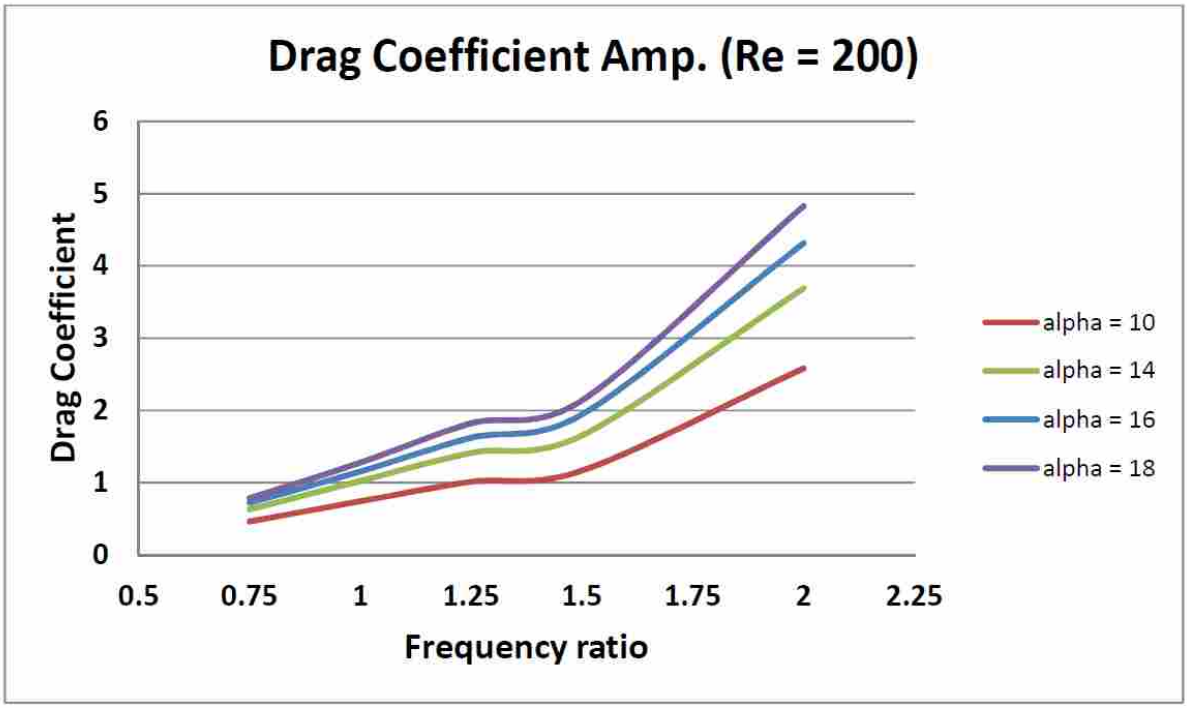


**Fig. (4.32):** Variations of drag force coefficient value at Reynolds numbers 200 and in different frequency ratio and oscillation amplitudes.

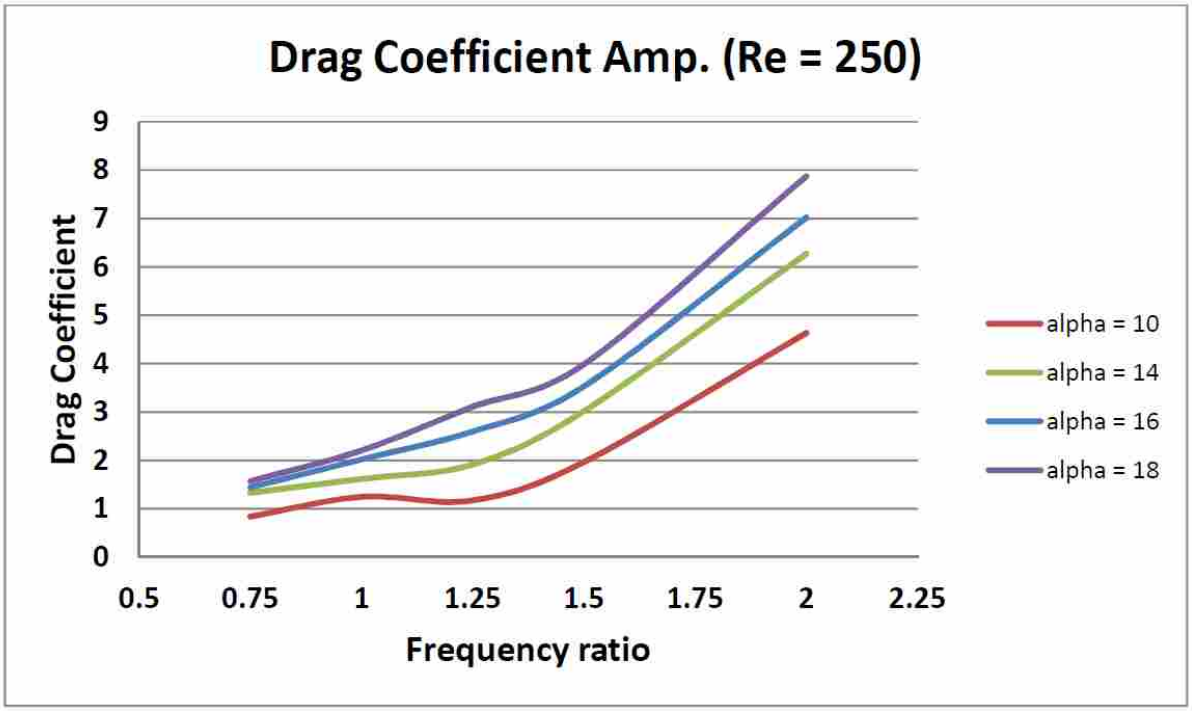


**Fig. (4.33):** Variations of drag force coefficient value at Reynolds numbers 250 and in different frequency ratio and oscillation amplitudes.

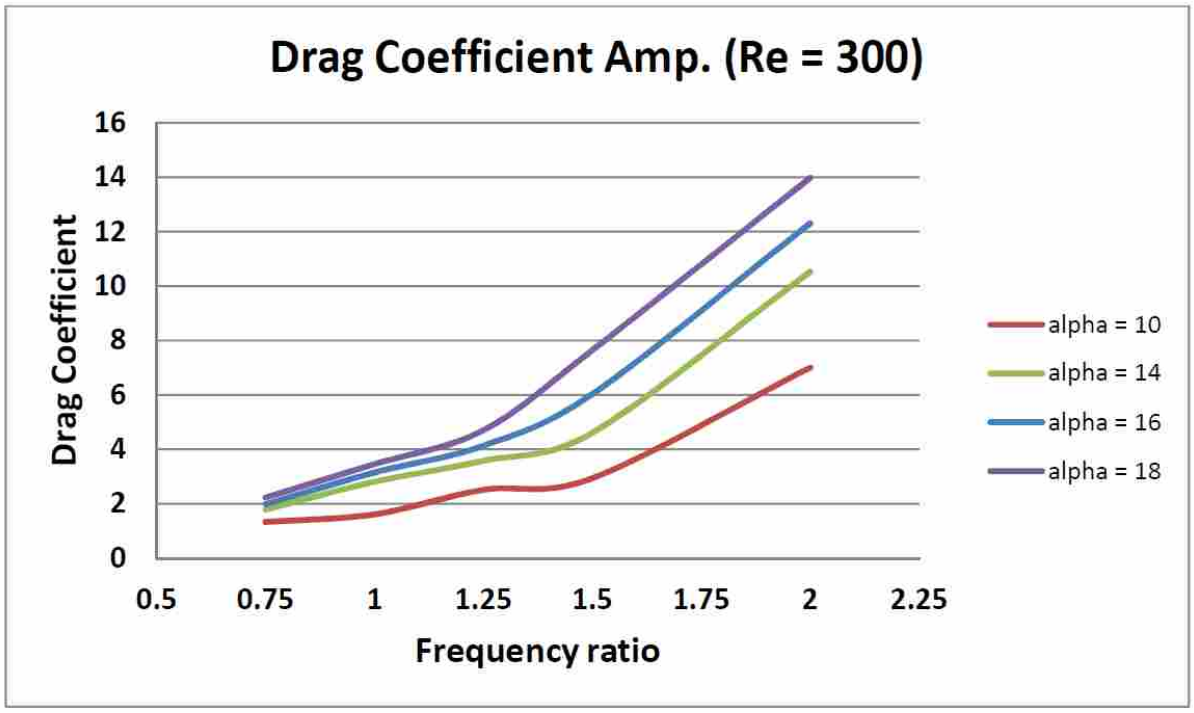


**Fig. (4.34):** Variations of drag force coefficient value at Reynolds numbers 300 and in different frequency ratio and oscillation amplitudes.

### 4.2.2. Properties of lift force and oscillations result from oscillation of wings

Lift force is an important variable in aerodynamic studies and fluid-solid interaction. As mentioned earlier, in problems in which the aerodynamic phenomena have oscillation, this variable is also oscillating. Fig. (4.35) shows this sinusoidal oscillation very well. This plot is for fixed wings arrangement which are installed at trigonometry angle $\pm 55$ and at installation angle zero. According to this figure, from the time 0 to 2.5sec the flow is forming. The effect of fluctuations resulted from numerical error and the beginning of the oscillatory instability in the flow from time 0.5s is quite evident. The increase in amplitude of the instability continues until the flow becomes semi-steady. From time 2.5sec onward, the flow become semi-steady and the instability amplitude remains constant.

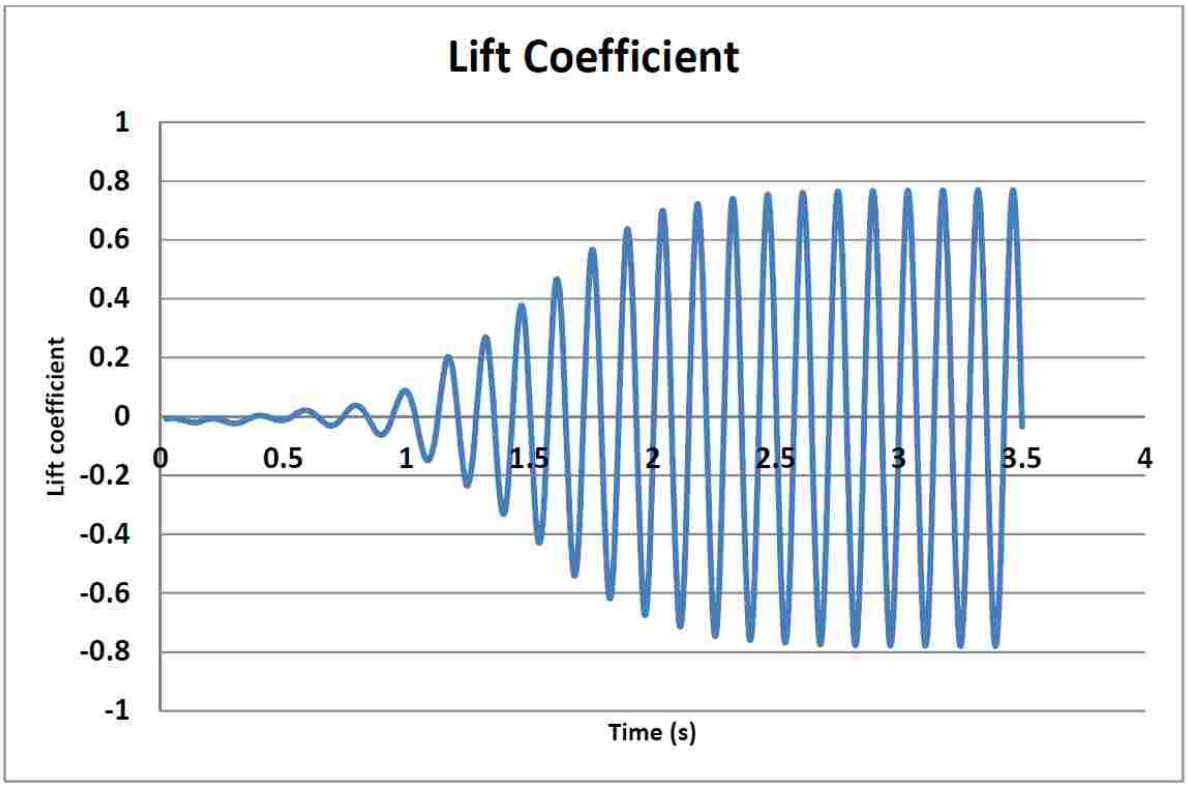


**Fig. (4.35):** Lift coefficient graphs for fixed wings installed at angle zero at trigonometry angle ±55.

Investigation of fast Fourier transform graphs of the lift force and different simulations shows that the drag force has different behavior comparing with lift force. The most important difference between that the fast Fourier transform plots of lift and drag forces is the presence of new picks which can not be seen is drag force graphs. Also, presence of too much noises in some runs is also noticeable. In this section, these differences will be addressed.

The differences can be considered equivalence with the shape of phenomena available in flow and vortices. In fact, presence of additional picks and noises both occurred when the vortices take specific shape in the flow. More detailed investigations and descriptions are provided in the next section.

**Results**

In this section, the results related to lift force coefficients in different simulations and also the fast Fourier transform of these data are presented. Given that due to the amplitude difference in different simulation, superposition of graphs is not applicable and because there are too many graphs, therefore only a part of them is presented as example.

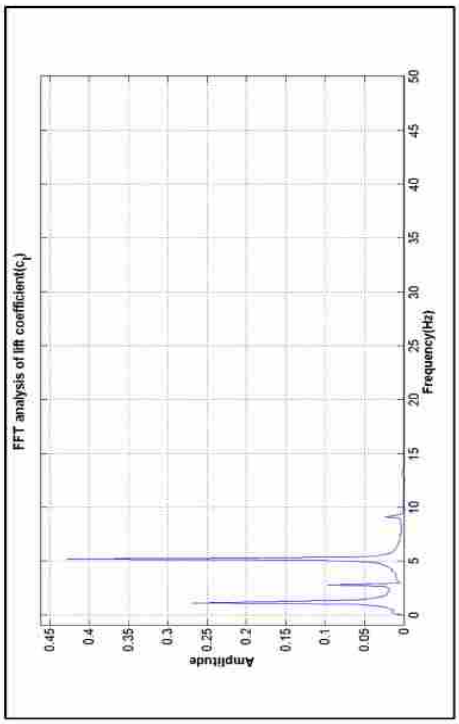


**Fig. (4.36):** Fast Fourier transform diagram of lift force coefficient at Reynolds number 200, frequency ratio 0.75 and oscillation amplitude 10 degree.

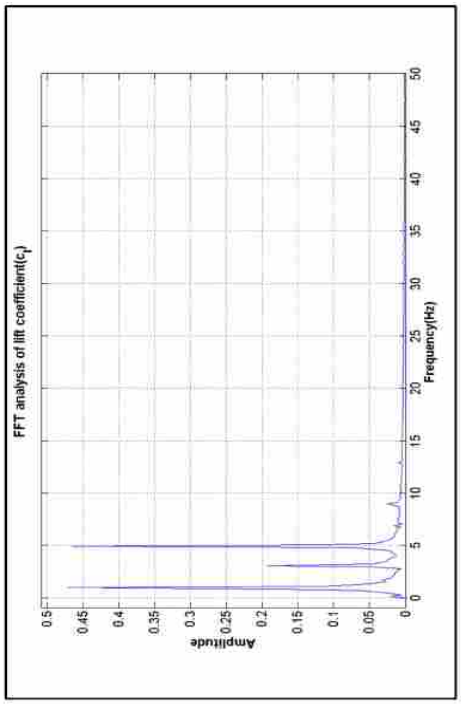


**Fig. (4.37):** Fast Fourier transform diagram of lift force coefficient at Reynolds number 200, frequency ratio 0.75 and oscillation amplitude 16 degree.

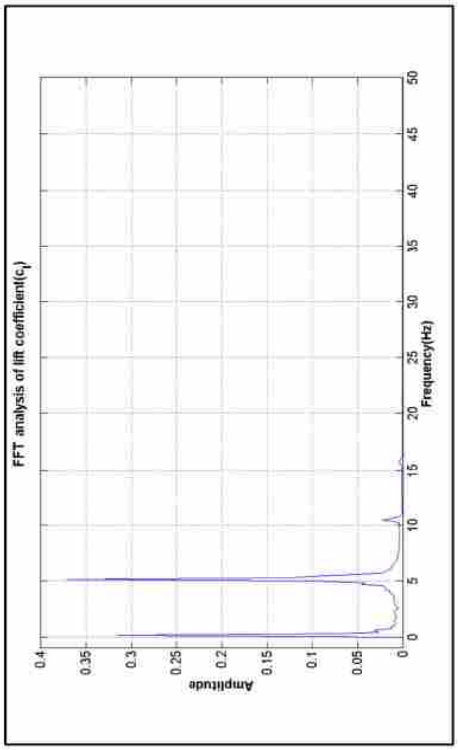


**Fig. (4.38):** Fast Fourier transform diagram of lift force coefficient at Reynolds number 200, frequency ratio 1 and oscillation amplitude 10 degree.

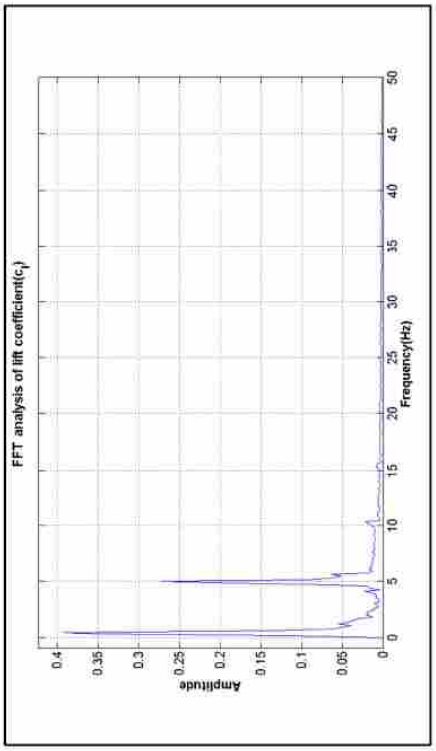


**Fig. (4.39):** Fast Fourier transform diagram of lift force coefficient at Reynolds number 200, frequency ratio 1 and oscillation amplitude 16 degree.

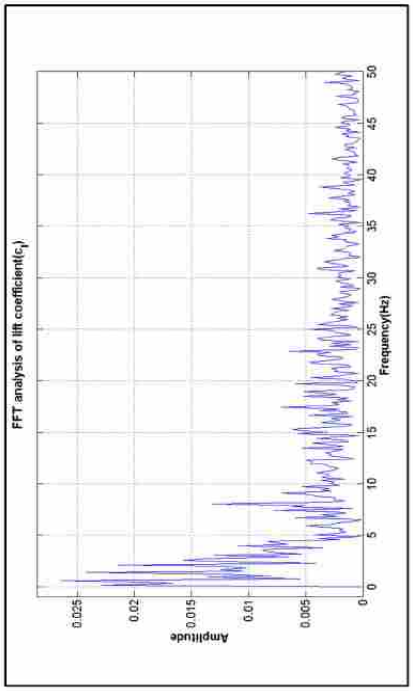


**Fig. (4.40):** Fast Fourier transform diagram of lift force coefficient at Reynolds number 200, frequency ratio 1.5 and oscillation amplitude 10 degree.

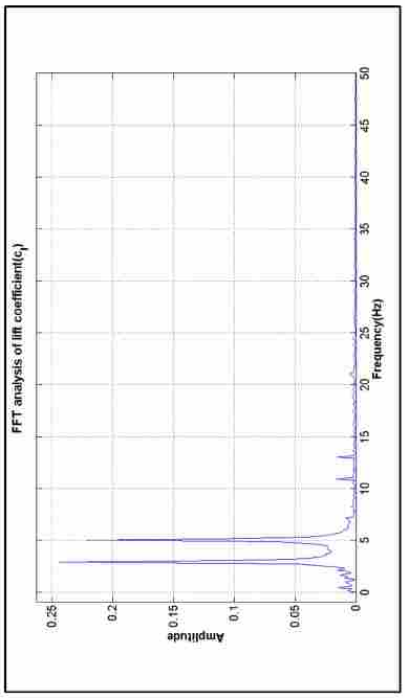


**Fig. (4.41):** Fast Fourier transform diagram of lift force coefficient at Reynolds number 200, frequency ratio 1.5 and oscillation amplitude 16 degree.

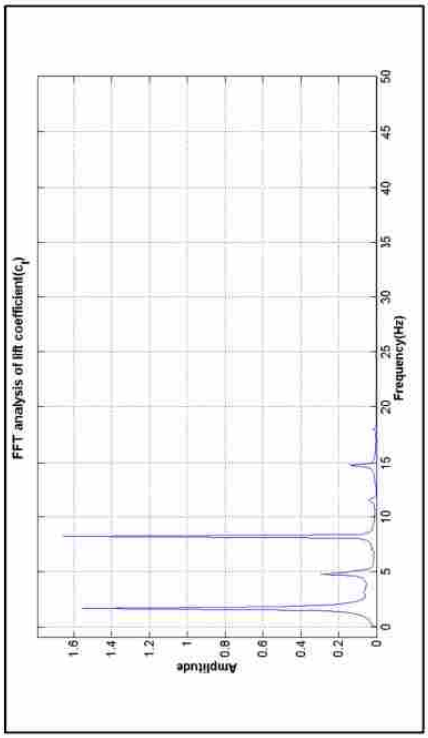


**Fig. (4.42):** Fast Fourier transform diagram of lift force coefficient at Reynolds number 300, frequency ratio 0.75 and oscillation amplitude 10 degree.

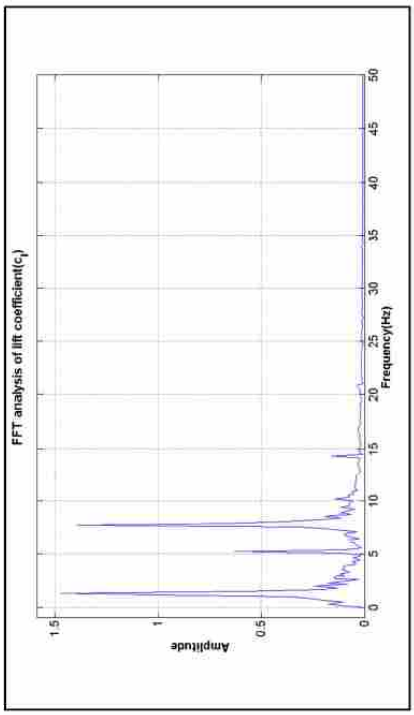


**Fig. (4.43):** Fast Fourier transform diagram of lift force coefficient at Reynolds number 300, frequency ratio 0.75 and oscillation amplitude 16 degree.

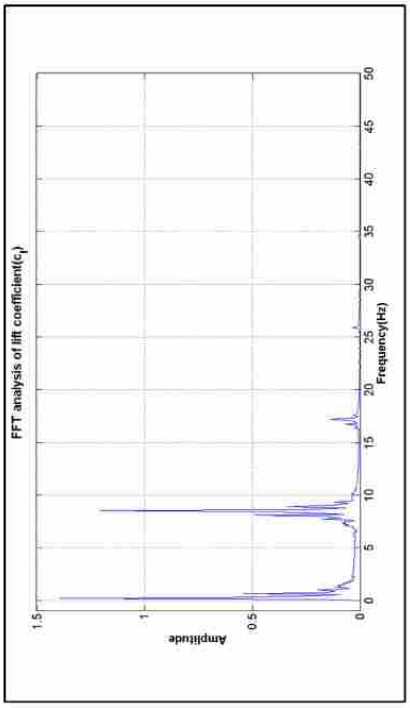


**Fig. (4.44):** Fast Fourier transform diagram of lift force coefficient at Reynolds number 300, frequency ratio 1 and oscillation amplitude 10 degree.

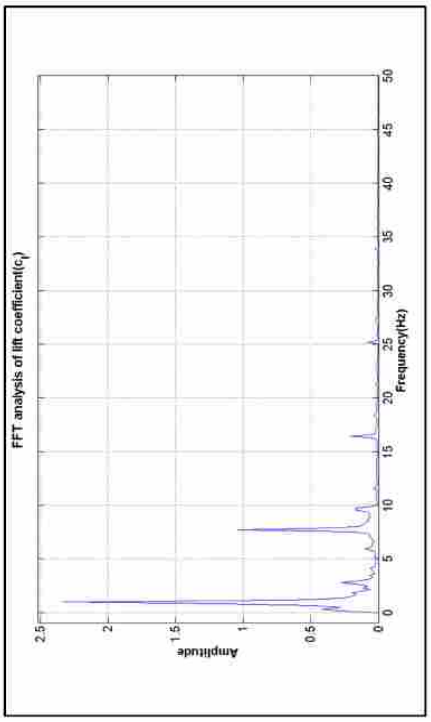


**Fig. (4.45):** Fast Fourier transform diagram of lift force coefficient at Reynolds number 300, frequency ratio 1 and oscillation amplitude 16 degree.

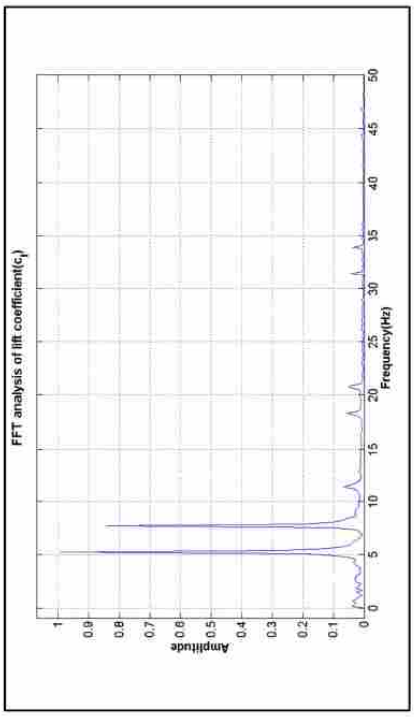


**Fig. (4.46):** Fast Fourier transform diagram of lift force coefficient at Reynolds number 300, frequency ratio 1.5 and oscillation amplitude 10 degree.

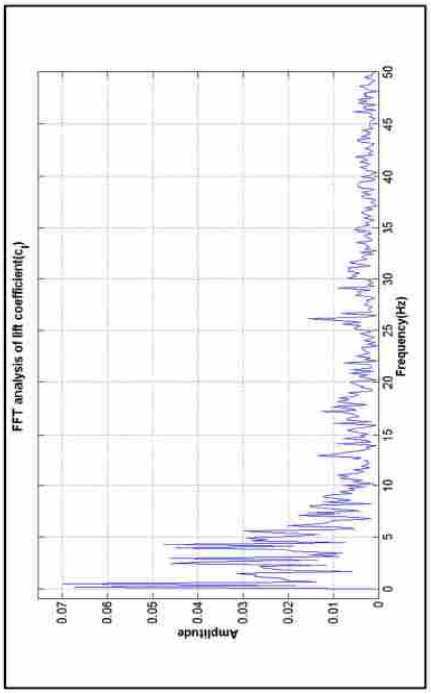


**Fig. (4.47):** Fast Fourier transform diagram of lift force coefficient at Reynolds number 300, frequency ratio 1.5 and oscillation amplitude 16 degree.

In all Figs. (4.36) to (4.47) there is a pick in oscillation frequency of planes. The amplitude of this pick is lower than that of the other picks. In other word, the effects of oscillatory motion of wings in very short amplitude can be observed in the behavior of lift coefficient during the time. It should be noted that unlike the symmetric geometry, the behavior of upper half of the domain is not similar to the behavior of the lower half. As a result, it can conclude that the wings' motion has effect o the lift coefficient. These graphs clearly show that the oscillatory motion has effect on the behavior of the lift force and this effect is negligible compares with the effect of other aerodynamic phenomena.

Generally, the graphs presented here, and those were not presented, can be divided in three basic categories. The first category is those graphs wherein the separate and distinguishable picks have been observed. In these plots, the waves are distinct from one another and the amplitudes of noises is low. In other word, the number of the effective waves on the lift coefficient is low and can be determined. In this category, frequency and amplitudes of the oscillations can be easily determined.

The second category includes those graphs wherein there are many effective picks. In fact, the amplitude of noises exist in FFT graph is of same order of waves' amplitude obtained from the aerodynamic phenomena and therefore it is not possible to distinguish between aerodynamic phenomena and noises. By comparing the amplitudes of the different waves shown in the graphs of the first and second categories, it can be concluded that in some special conditions, the amplitude of waves resulted from aerodynamic phenomena reduce dramatically. the reason having same order for amplitude of noises and amplitude of waves is due to this severe reduction in these waves. Given this small oscillation amplitude and because the oscillations of lift force occur around the zero value, it can be concluded that in this situation, the effect of oscillatory Karman vortices on the side force (lift) is practically eliminated.

The third category are those graphs wherein there is only one pick can be observed. These graphs are those wherein the frequency ration is 2.an example of these graphs is shown in Fig. (4.48).

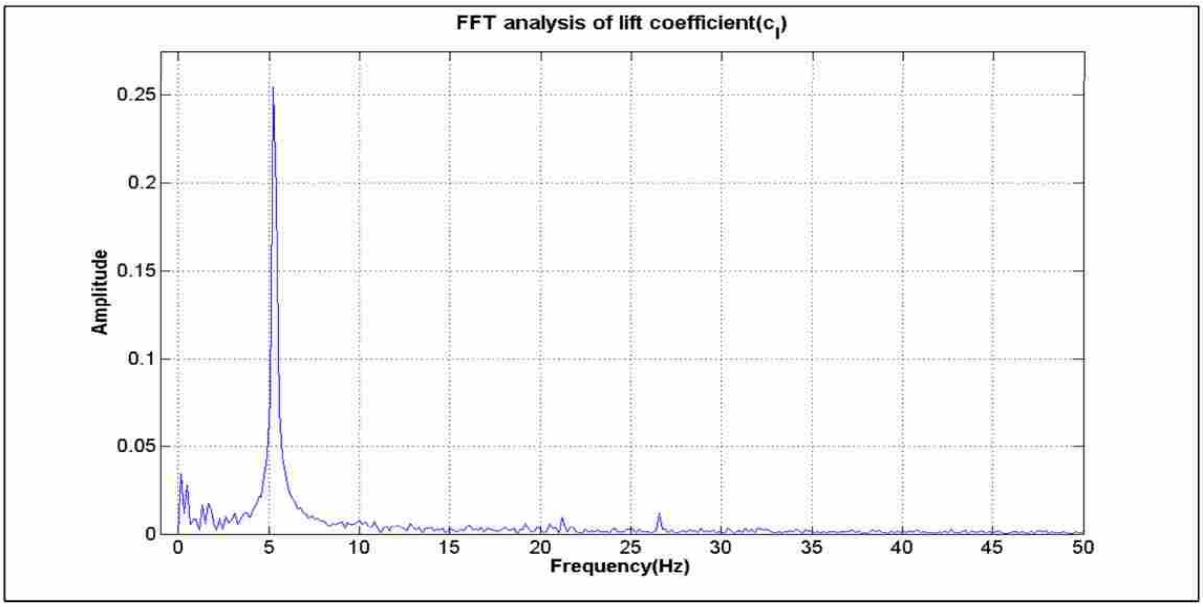


**Fig. (4.48):** Fast Fourier transform diagram of lift force coefficient at Reynolds number 200, frequency ratio 2 and oscillation amplitude 10 degree.

According to the categories obtained based on the shape of the FFT graphs, the behavior of flow can be divided in to three categories. The shape of separated vortices and also how the vortices formed, have some common properties in a same category which are different with the other categories. A more detailed explanation about these properties is presented in the next section.

In all graphs of the first category, there are two dominant picks. By investigating the frequencies of these picks and comparing them with the flow phenomena, it can be concluded that, with good accuracy, one of these two picks has is equivalent with the frequency of the vortex shedding. Also, the other pick indicates that there is an aerodynamic oscillatory phenomenon in the field. The justification for this existence and its relation to the shape of the vortices are discussed in the next section.

In the following table, the values related to frequencies of picks equal to the vortex shedding for different variables are provided. The empty boxes of this table is for the simulations wherein its FFT lift coefficient graph is in the second category.

**Table (4.5):** Comparison of vortex shedding frequency extracted from the FFT of lift force coefficient.

| **Frequency ratio** | **Reynolds number** | | |
|---|---|---|---|
| Frequency amplitude (degree) | **200** | **250** | **300** |
| **0.75** | | | |
| 10 | 5.158 | 6.667 | 8.216 |
| 14 | 5.006 | 6.512 | 7.884 |
| 16 | 5.009 | 6.41 | 7.723 |
| 18 | 4.856 | 6.24 | 7.72 |
| **1** | | | |
| 10 | 5.158 | 6.917 | 7.727 |
| 14 | 5.006 | 6.671 | 8.21 |
| 16 | 5.005 | 6.371 | 7.725 |
| 18 | 4.851 | 6.224 | 7.553 |
| **1.25** | | | |
| 10 | 5.158 | 6.616 | 8.216 |
| 14 | 4.854 | 6.203 | 7.596 |
| 16 | 4.701 | 6.078 | 7.392 |
| 18 | - | - | - |
| **1.5** | | | |
| 10 | 5.006 | 6.568 | 7.725 |
| 14 | 4.854 | 6.345 | 7.362 |
| 16 | - | - | - |
| 18 | - | - | - |
| **2** | | | |
| 10 | 5.253 | 7.177 | 8.623 |
| 14 | - | - | - |
| 16 | - | - | - |
| 18 | - | - | - |

Given that the frequencies presented in the Table (4.5) are equal to the frequency of vortex shedding, therefore these values are used based on the relation of Strouhal number, Table (4.6) presents the calculated Strouhal number.

**Table (4.6):** Strouhal number calculated with the frequency extracted from the FFT of lift force coefficient.

| **Frequency ratio**<br><br>Frequency amplitude (degree) | **Reynolds number** | | |
|---|---|---|---|
| | **200** | **250** | **300** |
| **0.75** | | | |
| 10 | 0.177 | 0.183 | 0.188 |
| 14 | 0.174 | 0.178 | 0.180 |
| 16 | 0.171 | 0.176 | 0.176 |
| 18 | 0.166 | 0.171 | 0.176 |
| **1** | | | |
| 10 | 0.177 | 0.190 | 0.199 |
| 14 | 0.171 | 0.183 | 0.187 |
| 16 | 0.171 | 0.175 | 0.176 |
| 18 | 0.166 | 0.171 | 0.172 |
| **1.25** | | | |
| 10 | 0.177 | 0.181 | 0.188 |
| 14 | 0.166 | 0.170 | 0.173 |
| 16 | 0.161 | 0.167 | 0.169 |
| 18 | 0.228 | 0.242 | 0.247 |
| **1.5** | | | |
| 10 | 0.171 | 0.180 | 0.176 |
| 14 | 0.166 | 0.174 | 0.168 |
| 16 | 0.275 | 0.289 | 0.296 |
| 18 | 0.275 | 0.292 | 0.297 |
| **2** | | | |
| 10 | 0.180 | 0.197 | 0.197 |
| 14 | 0.365 | 0.387 | 0.397 |
| 16 | 0.365 | 0.387 | 0.397 |
| 18 | 0.365 | 0.387 | 0.397 |

It should be noted that for the boxes wherein their information is not available in the Table (4.5), calculation of Strouhal number based on the lift frequency is not possible. To calculate the Strouhal number for these cases, the graphs related to the FFT of drag force are used. the results show that, in these special cases, the frequency related to the drag force is equal to the vortex shedding. The values related to the corresponding houses are defined by underline symbol. The dramatic increase in frequency of vortex shedding and as a result in Strouhal number in the second category of the flow behavior are considerable.

The final analysis of the lift force coefficient is related to the third pick of the FFT graph (equal to the change in size of vortices in the first flow category). By investigating the behavior of videos obtained from the flow rotation graphs, it can be found that this phenomenon can be equal to the Karman vortex shedding but with smaller frequency than the vortex shedding. In other word, this phenomenon periodically changes the size of the separated vortices. The frequency of this phenomenon is extracted from FFT graphs and is presented in Table (4.7). According to Fig. (4.7) and comparing with Tables. (4.5) and (4.6), it is clear that the

aforementioned aerodynamic phenomenon only occurs in the second category of flow behavior. In other word, in the second category of flow behavior wherein the vortices are shedding simultaneously with the frequency equal to the oscillation frequency of wings, this phenomenon is not observed and the vortices are separated with same size without periodic change in size. By increasing the Reynolds number, the frequency of this phenomenon increases. Of particular note is the dramatic decrease in the size of the frequency in the oscillation of the wings at frequency ratio 1.

**Table (4.7):** The values of vortex shedding frequency extracted from the FFT of lift force coefficient for aerodynamic phenomenon of vortex size change.

| **Frequency ratio** | **Reynolds number** | | |
|---|---|---|---|
| Frequency amplitude (degree) | **200** | **250** | **300** |
| **0.75** | | | |
| 10 | 1.124 | 1.5 | 1.643 |
| 14 | 1.062 | 1.232 | 1.478 |
| 16 | 0.9107 | 1.151 | 1.314 |
| 18 | 0.9105 | 0.9852 | 1.15 |
| **1** | | | |
| 10 | 0.1517 | 0.1537 | 0.1818 |
| 14 | 0.3034 | 0.3336 | 0.4926 |
| 16 | 0.455 | 0.6887 | 0.9862 |
| 18 | 0.4548 | 0.8118 | 1.149 |
| **1.25** | | | |
| 10 | 1.517 | 2.127 | 2.793 |
| 14 | 1.82 | 2.449 | 3.137 |
| 16 | 1.971 | 2.628 | 3.449 |
| 18 | - | - | - |
| **1.5** | | | |
| 10 | 2.882 | 3.941 | 5.26 |
| 14 | 3.186 | 4.23 | 5.644 |
| 16 | - | - | - |
| 18 | - | - | - |
| **2** | | | |
| 10 | - | - | - |
| 14 | - | - | - |
| 16 | - | - | - |
| 18 | - | - | - |

### 4.2.3. Qualitative Properties of the flow and shape of vortices

In addition to qualitative investigation done before, the qualitative properties of flow include shape of vortices and the relation between these shapes with the FFT graphs presented in previous sections are studied. As mentioned earlier, the shape of vortices in some simulations have very interesting properties which are related to the additional picks or/and noise exist in the FFT graphs of the lift force. In some simulations, the vortices are separated from the geometry simultaneously. It is while that in Karman vortex shedding phenomenon, the vortices are periodically shed, once from top and then from the down.

In FFT lift coefficient graphs for a case where vortices are simultaneously separated, distinguishing different waves is not possible. In other word, the FFT graphs of the simulations in which vortices are separated simultaneously are located in second category of FFT graphs.

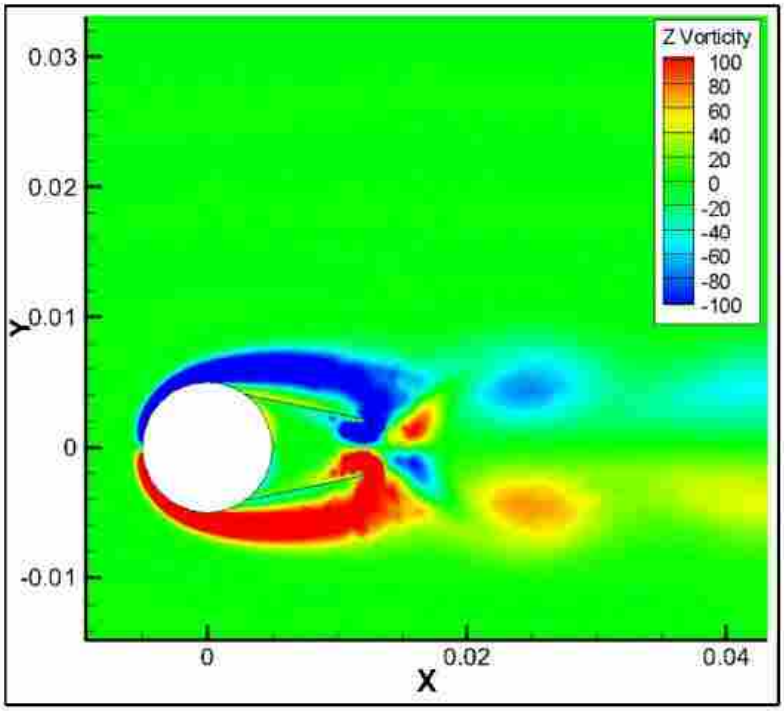


**Fig. (4.49):** Contour of flow vorticity vector for simulation at Reynolds number 200, frequency ration 2 and frequency amplitude 18 degree.

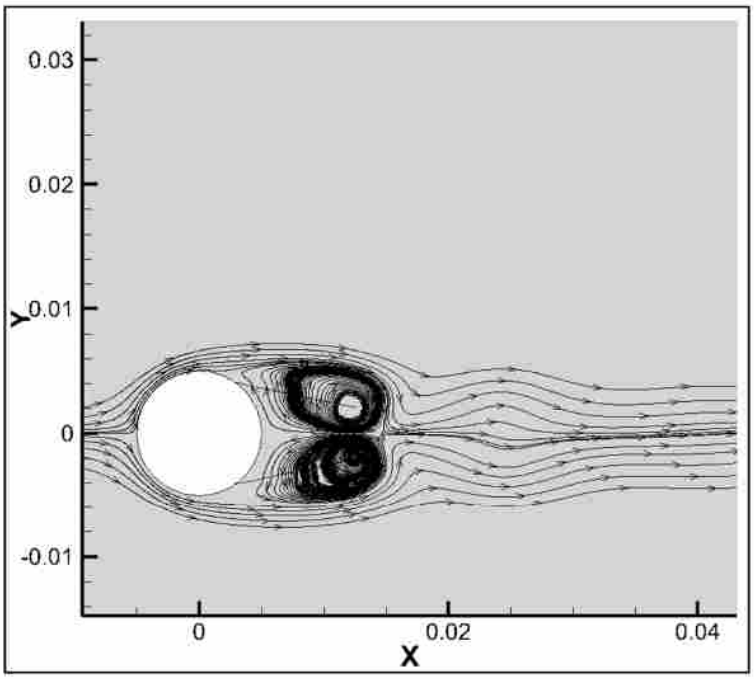


**Fig. (4.50):** Flow streamlines for simulation at Reynolds number 200, frequency ration 2 and frequency amplitude 18 degree.

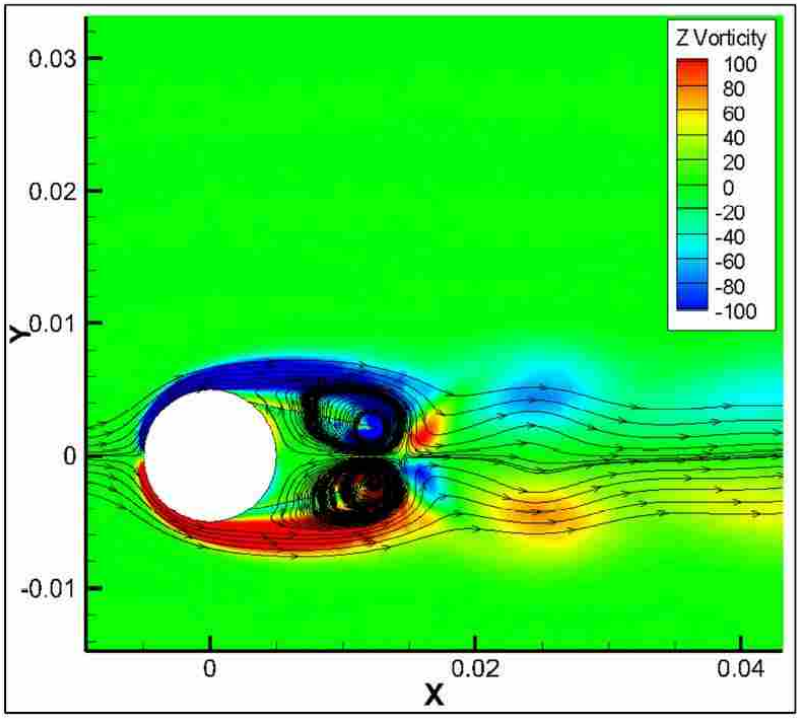


**Fig. (4.51):** Superposition of flow streamlines and contours for simulation at Reynolds number 200, frequency ration 2 and frequency amplitude 18 degree.

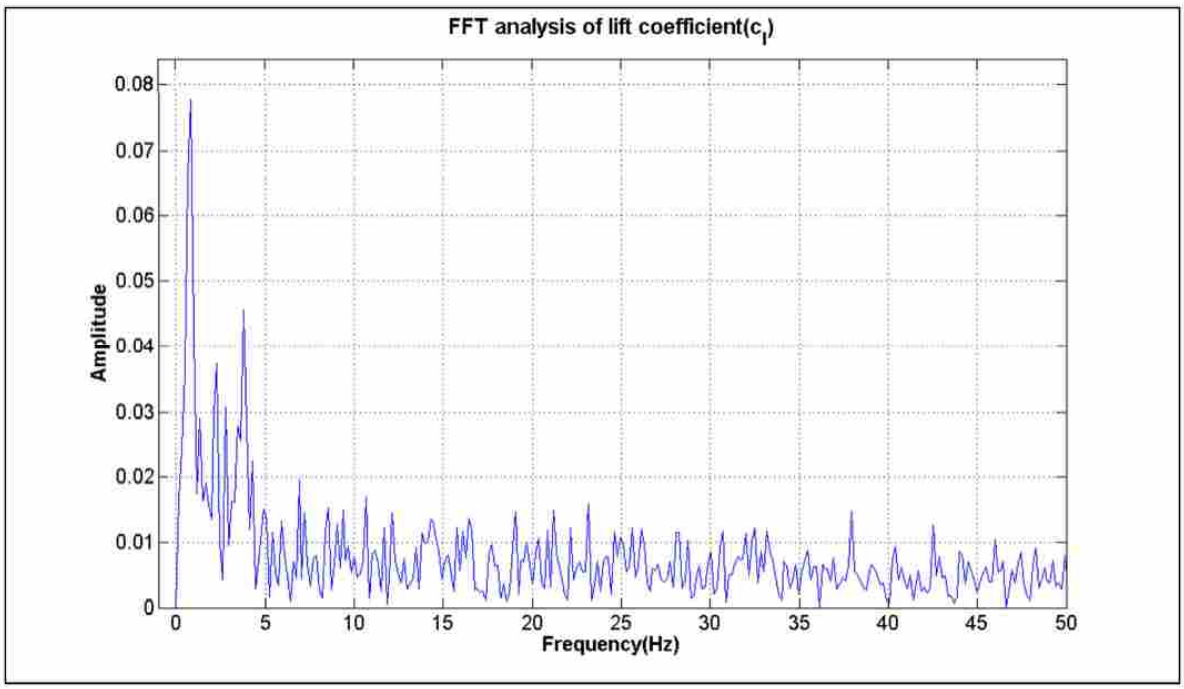


**Fig. (4.52):** Lift force coefficient FFT graph at Reynolds number 200, frequency ration 2 and frequency amplitude 18 degree.

Figs. (4.49) and (4.50) shows the flow vorticity contour and streamlines around a cylinder equipped with moving wings. In Fig. (5.41) the superposition of these two graphs is shown to determine the relation between the vorticity field and the vortices. The oscillation amplitudes of the wings, in this simulation, is 18-degree ant their oscillation is twice the natural frequency of vortex shedding. This simulation is performed at Re=200. As can be seen from Fig. (4.52), the vortices are shed simultaneously and fully symmetric. On the other hand, in this figure the symmetric of streamlines confirm the simultaneous vortices. Fig. (4.52) shows the FFT graphs related to this simulation. As can be seen, this graph has all properties of the second category FFT graphs. The amplitude of oscillations is very small and the noises and main waves are not distinguishable. In the other cases, the simultaneous vortex shedding is equal to the second category FFT graph.

For better understanding of the problem physic, the pressure and velocity contours are also evaluated. Fig. (4.53) shows the static pressure contours. The symmetricity of the field respect to the horizontal axis is quite clear and is in agreement with the symmetricity of the streamlines and vorticity graphs. As mentioned before, this symmetricity indicated the dissipation of lift force and the FFT of lift force coefficient shows this quantitively.

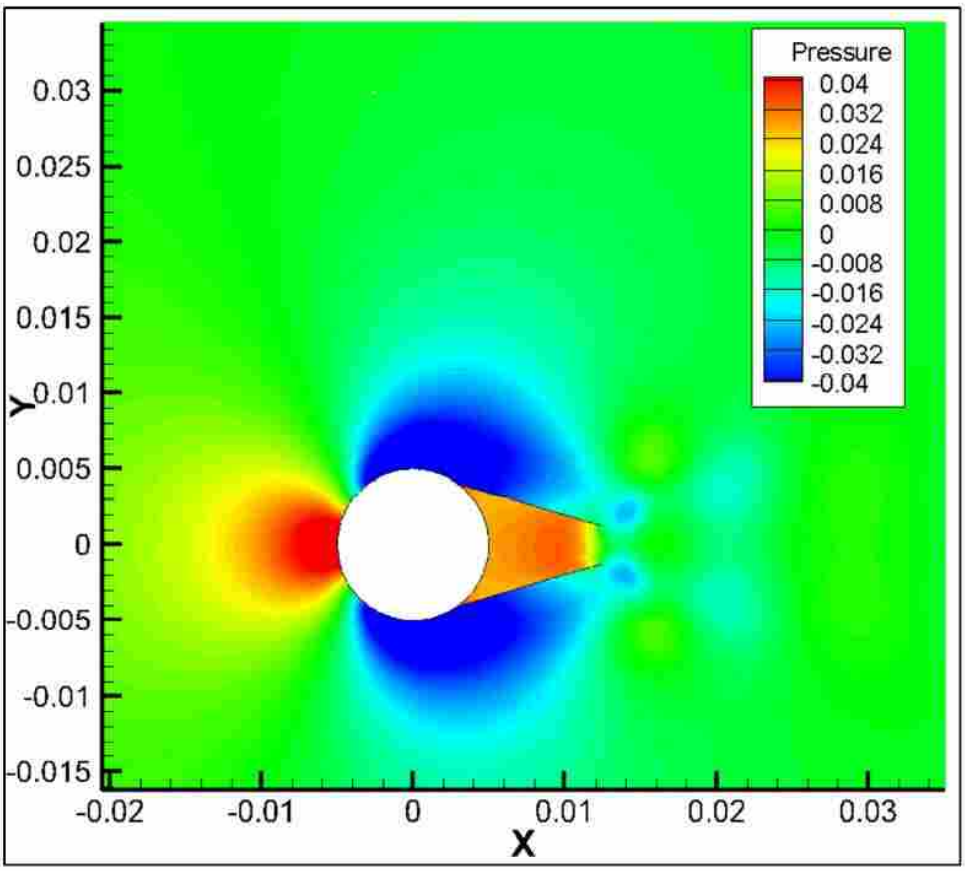


**Fig. (4.53):** Contours of the static pressure for simulation at Re=200, frequency ratio 2 and oscillation amplitude 18-degree.

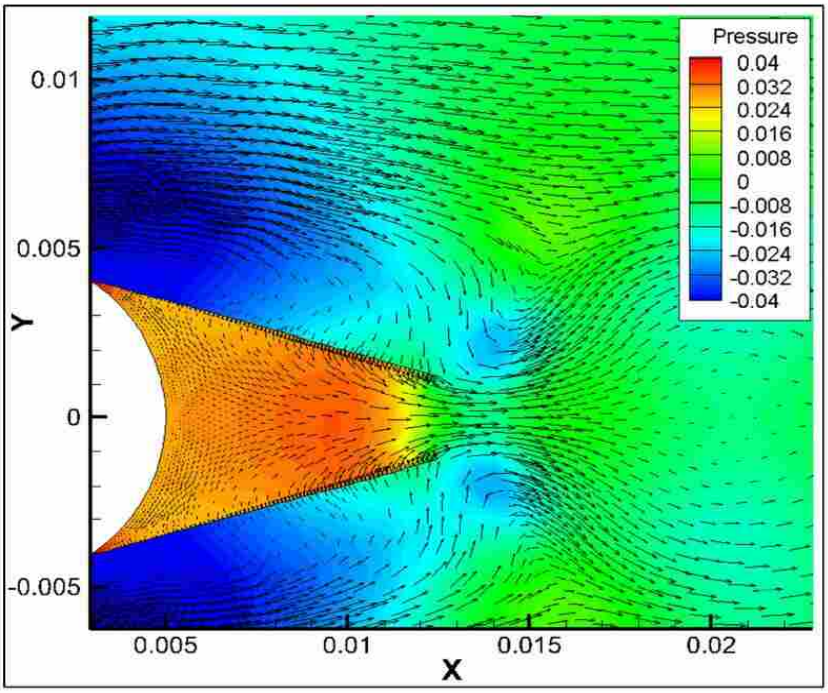


**Fig. (4.53):** Superposition of static pressure contours and velocity vectors for simulation at Re=200, frequency ratio 2 and oscillation amplitude 18-degree.

In Fig. (4.53) wings are getting closer to each other. An increase in pressure in the region between two wings illustrated this.

Given the Fig. (4.54), pressure increase in the region between these two wings leads to form a jet-like flow which exit this region. Immediately after exiting flow from the region between two wings, two vortices are forming on the tip of the wings and at downstream there are two vortices which are separated from the geometry simultaneously. The path of the velocity vector perfectly shows the presence of the vortices.

Fig. (4.55) shows the superposition of the velocity vector and pressure contour. In this figure, wings are moving away from each other and therefore the pressure in the region between two wings reduced. This reduction leads to a suction of flow in to this region. Vortices which are forming on the tip of the wings are shown by the velocity vectors.

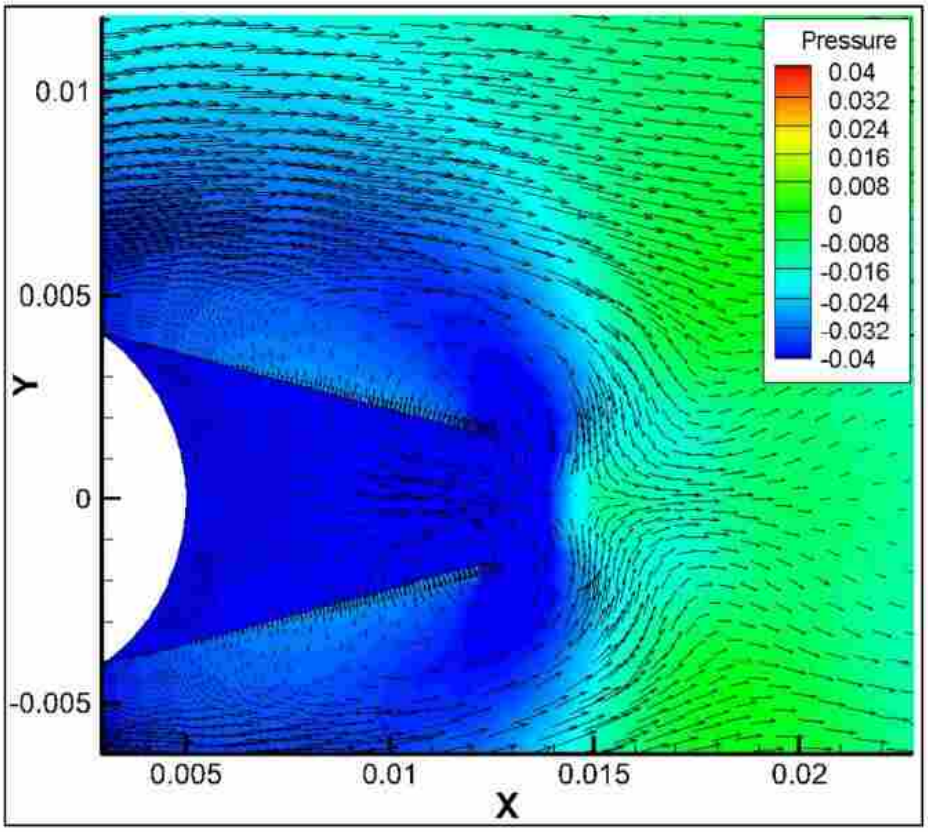


**Fig. (4.55):** Superposition of static pressure contours and velocity vectors for simulation at Re=200, frequency ratio 2 and oscillation amplitude 18-degree.

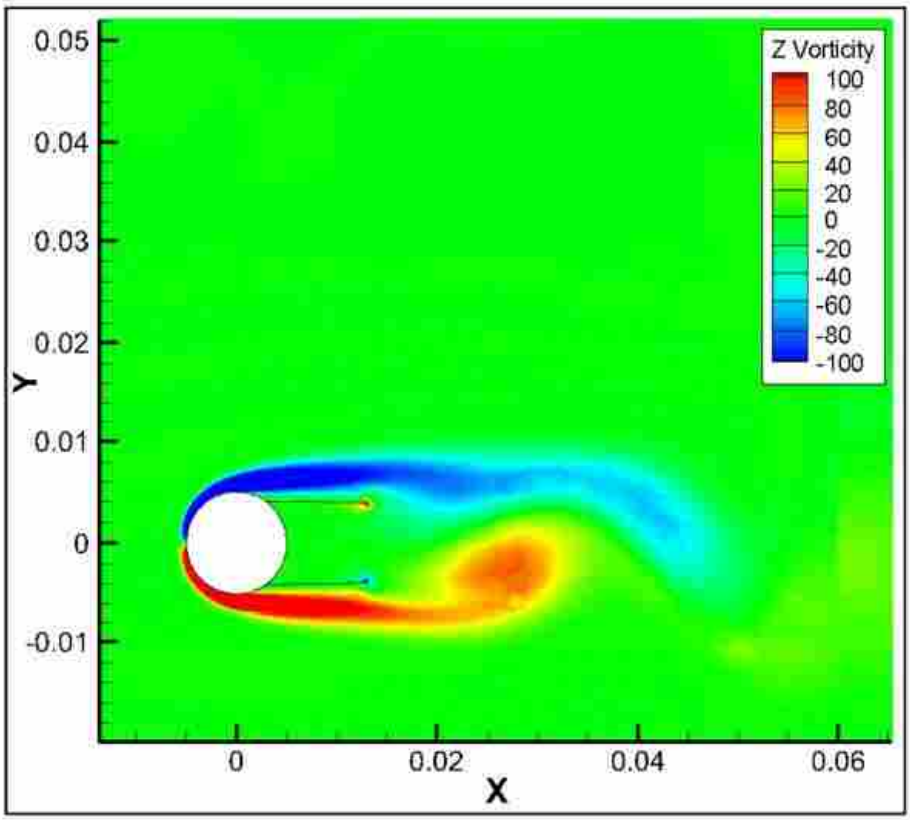


**Fig. (4.56):** Flow vorticity contours for simulation at Re=200, frequency ratio 0.75 and oscillation amplitude 10-degree.

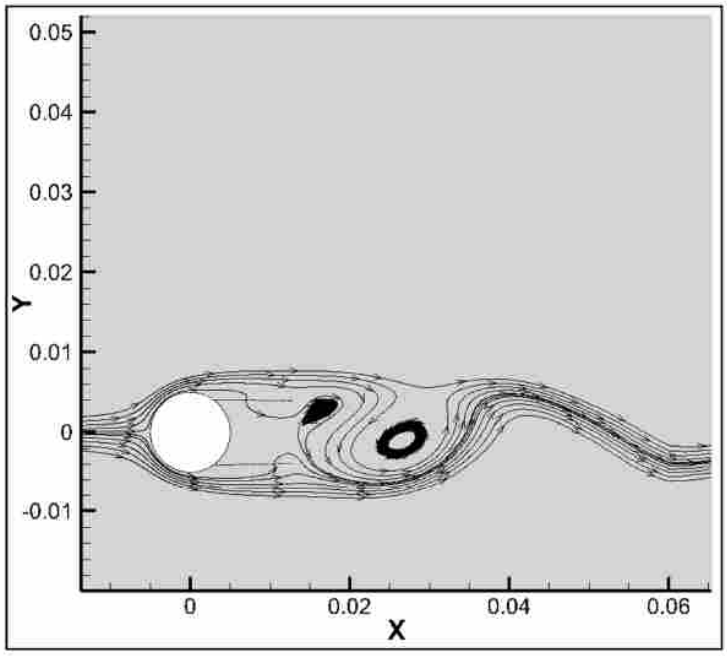


**Fig. (4.57):** Streamlines for simulation at Re=200, frequency ratio 0.75 and oscillation amplitude 10-degree.

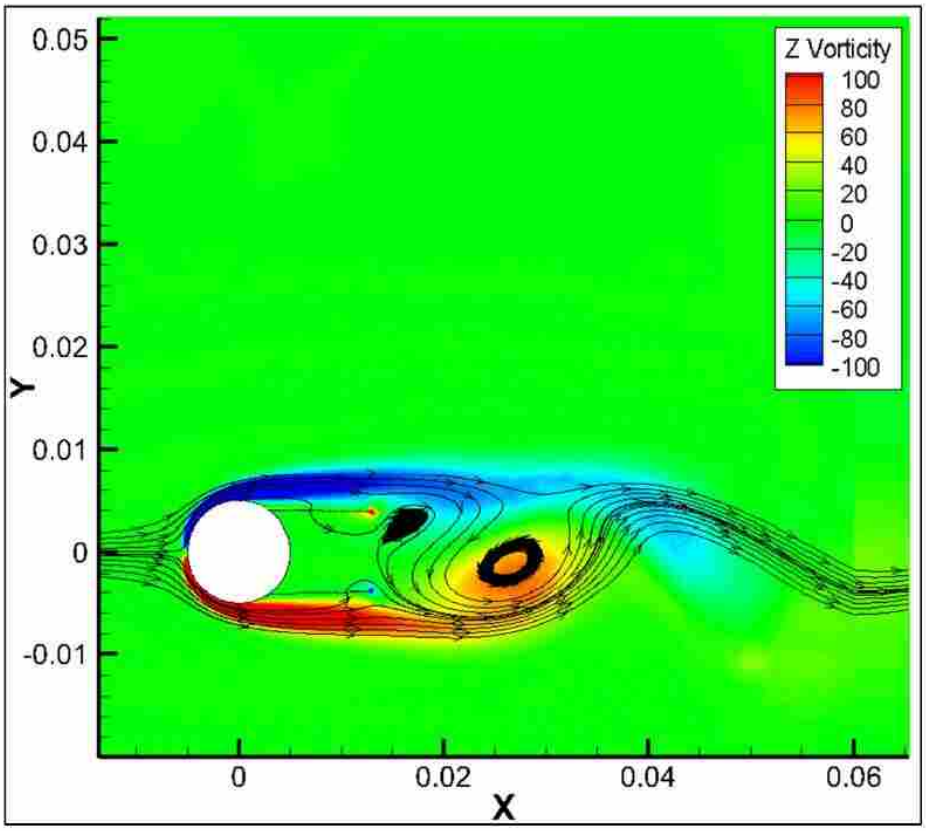


**Fig. (4.58):** Superposition of flow vorticity contours and velocity vectors for simulation at Re=200, frequency ratio 0.75 and oscillation amplitude 10-degree.

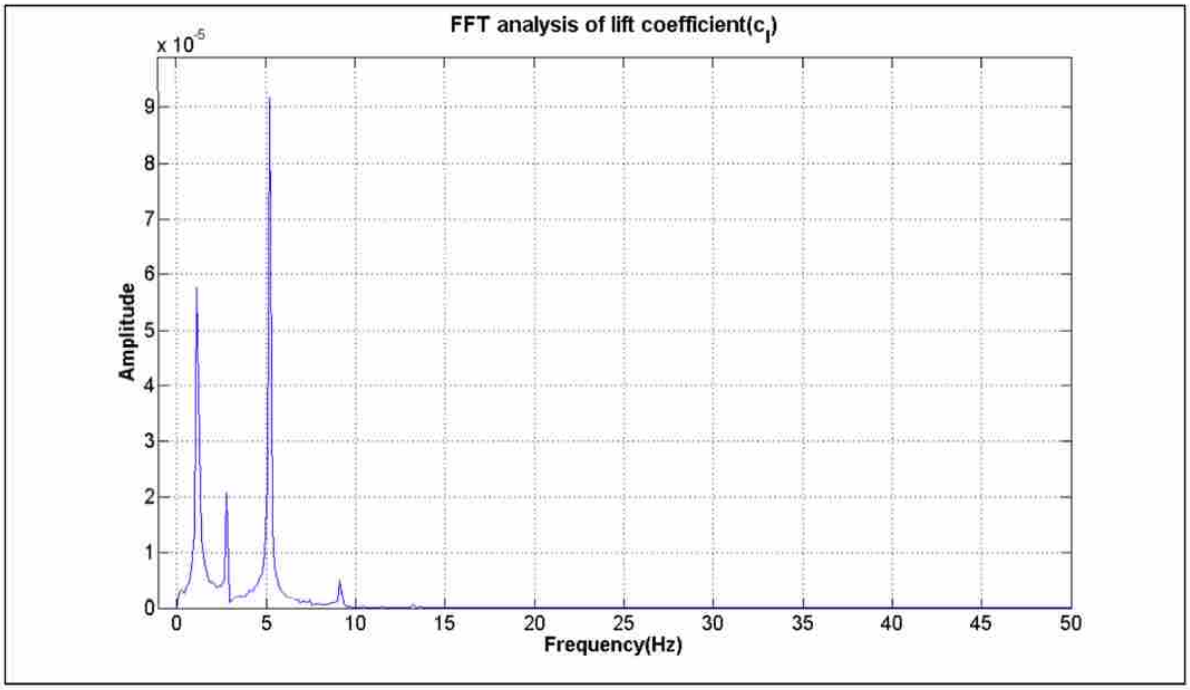


**Fig. (4.59):** Lift force coefficient FFT graph at Reynolds number 200, frequency ration 0.75 and frequency amplitude 10 degree.

Same as for Figs. (4.49)-(4.51), Figs (4.56)-(4-58) show the vorticity contour, streamlines, and superposition of vorticity contour and the streamlines for a same simulation. In this simulation, the oscillation amplitude of the wings is equal to 10-degree, their oscillation frequency is 0.75 which is equal to the natural frequency of vortex shedding. This simulation has been performed at Re=200.as can be seen, the general shape of the vortex shedding is same as the vortex shedding in the Von-Karman shedding phenomenon. Fig. (459) shows the FFT lift force coefficient graph for the considered simulation. It was previously described that one of the picks available in the FFT graph follows the vortex shedding with good approximation. Another pick is resulted from the effect of oscillations of the wings. The third pick shows a phenomenon in which the vortex shedding occurred more slowly than the other two phenomena. By investigating the shape of the vortex shedding during the time, it can be seen that the vortices are not separated from the surface with same size. The size variation of the vortices separated at different time steps itself has an oscillatory behavior. Investigating the animations obtained from the simulation show this behavior quite clear. Also, it can be seen that the slowest frequency of the phenomena observed in the FFT graph shows the size of the vortices with very good approximation.

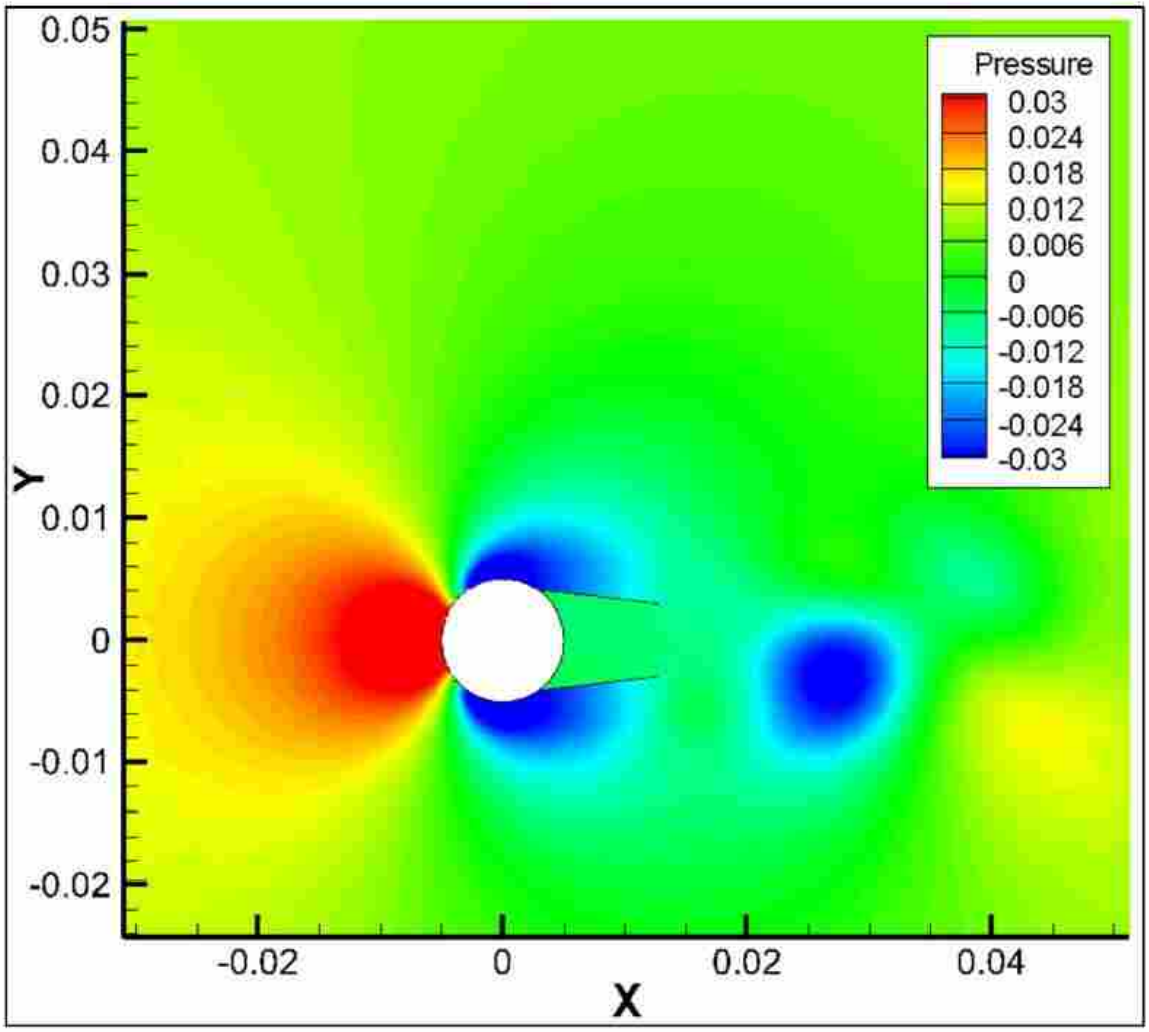


**Fig. (4.60):** Contours of the static pressure for simulation at Re=200, frequency ratio 0.75 and oscillation amplitude 10-degree.

In Fig. (4.60), wings are getting closer to each other. Increase in pressure in the region between two wings is much lower than that of the second category of the flow. The reason behind this difference in the pressure increase is that in the second category, the pressure field around the geometry only follows the movement of the wings and there is no other oscillatory phenomenon that has effect on it. But, in the first category, in addition to oscillation of the sings, the oscillation of the sized of the separated vortices (which are equivalent to the oscillation of the pressure field) is also effects on the field. Another dramatic difference between the graphs of two arrangement with different wings' oscillation (Figs. (4.53) and (4.60)) is the lack of symmetricity of flow respect to the horizontal axis in an arrangement with smaller oscillation. The difference between the first and second flow can be clearly seen in the pressure contours.

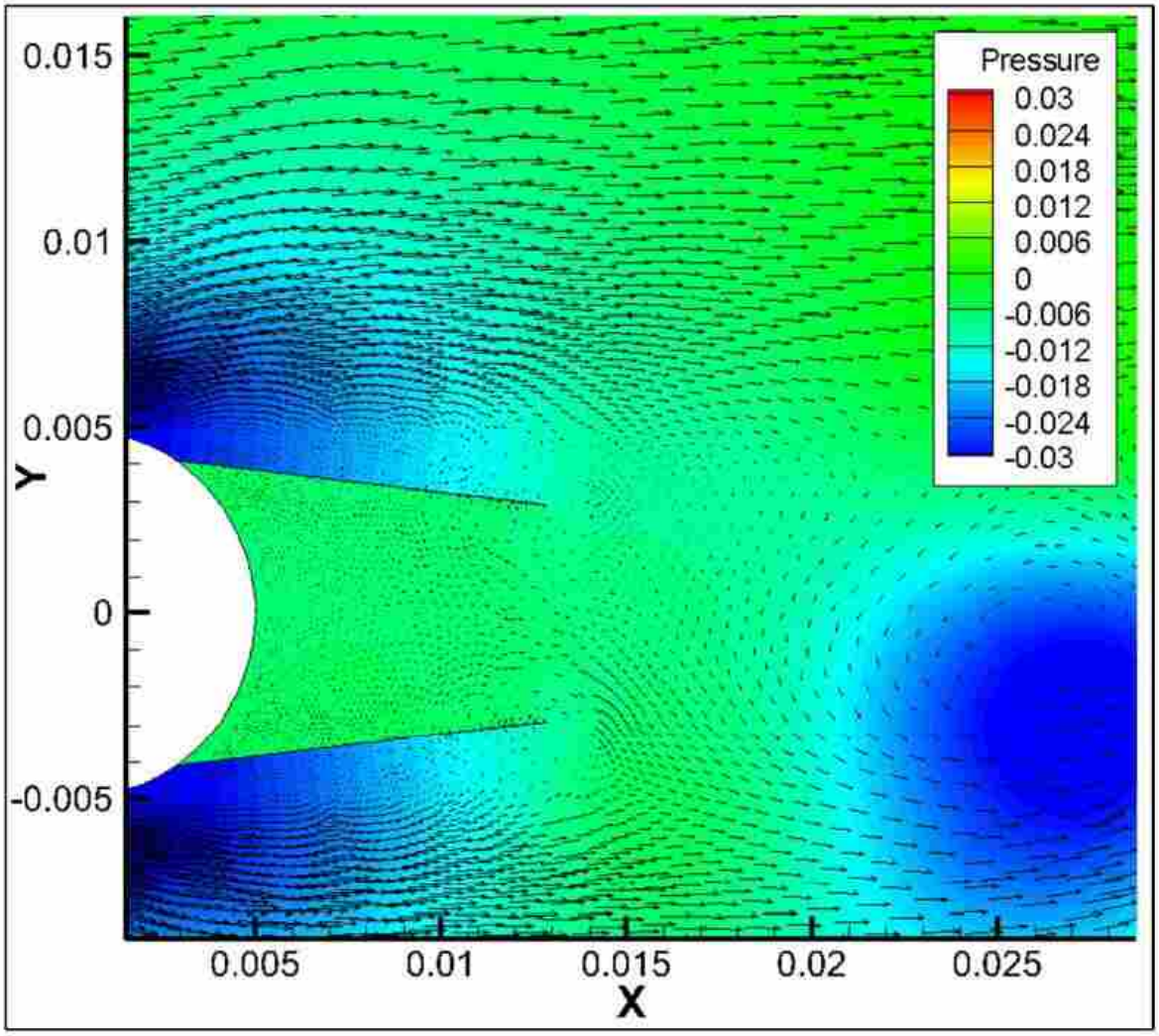


**Fig. (4.61):** Superposition of static pressure contours and velocity vectors for simulation at Re=200, frequency ratio 0.75 and oscillation amplitude 10-degree.

Unlike Fig. (4.54), in Fig. (4.61) an increase in pressure in the region between two wings is not too much that caused creating a jet-like flow. given the flow behavior in this category, two vortices are formed on the tip of the wings immediately after exiting from this region and then a big vortex separated from the bottom-wing can be observed. The main difference of this type with the second flow category is that the size of the vortex created on the tip of the bottom and top wings is not same which indicates the periodic behavior (like Karman vortices) of the vortex shedding. The path of the velocity vector shows the creation of the vortices quite clearly.

Fig. (4.62) shows the superposition of static pressure contours and velocity vectors. In this figure, wings are moving away from each other, therefore the region between two vortices has reduced. This pressure reduction is not as much as the second flow category. As a result, the flow suction in to this region is much lower.

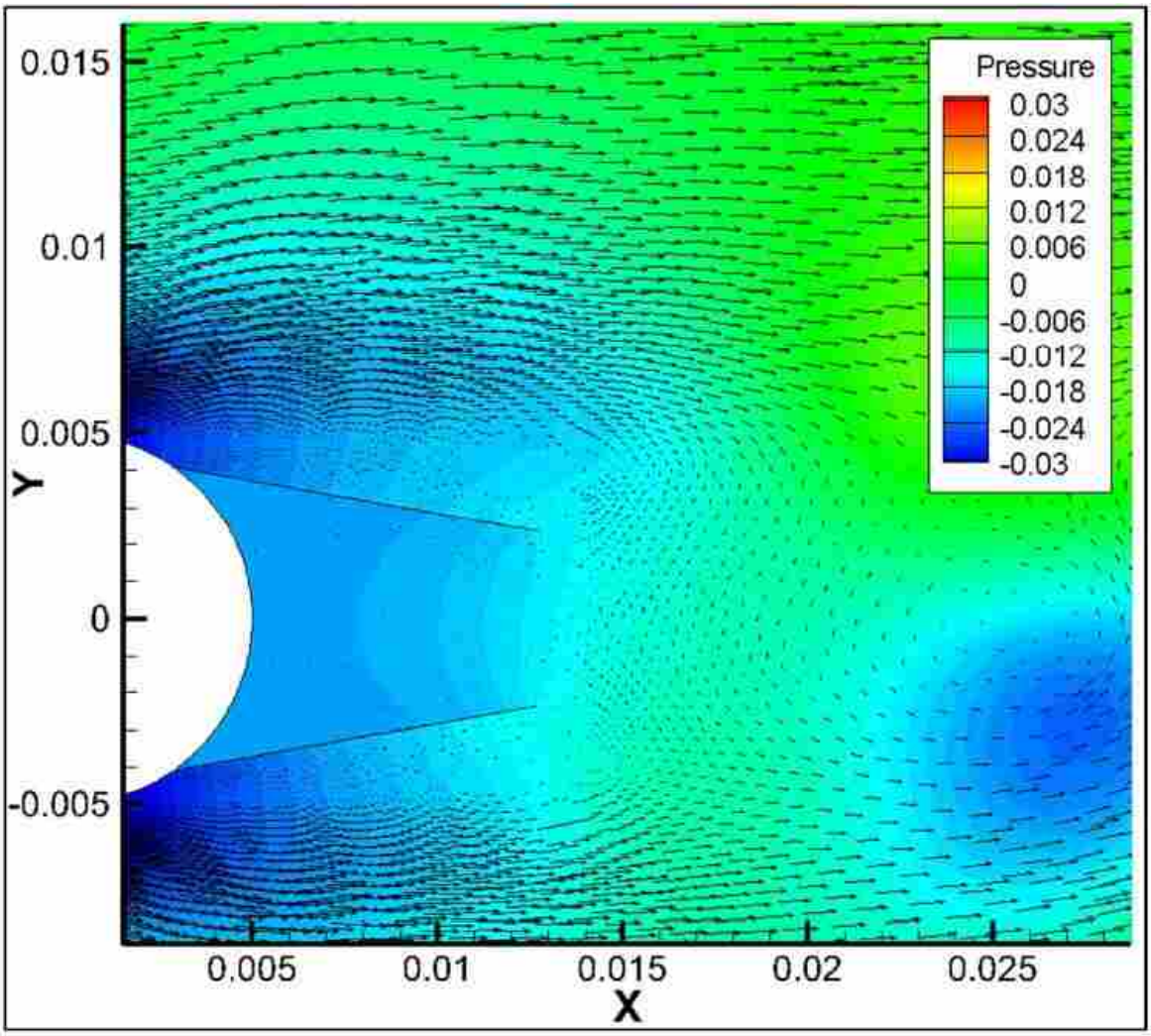


**Fig. (4.62):** Superposition of static pressure contours and velocity vectors for simulation at Re=200, frequency ratio 0.75 and oscillation amplitude 10-degree.

The following figures are provided to analyze the relation between the FFT graphs of the third category and the flow phenomena.

Figs. (4.63) to (6.65) shows the vorticity contour, streamlines and the superposition of vorticity contours and the streamlines, respectively. Simulation has been performed at Re=200 and the oscillation amplitude of the wings is 10-degree. Also, the oscillation frequency of the wings is twice the natural frequency of vortex shedding at same Reynolds number.

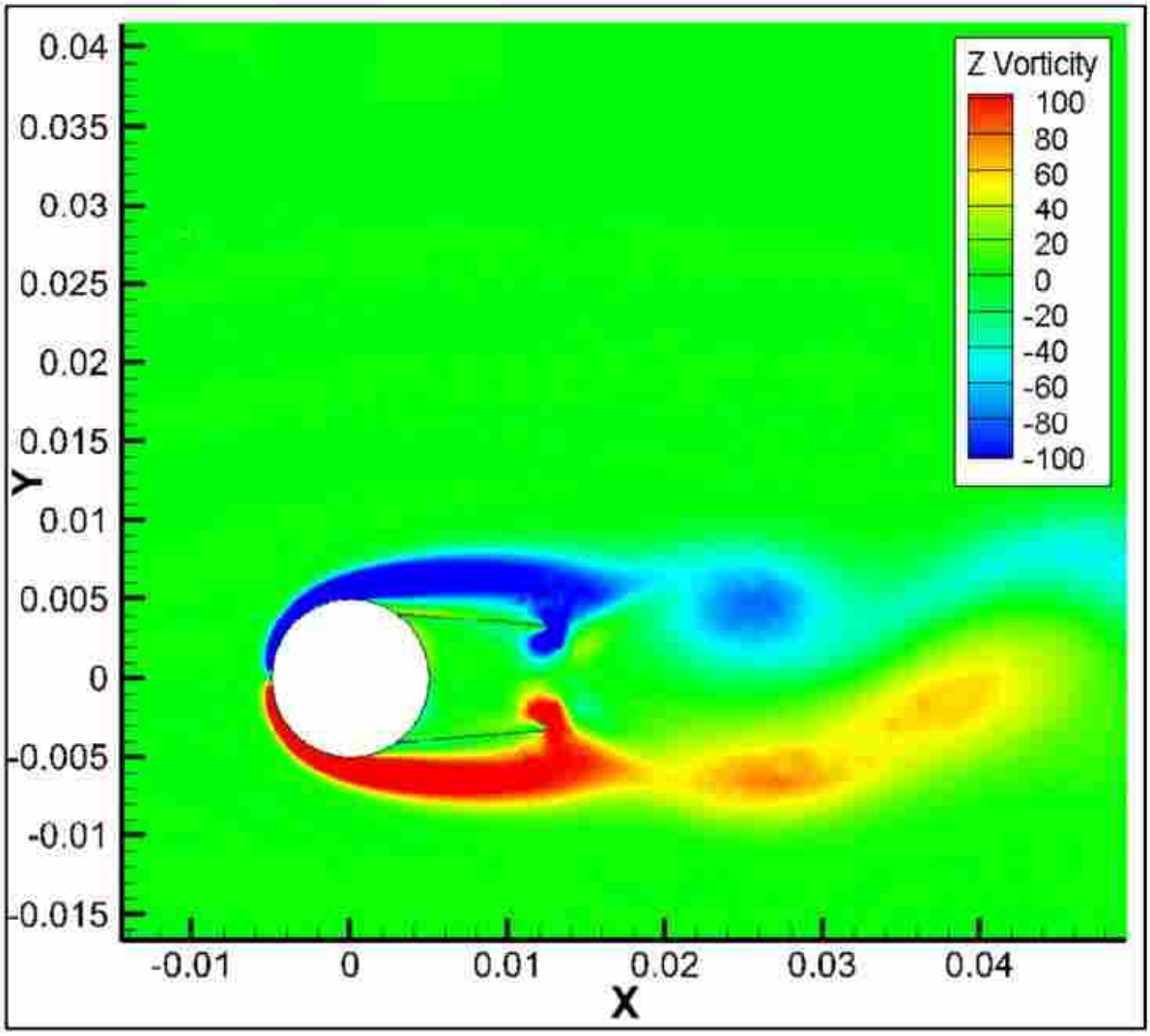


**Fig. (4.63):** Contours of the static pressure for simulation at Re=200, frequency ratio 2 and oscillation amplitude 10-degree.

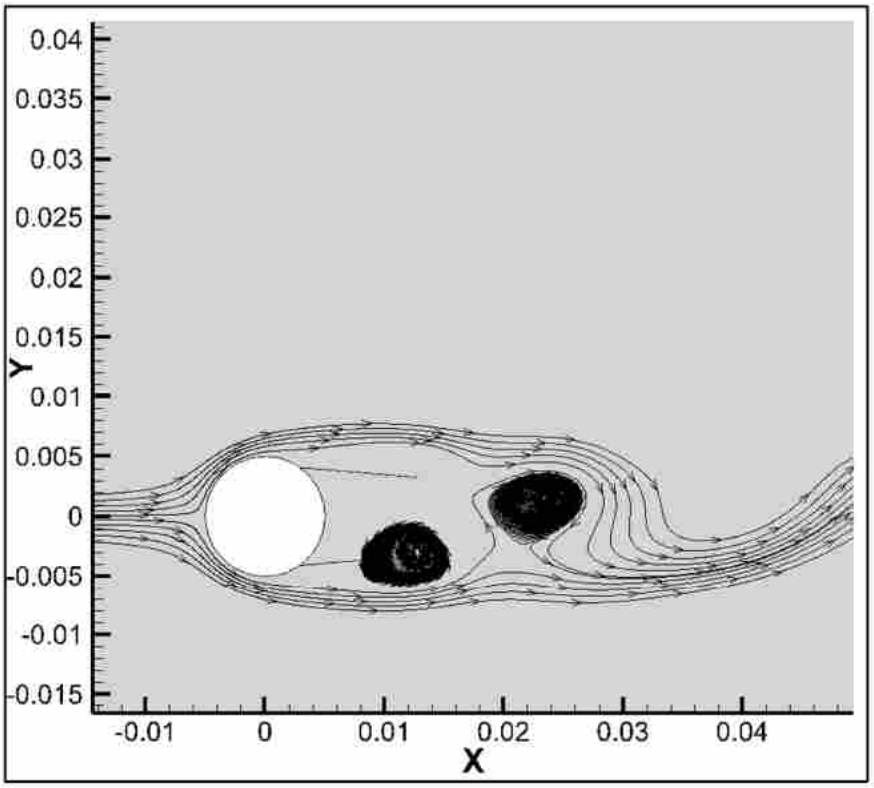


**Fig. (4.64):** Streamlines for simulation at Re=200, frequency ratio 2 and oscillation amplitude 10-degree.

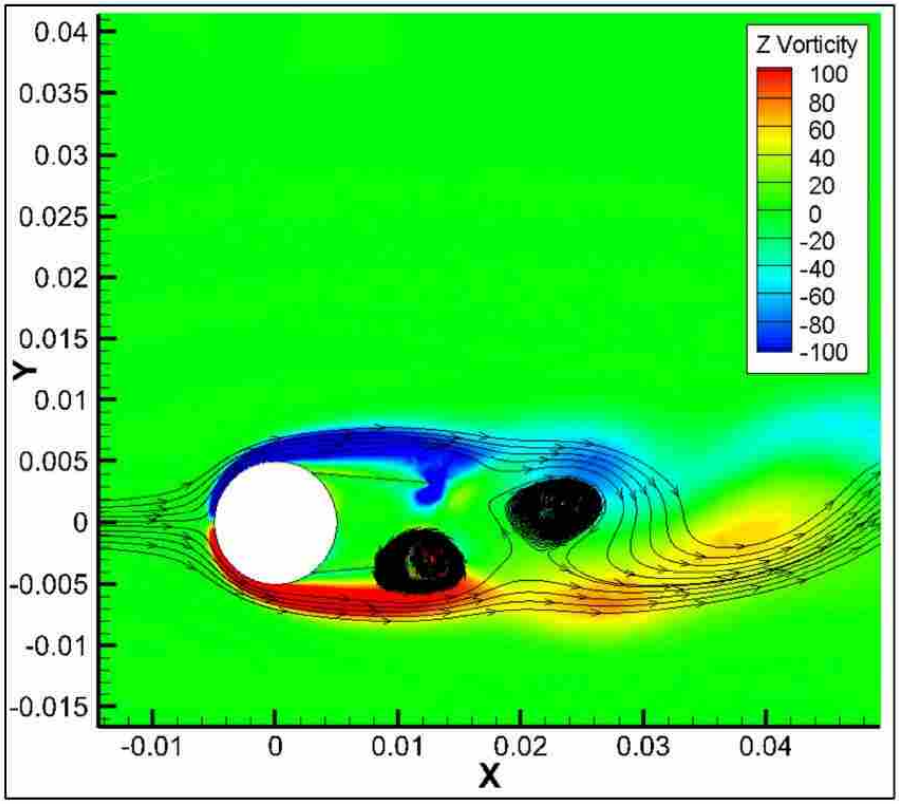


**Fig. (4.65):** Superposition of flow vorticity contours and velocity vectors for simulation at Re=200, frequency ratio 2 and oscillation amplitude 10-degree.

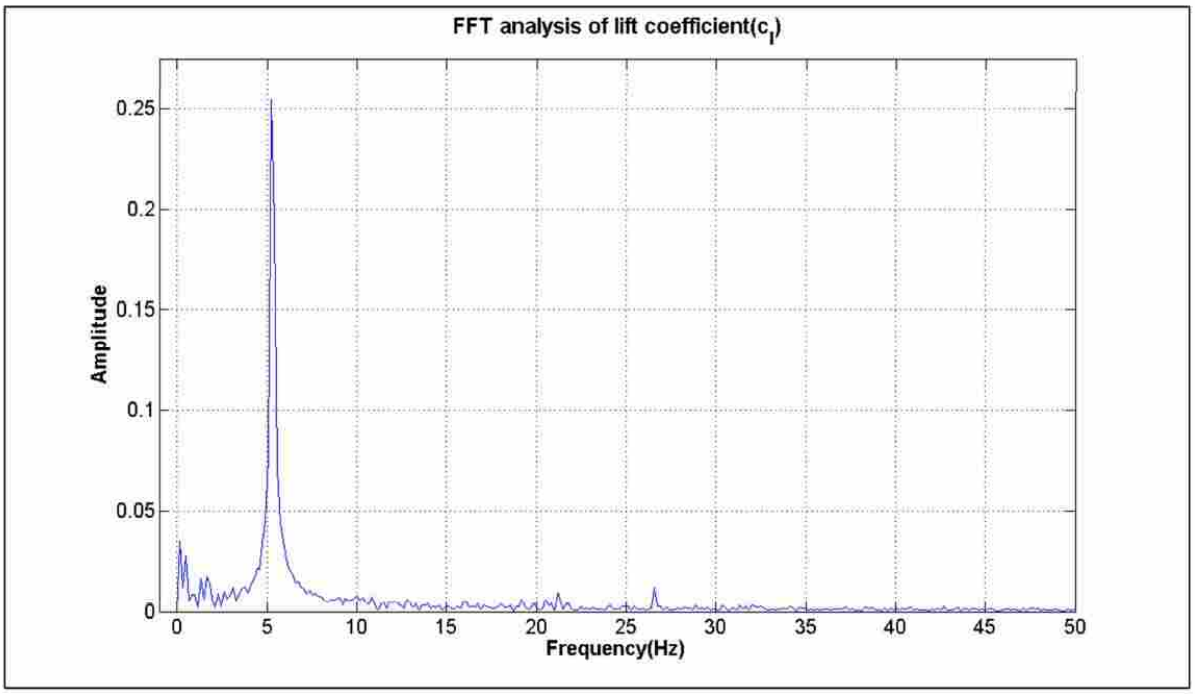


**Fig. (4.66):** Lift force coefficient FFT graph at Reynolds number 200, frequency ration 2 and frequency amplitude 10 degree.

As can be seen from the FFT graph in Fig. (4-66), there is only one dominance phenomenon on the oscillations of the lift force. By investigating the frequency extracted from FFT graphs of the third category and comparing them with the frequency of vortex shedding it can be observed that the frequency extracted from the FFT graph is exactly equal to the frequency of vortex shedding. On the other hand, in the simulations related to the FFT graphs on the third category, in addition to the vortex shedding phenomenon, the presence of an aerodynamic phenomenon can be observed. Near the geometry, with every complete oscillation of wings, one vortex is created at the end of the wings. Given that the frequency of sings' oscillation is exactly twice the natural frequency of the vortex shedding, it is expected that the Von-Karman shedding phenomenon occurs at exactly frequency equal to the half of the oscillations of the wings. Superposition of the oscillation of wings and the tendency of vortices to shed lead to strength the natural vortex shedding. In fact, both vortices resulted from two consecutive oscillation are attached with each other and creates a bigger vortex region. Since the natural frequency of shedding is exactly half of the frequency of vortex shedding due to the oscillation of the wings, a bigger vortex region (results from attachment of two smaller vortices), are moving away from the geometry at the natural frequency shedding. This new vortex region has been considered as a criterion for calculating the vortex shedding. It should be noted that two small vortex regions are attached together near the geometry and immediately form bigger vortex region. This means that a region which is under effect of two smaller vortices is not too much wide. Also, the time of existence of two small vortices is very low and they attached together. Immediately after creation of this large vortex region, stimulation of field due to the tendency to natural shedding caused that the larger region moving away from the geometry with same natural frequency. This superposition can increase the oscillation amplitude of the lift coefficient. Fig. (4.67) shows the static pressure contours.

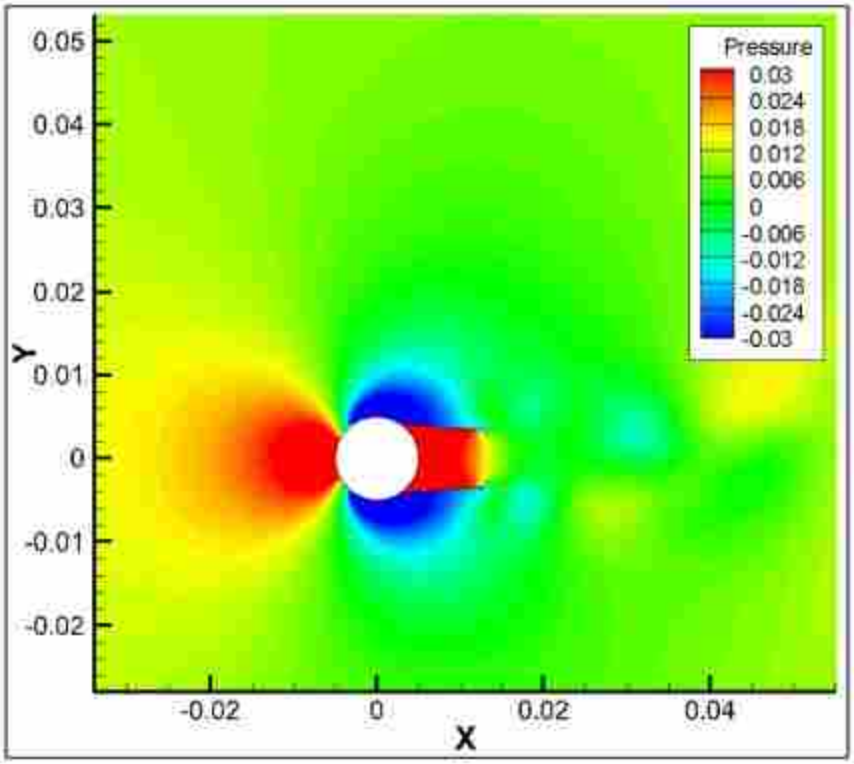


**Fig. (4.67):** Contours of the static pressure for simulation at Re=200, frequency ratio 2 and oscillation amplitude 10-degree.

In Fig. (4.67) wings are getting closer to each other. Increase in pressure in the region between two wings indicates this scenario. The reason of this dramatic difference of the contours between these two arrangements, which is the only difference between the oscillation amplitude of the wings (Figs. (4.53) and (4.67)), is the lack of symmetricity of the flow respect to the horizontal axis of the flow in arrangement with smaller oscillation amplitude. The small spots in this figure in which their pressure value is negative indicate the regions with vorticity or vortices.

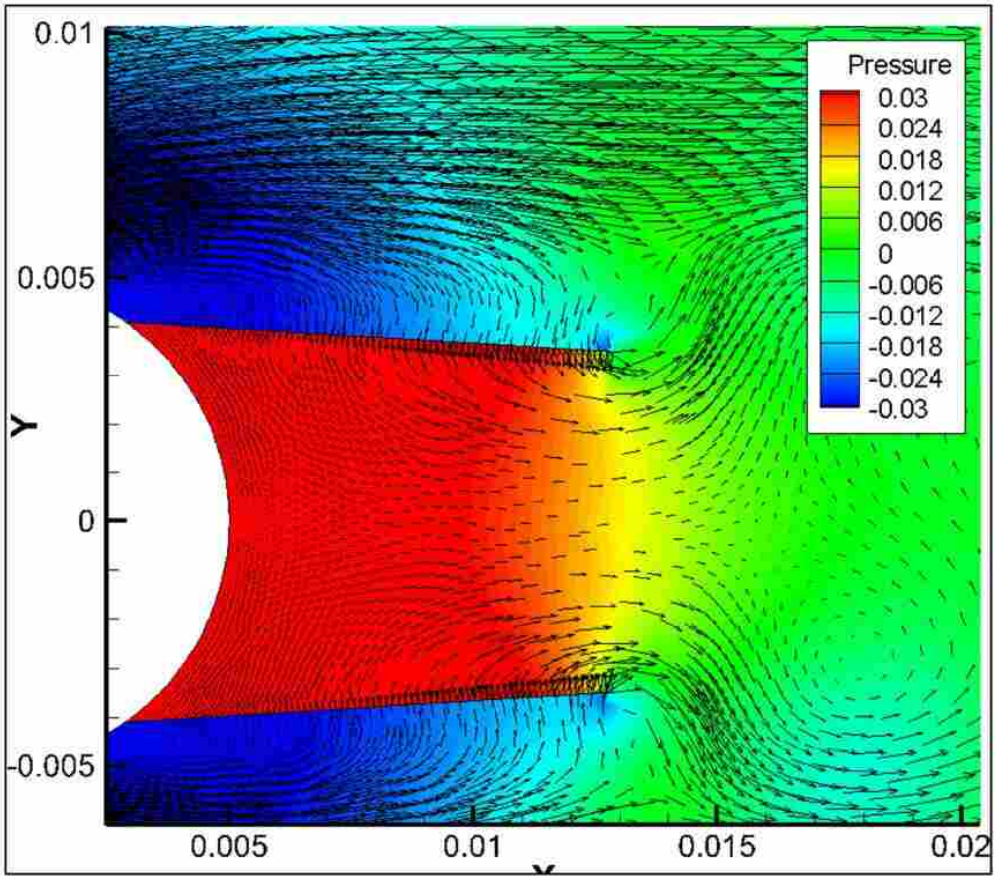


**Fig. (4.68):** Superposition of static pressure contours and velocity vectors for simulation at Re=200, frequency ratio 2 and oscillation amplitude 10-degree.

Same as with Fig. (4.54), in the Fig. (4.68) the increase in pressure in the region between two wings causes a jet-like flow to be created which exits from this region. Given the flow behavior in this category, two vortices which are created on the tip of the wings immediately after exiting from the region between these two wings can be observed. the main difference compare with the second category of flow is that the size of the vortices created on the tip of the top wing is different from than that of the bottom wing which indicates the periodic behavior (like Karman vortices) of the vortex shedding. The pass of velocity vectors shows the presence of these vortices quite clearly.

Fig. (4.69) also shows the superposition of pressure contour and velocity vectors plots. In this figure, wings are moving away from each other, therefore the pressure of the region between two wings reduces. This reduction in pressure has caused a flow suction in to this region. The vortices forming on the tip of the wings are shown using the velocity vectors.

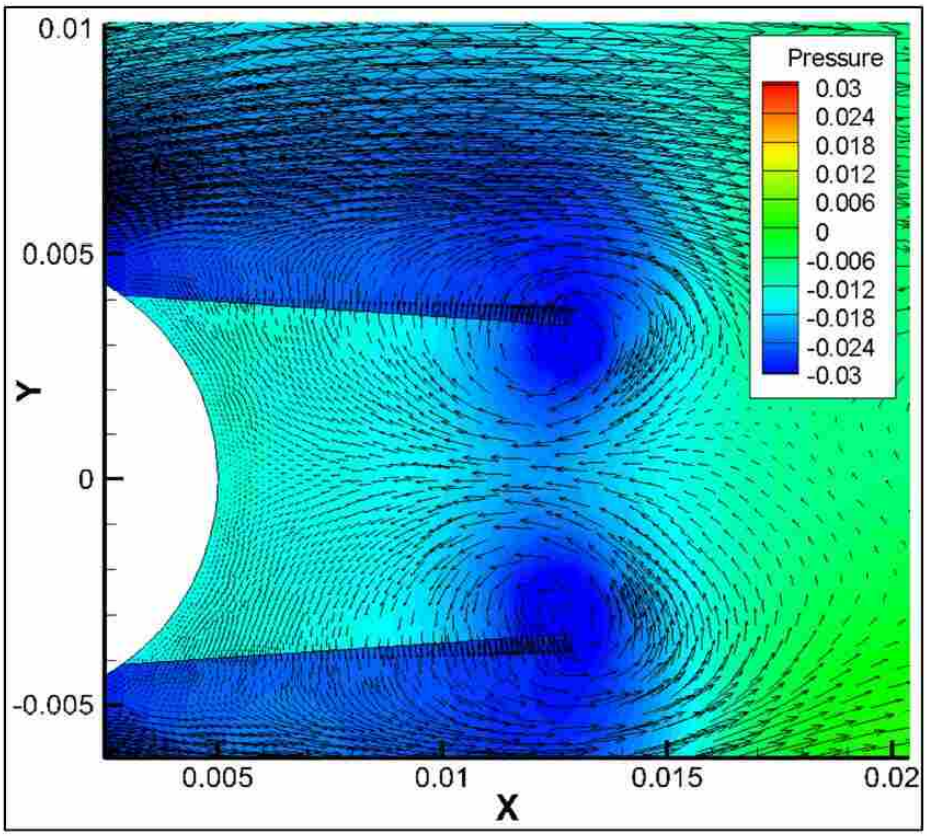


**Fig. (4.69):** Superposition of static pressure contours and velocity vectors for simulation at Re=200, frequency ratio 2 and oscillation amplitude 10-degree.

### 4.2.3.1. Classifying the flow behavior using the dimensionless numbers

As mentioned earlier, in this research the behavior of flow was divided in to three categories. This difference has the same behavior for every three selected Reynolds number. therefore, only two variables, oscillation amplitude and oscillation frequency, create this difference. With more attention to the trend of these variations it is obvious that a combination of the two variables of oscillation amplitude of the wings and their oscillations (the ratio of frequency to the natural frequency of shedding) dominated the flow behavior. Therefore, classifying the behavior in to three categories can also be explained using a dimensionless value which is a the multiplying the frequency ratio and the amplitude of the oscillation (which itself are dimensionless values). Therefore, according to the relations of the range of dimensionless values, each of these ranges denotes one of the categories of the flow behavior.

$$\beta = FR \times A \tag{4.1}$$

where, FR is the frequency ratio and A is the oscillation amplitude of the wings. for more clarity of this, Table (4.8) shows the three-categories classification of the flow behavior for different arrangements. In Table (4.8), white, orange and green houses show the first, second and third categories of the flow behavior, respectively. According to Table (4.7) it is evident that by

increasing the frequency ratio of the oscillation amplitude required by the wings to convert the flow from category 1 to category 2 has the descending trend. Therefore, according to Eq. (4.1) and given the Table (4.7) the range of dimensionless value β can be determined.

β=22.5 denotes the boundary of the first and second categories at frequency ratio 1.25. be increasing the value of β, the behavior of flow changes to the second category and the reduction in the value of β denotes the flow behavior of first category.

About the value of β in the third category of flow behavior we cannot say anything. Based on the results obtained for correct coefficients of the frequency ratio, the third signal having low frequency is not exists. For example, at frequency ratio twice the natural shedding frequency, the aforementioned signal is eliminated and a type of flow behavior is observed which is different from the incorrect ratios. More information is needed to make a definitive comment on the relation between the β number and the third category of flow. This remains as a future work.

**Table. (8.4):** Classification of flow behavior based on problem arrangement.

| **Frequency ratio** Frequency amplitude(degree) | **Reynolds number** | | |
|---|---|---|---|
| | **200** | **250** | **300** |
| **0.75** | | | |
| 10 | First type | | |
| 14 | | | |
| 16 | | | |
| 18 | | | |
| **1** | | | |
| 10 | First type | | |
| 14 | | | |
| 16 | | | |
| 18 | | | |
| **1.25** | | | |
| 10 | First type | | |
| 14 | | | |
| 16 | | | |
| 18 | Second type | | |
| **1.5** | | | |
| 10 | First type | | |
| 14 | | | |
| 16 | Second type | | |
| 18 | | | |
| **2** | | | |
| 10 | Third type | | |
| 14 | Second type | | |
| 16 | | | |
| 18 | | | |

# Conclusions
# And
# Future works

This section has addressed an overview on the previous chapters and summarized them. Analysis of the results which has been done in the previous chapters and presenting conclusion based on them will be done in this chapter. Then, some recommendations will be presented as the futures work for the interested research in this field to study on them and solve the problems with more applications and/or to use better and more precise methods for solving their problems. In this thesis, the effect of the installing the oscillatory slender wings on the cylinder on the Von-Karman vortex shedding and oscillating variations of the lift and drag coefficients was investigated.

## 1. Conclusions

Von-Karman vortex is an unsteady phenomenon caused by the laminar flow instabilities around a cylinder. Due to this phenomenon, some vortices are formed and separated periodically on the lower and upper parts of the cylinder. Although the laminar nature of the flow preserved, but some vortices effects on a part of the field until the complete dissipation.

In this research the effect of installation of two oscillatory slender wings having 180-degree phase differences has been investigated. In chapter 2, the governing equations of the flow were studied. Given that the Navier-Stokes equations have been used in the simulations, these equations were simplified based on the problem, since the Karman vortex shedding around the cylinder in the laminar flow regime is of concerned, one of the most simplifications is the lack of turbulences in the flow. Given that the simulations are performed using AnsysFluent too for validation, the type of the boundary conditions required for the simulation were defined. Because the velocity is known on the inlet boundary, therefore the best boundary condition for the inlet is the velocity. Non-slip condition is defined for the walls in the software. Based on the similar simulations which are done, the Pressure outlet condition was used for the outlet boundary.

Given the selecting of Ansys Fluent software as the validation solver and since this software solves the Navier-Stokes equations based on the finite volume methods, these methods were described in chapter 3. Considering the flow as laminar lead to some specific requirement in the grid. This along with low Mach number determine the overall shape of the field and the quality of the grid. In addition, numerical validations and grid comparison with grids available in the reference papers have led to a final grid which was explained in chapter 3. Given the problem and requirement for remeshing method, the requirements of the solver in the desired grid should be taken in to account. For this purpose, the introduced grid has been considered as an unstructured grid with good quality to simulate the boundary layer. Diffusion of the vortices separated from the geometry occurred in the region behind the body which known as the Karman street. Based on this, the grid created in this region has better quality than the other regions.

Geometry changing during the solution and using remeshing method lead to change in grid quality during the solution. In chapter 3, the properties of the grid and the settings required to optimize the quality during the solution were reviewed and studied.

In this research it was indicated that the oscillations of the lift coefficient can be minimized under some specific conditions. In the conditions, the oscillations of the lift force are of the same order as the noises available in their oscillations. The sources of these noises can be the numerical error, error results from changing the grid quality during the time and the other error

sources. The shape of diffusion of vortices, in such condition, does not follow the general diffusion shape of the Karman shedding phenomenon and the vortices are separated from the geometry simultaneously and advances in the field perfectly symmetrical.

It was shown that the effects of the wings, vortex shedding and slower aerodynamic phenomena are effective on the lift force coefficient. It is while that the drag force coefficient has more effect on the oscillation of the wings that the other variables and the effect of other phenomena on this coefficient can be neglected. In this research, it was found that in some cases related to the frequency ratio of the oscillation of the wings twice than the natural shedding, the number of the waves governed the behavior of the lift coefficient decrease to a single wave. It was shown that the frequency of this wave is equal to the frequency of the vortex shedding. Also, the behavior of the vortices in this case was analyzed. It was found that in this case the vortex region moving away from the geometry is the result of the attaching smaller vortices which create from two consecutive oscillations of the wings.

**2. Future work recommendations**

Given the studies done in this project and given the various aspects which can be improved, it is recommended that the following activities be done in the future.

**1. Increase the number of wings:**

Given the mutual effects of the effective parameters on the physic of the Karman vortices, increasing the number of wings can be a good research field to achieve the more optimal and/or to more precise controlling the behavior of vortices. For example, the effect of the installing planes as fractal and study its effects on the flow in micro and nano scales can be interesting topic.

**2. Installation angle, location angle, the ratio planes' length to cylinder's length and the oscillatory function of wings**

In this research, installation angle and location of the wings were selected based on the minimum oscillation amplitude of the lift force coefficient. But, this condition is not the only determining factor of the problem's arrangement and the method for selecting these parameters itself can be a research field. Also, the wings were applied under a simple oscillation harmonic function. Changing the oscillation function of the wings can be an interesting topic for the future researches.

**3. 3D simulation**

In the present research, only 2D simulation has been addressed. One of the complexities of the aerodynamic flows is the variations of the flow behavior at the end of the bodies. The mutual effect of the edge flow at two ends of the cylinder and Karman vortices can be very interesting and important. Changing the simulation from 2D to 3D and investigating the effect of the wings' installation can be the next step of the present research.

**4. Using flexible planes rather than solid wings**

In the present study, wings are considered as the solid planes. One of the methods for controlling the Karman vortex shedding is the use of the flexible planes. Using these planes and repeating the simulations can be the continues of this project and can be studied.

## 5. Discussion on the dimensionless number β

For definite comment on the relation of dimensionless value β and the third type of the flow and generally the correct frequency ratios, information and studying on the more arrangement are required. It is recommended that the number of arrangement under study increases and more correct ratios of the natural frequencies studied.

# Bibliography


[1] L. S. G. Kovasznay, "Hot-Wire Investigation of the Wake behind Cylinders at Low Reynolds Numbers," *Proc. R. Soc. London A Math. Phys. Eng. Sci.*, Vol. 198, no. 1053, pp. 174–190, 1949.

[2] Roshko, "On the drag and shedding frequency of two-dimensional bluff bodies," *NACA Tech. Note 3169*, no. July 1954, pp. 1–30, 1954.

[3] L. Prandtl, O. G. Tietjens, and J. P. Den Hartog, *Applied hydro-and aeromechanics*. Dover Publications, 1957.

[4] P. W. Bearman and M. M. Zdravkovich, "Flow around a circular cylinder near a plane boundary," *J. Fluid Mech.*, Vol. 89, no. 01, p. 33, 1978.

[5] Y. Lecointe and J. Piquet, "On the use of several compact methods for the study of unsteady incompressible viscous flow round a circular cylinder," *Comput. Fluids*, Vol. 12, no. 4, pp. 255–280, 1984.

[6] M. Braza, P. Chassaing, and H. H. Minh, "Numerical study and physical analysis of the pressure and velocity fields in the near wake of a circular cylinder," *J. Fluid Mech.*, Vol. 165, no. 1986, pp. 79–130, 1986.

[7] D. Rockwell, "On vortex formation from a cylinder. Part 2. Control by splitter-plate interference," *JFM*, pp. 1–3, 1987.

[8] C. H. K. Williamson, "Oblique and parallel modes of vortex shedding in the wake of a circular cylinder at low Reynolds numbers," *J. Fluid Mech.*, Vol. 206, no. -1, p. 579, 1989.

[9] R. D. Blevins, *Flow-induced vibration*, Second edi. Van Nostrand Reinhold, 1990.

[10] A. Williamson, C. H. K. and Roshko, "Measurements of base pressure in the wake

of a cylinder at low Reynolds numbers," *Zeitschrift f'ur Flugwissenschaften und Weltraumforsch.*, Vol. 14, pp. 38–46, 1990.

[11] a. Roshko, "Perspectives on bluff body aerodynamics," *J. Wind Eng. Ind. Aerodyn.*, Vol. 49, no. 1–3, pp. 79–100, 1993.

[12] G. D. Miller and C. H. K. Williamson, "Control of three-dimensional phase dynamics in a cylinder wake," *Exp. Fluids*, Vol. 18, pp. 26–35, 1994.

[13] C. H. K. Williamson, "Vortex Dynamics in the cylinder wake," *Annu. Rev. Fluid Mech.*, Vol. 28, pp. 477–539, 1996.

[14] C. H. K. Williamson and R. Govardhan, "VORTEX-INDUCED VIBRATIONS," *Annu. Rev. Fluid Mech.*, Vol. 36, no. 1, pp. 413–455, Jan. 2004.

[15] E. Naudascher and D. Rockwell, *Flow-Induced Vibrations: An Engineering Guide*. Courier Corporation, 2012.

[16] A. Okajima, "Strouhal numbers of rectangular cylinders," *J. Fluid Mech.*, Vol. 123, p. 379, 1982.

[17] R. W. Davis and E. F. Moore, "A numerical study of vortex shedding from rectangles," *J. Fluid Mech.*, Vol. 116, p. 475, 1982.

[18] R. W. Davis, E. F. Moore, and L. P. Purtell, "A numerical-experimental study of confined flow around rectangular cylinders," *Phys. Fluids*, Vol. 27, no. 1, p. 46, 1984.

[19] a Okajima, "Numerical simulation of flow around rectangular cylinders," *J. Wind Eng. Ind. Aerodyn.*, Vol. 33, pp. 171–180, 1990.

[20] K. Kelkar and S. Patankar, "Numerical prediction of vortex shedding behind a square cylinder," *Int. J. Numer. Methods Fluids*, Vol. 14, no. May 1991, pp. 327–341, 1992.

[21] A. Okajima, H. Ueno, and H. Sakai, "Numerical Simulation O F Laminar and Turbulent Flows Around Rectangular," Vol. 15, no. March, pp. 999–1012, 1992.

[22] C. Norberg, "Flow around rectangular cylinders: Pressure forces and wake

frequencies," *J. Wind Eng. Ind. Aerodyn.*, Vol. 49, no. 1–3, pp. 187–196, 1993.

[23] A. Sohankar, L. Davidson, and C. Norberg, "Numerical simulation of unsteady flow around a square two-dimensional cylinder," 1995, p. 4.

[24] A. Sohankar, C. Norbergb, and L. Davidson, "Numerical simulation of unsteady low-Reynolds number flow around rectangular cylinders at incidence," *J. Wind Eng. Ind. Aerodyn.*, Vol. 69–71, pp. 189–201, Jul. 1997.

[25] A. Sohankar, C. Norberg, and L. Davidson, "Low-Reynolds-number flow around a square cylinder at incidence: study of blockage, onset of vortex shedding and outlet boundary condition," *Int. J. Numer. Methods Fluids*, Vol. 26, no. 1, pp. 39–56, Jan. 1998.

[26] S. Sen, S. Mittal, and G. Biswas, "Flow past a square cylinder at low Reynolds numbers," *Int. J. Numer. Methods Fluids*, Vol. 67, no. 9, pp. 1160–1174, Nov. 2011.

[27] E. A. GILLIES, "Low-dimensional control of the circular cylinder wake," *JFM*, Vol. 371, pp. 157–178, 1998.

[28] V. Gattulli and R. Ghanem, "Adaptive control of # ow-induced oscillations including vortex e ! ects," Vol. 34, pp. 853–868, 1999.

[29] C. Homescu, I. M. Navon, and Z. Li, "Suppression of vortex shedding for flow around a circular cylinder using optimal control," Vol. 69, no. March 2001, pp. 43–69, 2002.

[30] H. Akilli, B. Sahin, and N. Filiz Tumen, "Suppression of vortex shedding of circular cylinder in shallow water by a splitter plate," *Flow Meas. Instrum.*, Vol. 16, no. 4, pp. 211–219, Aug. 2005.

[31] S. Turki, "Numerical Simulation of Passive Control on Vortex Shedding Behind Square Cylinder Using Splitter Plate," *Eng. Appl. Comput. Fluid Mech.*, Vol. 2, no. 4, pp. 514–524, Jan. 2008.

[32] Y. Sudhakar and S. Vengadesan, "Vortex shedding characteristics of a circular cylinder with an oscillating wake splitter plate," *Comput. Fluids*, Vol. 53, pp. 40–

52, Jan. 2012.

[33] Y. Hu and J. Wang, "The effects of attached flexible tail length on the flow structure of an oscillating cylinder," *Sci. China Physics, Mech. Astron.*, Vol. 56, no. 2, pp. 340–352, Jan. 2013.

[34] S. Kunze and C. Brücker, "Control of vortex shedding on a circular cylinder using self-adaptive hairy-flaps," *Comptes Rendus Mécanique*, Vol. 340, no. 1–2, pp. 41–56, Jan. 2012.

[35] a. Igbalajobi, J. F. McClean, D. Sumner, and D. J. Bergstrom, "The effect of a wake-mounted splitter plate on the flow around a surface-mounted finite-height circular cylinder," *J. Fluids Struct.*, Vol. 37, pp. 185–200, Feb. 2013.

[36] Y. Qiu, Y. Sun, Y. Wu, and Y. Tamura, "Effects of splitter plates and Reynolds number on the aerodynamic loads acting on a circular cylinder," *J. Wind Eng. Ind. Aerodyn.*, Vol. 127, pp. 40–50, Apr. 2014.

[37] M. Eckert, *The Dawn of Fluid Dynamics: A Discipline Between Science and Technology*. Wiley, 2007.

[38] J. . Anderson, *Fundamentals of Aerodynamics*, 5th ed. McGraw-Hill Education; 5th edition (February 12, 2010), 2010.

[39] A. Roshko, "On the Development of Turbulent Wakes From Vortex Streets."

[40] D. J. Tritton, "Experiments on the flow past a circular cylinder at low Reynolds numbers," *J. Fluid Mech*, Vol. 6, no. 4, pp. 547–567, 1959.

[41] E. Berger, "transition of the laminar vortex flow to the turbulent state of the karman vortex street behind an oscillating cylinder at low reynolds number," in *Jahrbuch der Wissenschaften Gesselschaft*, 1964, pp. 164–172.

[42] C. H. K. WILLIAMSON and G. L. BROWN, "A SERIES IN 1/√Re TO REPRESENT THE STROUHAL–REYNOLDS NUMBER RELATIONSHIP OF THE CYLINDER WAKE," *J. Fluids Struct.*, Vol. 12, no. 8, pp. 1073–1085, 1998.